

WTI Onderzoek en ontwikkeling landelijk toetsinstrumentarium

Product 5.12 Analyses grass erosion in wave run-up and wave
overtopping conditions

Jentsje van der Meer (Van der Meer Consulting)
Gijs Hoffmans (Deltares)
Andre van Hoven (Deltares)



1209437-005

Title

WTI Onderzoek en ontwikkeling landelijk toetsinstrumentarium

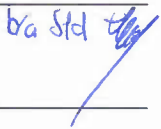
Client	Project	Reference	Pages
Rijkswaterstaat Water, Verkeer en Leefomgeving	1209437-005	1209437-005-HYE-0003-	95

Trefwoorden

erosion, grass, revetment, wave run-up, critical velocity, wave run-up simulator, grass erosion model, grass pull out strength, pressure gradient, Colijnsplaat, Zeelandbrug, large scale test, grass erosion database

Summary

Within the framework of WTI, Research and Development of Flood Defence Assessment Tools (Wettelijk Toetsinstrumentarium), which is called in Dutch: WTI-2017 "Onderzoek en ontwikkeling landelijk toetsinstrumentarium", research was carried out to develop an erosion model for grass in the wave run-up zone consistent with the current model in use for the wave overtopping zone. In order to use the erosion model for wave overtopping in the wave run-up zone it was necessary to re-evaluate all wave overtopping tests and to incorporate the flow velocity increase on the slope. This led to a re-evaluation of previously measured critical velocities U_c and cumulative overload D. To validate the erosion model in the wave run-up zone a wave run-up simulator was constructed and tested. The wave run-up generated by the simulator was measured at a test location near the village of Colijnsplaat (Zeeland, The Netherlands). The simulator performed well and four 2 meter wide test strips on the dike were tested with an increasing wave overtopping load. Storm conditions were simulated with a H_{m0} of 2 m and a (simulated) water level increasing to just below the transition between the hard revetment and the grass revetment. The grass proved to be very erosion resilient and (unfortunately) did not fail. The validation was therefore not optimal, however it the proven strength of the grass has added to the confidence in the model. Apart from the large scale erosion tests small sod pull out tests were performed. The pull-out tests were carried out 'in one go' and fatigue tests were done at ca. 80% of the maximum stress with up to 100 repetitions. The small tests will hopefully link this measurable field parameter to the grass erosion model parameter U_c using the turf element model. The objective of WTI-2017 programme is to provide a new set of safety assessment tools for water defences in 2017. This report is product 5.12 of 2014.

Versie	Datum	Auteur	Paraaf	Review	Paraaf	Goedkeuring	Paraaf
1	Nov. 2014	Jentsje van der Meer (Van der Meer Consulting) Gijs Hoffmans Andre van Hoven		Mark Klein Breteler		Leo Voogt	
2	Jan. 2014	Jentsje van der Meer (Van der Meer Consulting) Gijs Hoffmans (Deltares) Andre van Hoven (Deltares)		Mark Klein Breteler		Leo Voogt	

State
final

Contents

1	Introduction	1
1.1	Framework	1
1.2	Back ground research on erosion of grass in the wave run-up zone	1
1.3	Research steps from erosion model on landward slope to the seaward slope	2
1.4	Readers guidance	2
2	Wave run-up simulation	3
2.1	Design, construction and testing of the wave run-up simulator	3
2.1.1	Introduction	3
2.1.2	Design of the wave run-up simulator	3
2.1.3	Calibration of the prototype against a dike slope	5
2.1.4	Observations on the machine and possible improvements	14
2.2	Hydraulic measurements near the Zeelandbrug	15
2.2.1	Calibration for steering files	15
2.2.2	Set-up for the hydraulic measurements	18
2.2.3	Analysis of measurements	24
2.2.4	Wave overtopping by wave run-up simulation	27
3	Extension and modification of the database	31
3.1	Overall view of modifications and extensions	31
3.2	Recalculation of the cumulative overload for all observed conditions	31
4	Re-analysis on cumulative overload	35
4.1	Summary of original analysis on cumulative overload	35
4.2	Re-analysis of various hydraulic regimes at the Vechtdijk	35
4.3	Re-analysis of all tested locations	41
4.3.1	Method of analysis	41
4.3.2	Delfzijl	41
4.3.3	Boonweg	41
4.3.4	St Philipsland	42
4.3.5	Kattendijke	42
4.3.6	Afsluitdijk	42
4.3.7	Vechtdijk	44
4.3.8	Tielrode	44
4.3.9	Tholen	44
4.3.10	Nijmegen	45
4.3.11	Millingen	45
4.3.12	Noord-Beveland	45
4.4	Summary of the re-analysis	45
4.5	Re-analysis of the graphical method in the Handreiking	46
5	Evaluation of tests near the Zeelandbrug	49
5.1	Damage development	49
5.2	Front velocities during run-up	51
5.3	Cumulative overload	54
5.4	Cumulative overload for pilot test at Tholen	56
5.5	Conclusions on validation cumulative overload for wave run-up	58

6 Evaluation of tests with regard to pressure gradients over the grass sod	61
6.1 General	61
6.2 Laboratory pressure measurements	62
6.3 Field pressure measurements	63
6.3.1 Rivierenland	63
6.3.2 Noord-Beveland (Colijnsplaat)	65
6.4 Soil properties	69
6.5 Pluto calculations	70
6.6 Conclusions	73
7 Evaluation of tests with regard to the grass pull out strength versus critical velocity	75
7.1 Introduction	75
7.2 Performance of turf-tensile tests	75
7.3 Root investigation	78
7.4 Analysis	79
7.5 Critical flow velocity	83
7.6 Conclusions and recommendations	84
8 Procedures for the cumulative overload method	89
8.1 Introduction	89
8.2 Procedure for wave overtopping	89
8.3 Procedure for wave run-up	91
8.4 Procedure wave overtopping in WT12017	92
8.5 Procedure wave run-up in WT12017	92
9 Conclusions and recommendations	97
9.1 Conclusions	97
9.2 Recommendations	97
Appendices	
References	1
A Pictures of the construction stages of the wave run-up simulator	A-1
B Design drawings of the wave run-up simulator	B-1
C Pictures of the calibration at the Vossemeerdijk	C-1
D Measurements of velocity along the slope for various filling levels, during calibration at the Vossemeerdijk.	D-1
E Measurements of velocity and flow thickness along the slope during the hydraulic measurements at the Zeelandbrug and for various filling levels	E-1
F Cumulative overload for various test conditions and various acceleration factors	F-1
G Experimental results force and displacements (grass sods)	G-1

1 Introduction

1.1 Framework

This research has been carried out in the framework of WTI, Research and Development of Flood Defense Assessment Tools (Wettelijk Toetsinstrumentarium), which is called in Dutch: WTI-2017 “Onderzoek en ontwikkeling landelijk toetsinstrumentarium”. The objective of WTI-2017 programme is to provide a new set of safety assessment tools for water defences in 2017, while Cluster 5 of this program is focusing on dike revetments and residual strength. This is product 5.12 of 2014.

The report was written by two authors and edited by André van Hoven (Deltares). Jentsje van der Meer (Van der Meer Consulting) wrote chapters 2 to 5 and 8 and Gijs Hoffmans (Deltares) chapters 6 and 7. The research was carried out and discussed in the Project-team which also holds representatives from Alterra and Infram. The report represents a joint effort in the research in grass erosion.

1.2 Back ground research on erosion of grass in the wave run-up zone

One of the failure mechanisms within WTI2017 is erosion of grass on the seaward slope in the wave run-up zone. The definition of the zone is given in Figure 1.1. The division between the wave impact and wave run-up zone is the water level called Dutch: Toetspeil. The water level is generated within safety assessment software tool ‘Ringtoets’. The upper boundary is the seaward crest line. If a grass revetment is present in both the wave run-up zone and the wave impact zone, the assessment of the wave impact zone will be decisive, and the assessment in the run up zone can be discarded. In many cases where there is a high probability of large waves, the impact zone is protected by a hard revetment, while wave run-up will reach the grass cover above the hard revetment.

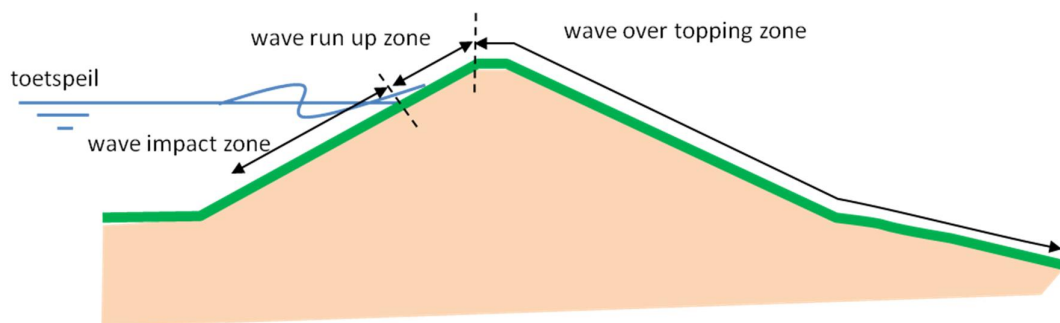


Figure 1.1 Grass revetment wave attack-zone definition for erosion mechanisms

For erosion of grass in the wave overtopping zone a failure model, the cumulative overload model, was developed and reported for use in the prolonged third safety assessment round [RWS 2012]. The model uses a grass quality description ‘closed’, ‘open’ and ‘fragmented’ sod. For erosion in the wave impact zone the same quality description is used. However, for the wave run-up zone the old VTV2006 model was still in use, describing the grass quality in a different way. Also the erosion model in the wave run up zone was not consistent with the model in the wave overtopping zone, while the load and mechanism are basically the same. Therefore in 2013 research was started aimed at developing an erosion model similar to the model in the overtopping zone, using the same grass quality description [Deltares 2013].

1.3 Research steps from erosion model on landward slope to the seaward slope

The first hypothesis was that the model was usable for the seaward slope without any adaptations, just using the run-up velocity instead of the velocity at the dike crest [Deltares 2013]. To validate the hypothesis a wave run-up simulator was designed and tested (Section 2). In the winter season of 2013-2014 a validation test was performed at a dike near Colijnsplaat in Zeeland [Infram 2014]. Evaluation of the test and validation of the model is given in section 5, 6 and 7.

To adapt the grass erosion model from the landward slope for the seaward slope, all previous overtopping tests had to be re-evaluated (sections 3 and 4). The model as described in RWS 2012 holds no distinction between steep and gentle slopes and short and long slopes and just uses the velocity at the crest, while acceleration of the overtopping wave volumes was observed and measured in several cases. The method using the velocity at the crest is applicable because the overtopping tests, on which the model is based, were performed at both steep and gentle slopes and short and long slopes, e.g. a representative cross-section of dikes in the Netherlands. A sufficient amount of safety between expected failure of the grass revetment and the safety assessment criterion ensures the method is safe for all cross sections. However, on the seaward slope, the run-up velocity is much larger than at the crest, requiring a better effort to take into account the actual velocity. The re-evaluation is described in section 3 and 4 and leads to an adjustment of both the characteristic damage numbers and the critical velocity.

Further steps will be needed to implement the model in the WTI2017. The further steps include, implementing the model in software, decide on safety factors to cover uncertainties left after the model validation and variations and uncertainties in the grass strength parameter. These steps are not part of this report.

1.4 Readers guidance

- The design process, testing and performance of the wave run-up simulator is given in section 2, the section also holds references to Appendix A and B where pictures and the design drawings of the simulator are given.
- Section 3 describes the extension of the test database with the latest tests in Millingen and Nijmegen and with slope parameters and the place relative to the crest where damage occurred. This makes it possible to take into account the acceleration of the flow on the landward slope.
- Section 4 holds the actual re-evaluation leading to different characteristic damage numbers and critical velocity.
- The general evaluation of the wave run-up tests is given in section 5. The tests were performed to validate the adapted erosion model.
- Sections 6 and 7 also describe the evaluation of the tests, however focused on the load (pressure gradient over the grass sod) and the strength (pull out strength of the sod, which is related to the critical velocity).
- A procedure to calculate the cumulative overload in the wave run-up zone for implementation in software is given in section 8.
- Section 9 holds the combined conclusions and recommendations from all sections.

2 Wave run-up simulation

2.1 Design, construction and testing of the wave run-up simulator

2.1.1 Introduction

A first pilot test on wave run-up has been performed at a seadike at Tholen in 2012. That test gave insight in how a run-up simulation works and gave also damage that could physically be explained: at the transition from an almost horizontal berm to the upper slope, where the flow of water has to change direction. The test itself was a pilot test as the wave overtopping simulator had been used with modified steering of the machine. The following aspects were observed:

- The test itself was a success with damage at the transition from berm to upper slope.
- The up-rushing wave tongue seems to simulate run-up well, but the whole run-up and run-down process was not simulated correctly. The main reason was that the wave overtopping simulator had a large volume and water was still flowing out of the machine when the highest run-up point had been reached on the slope and run-down had started. These two flows with opposite direction met each other on the slope, giving a jump or bump of water. This observation led to the conclusion that a good wave run-up simulator should contain less water and should have a slender shape over the full height.
- The large amount of water that came down the slope, gave very large forces on the side walls, this in contrast to wave overtopping. All the down rushing water could not flow down freely as the outflow of the simulator was placed only 0.2 m above the soil and this opening was too small to release all the water.

The second point has led to the decision to design and construct a simulator that would be able to simulate wave run-up more closely to reality. The last point will be solved when the logistics of testing with the wave run-up simulator will be set-up.

In memo vdm13391.27513.1 of 27 May 2013 two solutions for an improved wave run-up simulator have been discussed. One was a modification of the present wave overtopping simulator. A slender inner box with constant cross-section could be constructed in the existing box and could then be enlarged in height by a new slender box. The other idea was to take more or less the dimensions of the wave impact generator (0.4 m by 2 m) and to limit the width of the test section to 2 m only (which is 4 m for wave overtopping). This last option has been chosen for the new design of the wave run-up simulator.

2.1.2 Design of the wave run-up simulator

The principle idea was to develop a kind of drawer valve mechanism, a 110° bend to lead the vertically falling water onto a slope, and a high and slender box with everywhere the same cross-section. The simulator should be placed on a frame with adjustable legs, in order to keep the simulator in an upright position. Where possible modules with the correct cross-section should be used from the development of the wave impact generator. The principle idea of the drawer valve mechanism is shown in Figure 2.1, the bend and the full simulator in Figure 2.2.

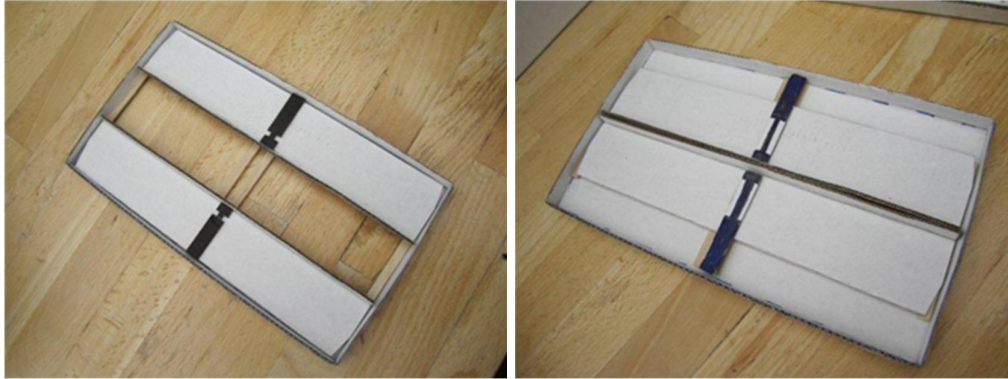


Figure 2.1. Drawer type valve mechanism (open left, closed right)



Figure 2.2. The drawer type valve mechanism left with the 110 degree bend. At right the complete machine on a frame with adjustable legs and a height of about 7 m

The actual design was made in August and September 2013, but was modified at some places during fabrication of the machine. The drawer type valve mechanism is a flat box with two valves of 0.2 m wide that slide horizontally over a bronze guide. In contrast to the valve mechanisms in the overtopping and impact simulators, a larger water pressure will close the valve and leakage will diminish with a higher filling grade of the box.

When the valve system was finished, it was first tested with only 0.1 m of water (the height of the flat box with the valve). Later the first boxes were filled up to 3 m height and when the full simulator had been constructed, up to 7 m height.

Figure 2.2 shows a cross-section of 0.4 m by 2 m over the full height. It was felt during the design that the front and back side of 2 m by 7 m could get quite some wind forces that could make the whole set-up less stable. For that reason the design was changed for the upper part to a cross-section of 0.8 m by 1.0 m with a transition section in between. Everywhere the cross-section was kept the same and internal guiding walls were constructed to guide the flow as smoothly as possible. The flow has to change slightly from direction when it leaves the simulator, but there are no narrow or wide sections that can induce dissipation of energy.

A special U-shaped “fork” was designed and constructed in order to place and dismantle the various models in an easy way with a fork lift truck or small crane. Also a pump inlet was made at half of the height of the simulator. This was done to avoid an inlet over the top at 7 m height, which was considered as very high and may be not required in most test cases. Due to the modular system, however, it is also possible to place the module with the pump inlet at the top of the simulator. The advantage of this last set-up is that all pumped water flows freely into the simulator, where with an inlet half way, the pump has to pump the water up into the simulator when the filling level becomes higher than the pump inlet. This gives a reduced capacity to the pump and then the pumping rate could be not any longer constant (due to the pressure). How large this effect is depends on the pump capacity, but a steering file is easiest to construct if for the whole filling process a constant discharge can be realized.

Appendix A gives a large series of pictures of the construction stages of the simulator as well as the final test with filling it completely with water. Appendix B gives the design drawings.

The filling test up to 7 m height showed that the pressures on the lowest parts of the simulator are enormous. A filling height of 7 m gives 5-7 m water column pressure on the lowest parts. This was no problem for the newly constructed upper parts of 1.0 m by 0.8 m and the transition part and it was also no problem for the valve system. But the lowest section of 0.4 m by 2 m was taken as a leftover of the design of the wave impact generator and this section had not been designed for these high water pressures. The steel plates were only 2 mm thick (the new parts are 4 mm thick) and even with strengthening at various points over the width of 0.4 m (the bolds on the pictures), the plates bended and the bolds were about to pull through the plates. The conclusion was clear: using the existing section seemed to be cheap, but it appears that a new and much stronger section had to be constructed. A new module of 0.4 m by 2.0 m was made by 4 mm thick steel in December.

Also the bend gets very large water pressures and needed to be strengthened by steel girders. Also this outflow guidance was strengthened in December. Moreover, the bend was designed with a 110° curvature, based on an upper slope of a dike of 1:3. When visiting possible locations in Zeeland for further testing with the wave run-up simulator it became clear that almost in all locations the up-rushing flow should start on a more or less horizontal berm and not at a slope. This means that the outflow should also have the possibility for a curvature of 90°. This was not foreseen at the beginning of the design and was modified after the calibration test in January.

2.1.3 Calibration of the prototype against a dike slope

In the week of 6-10 January 2014 the wave run-up simulator was tested on a dike slope. This dike was at the Vossemeerdijk, close to Ketelhaven, in the Province of Flevoland. Host of the testing was Waterboard Zuiderzeeland. Pictures of the set-up and the calibration itself are given in Appendix C.

The inclination of the dike slope was measured every metre over a length of about 16 m. The measurement was performed twice with about 1 m distance between the measurements (the test section was 2 m wide). Figure 2.3 gives the measurements and shows from the outflow of the simulator over a length of about 13 m a fairly constant slope of 1:2.7. The slope gets a little gentler above 13 m, but actually this area was not or hardly reached by the wave run-up simulator.

The opening and closing of the valve was performed by the hydraulic system of the rented crane. During real testing in Zeeland a more power full power pack will be used, which

means that opening and closing will then be a little faster. The opening and closing time was checked and appeared to be quite close to 0.5 s. This was fast enough to give a direct and nice outflow of water.

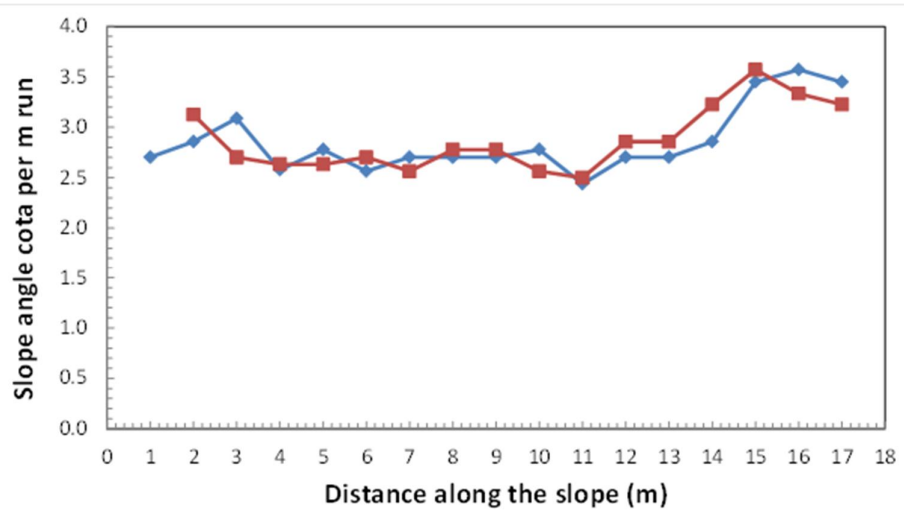


Figure 2.3. Inclination of the dike slope (cota) measured every m along the slope

A few filling levels were tried to see how the machine worked. With a filling level of 6 m the whole simulator displaced back suddenly by about 0.6 m when the valve was opened. It became clear that a sudden release of water, with a large pressure on the valve, gives also quite a backward force due to the forced bending of the water in order to run-up the slope. This backward force was able to displace the simulator as a whole. In order to avoid this, the four adjustable legs were secured by placing wooden poles against the plates of the adjustable legs, see also Appendix C. After this event the simulator was vertically repositioned.

The actual calibration started by filling to a predefined level, releasing the water and measuring visually the run-up height along the slope. On this slope every m was indicated by a painted mark on the grass. The filling levels started with 0.5 m and were increased every time after three similar filling levels had been released. The highest filling level is 7.3 m and then the upper box overflows.

This new wave run-up simulator was made to improve the behaviour of the up-rushing water on the slope compared to the pilot test at Tholen. And there was indeed a large improvement. The water released very fast from the simulator and running up was also fast and nice. The box of the simulator was empty before the run-down started and the “bump” at Tholen did not occur. It was also observed that the run-up over the full run-up area was fairly thin, not as thick as at Tholen. When the run-down started the water disappeared underneath the simulator as the outflow guidance (bend) was placed 0.2 m above the grass. All water disappeared directly, only a little was left with the largest filling levels. This behaviour was much better than at Tholen, where the largest filling levels needed sometimes more than 15 s to have all the water released from the slope and before the next run-up could be released.

It can be concluded that the simulated run-up with the new and slender simulator looked much like real run-up, fast and high with a fast run-down. Due to the fast release of the run-down the water pressures on the side boards were also much smaller than in Tholen,

where this was a real problem. Actually, the system of side boards with wooden poles, as always used for wave overtopping tests, proved to be sufficient for the new wave run-up tests. Although connecting the sideboards over the 2 m wide test area, certainly close to the outflow guidance, is recommended during real testing.

The measured run-up levels along the slope for each filling level are given in Table 2.1. Figure 2.4 shows the run-up level along the slope as function of the filling level. The repetition of run-up levels is very good; the scatter between the three repeated filling levels is small. The largest run-up level exceeded 13 m on the slope, which gives a vertical run-up level of 5 m! The curve in Figure 2.4 is not completely linear as it bends slowly. But the trend can very well be used to create a steering file for the actual tests.

Filling level [m]	Run-up along the slope (m)			
	1st	2nd	3rd	average
0.5	2.6	2.8	2.8	2.7
1.0	4.1	4.4	4.4	4.3
1.5	5.4	5.4	5.4	5.4
2.0	6.2	6.4	6.2	6.3
3.0	8.0	8.0	8.1	8.0
4.0	10.0	9.9	10.0	10.0
5.0	11.4	11.4	11.4	11.4
6.0	12.4	12.4	12.4	12.4
7.0	13.1	13.1	12.9	13.0
7.3	13.4			13.5

Table 2.1. Run-up levels along the slope for specific filling levels

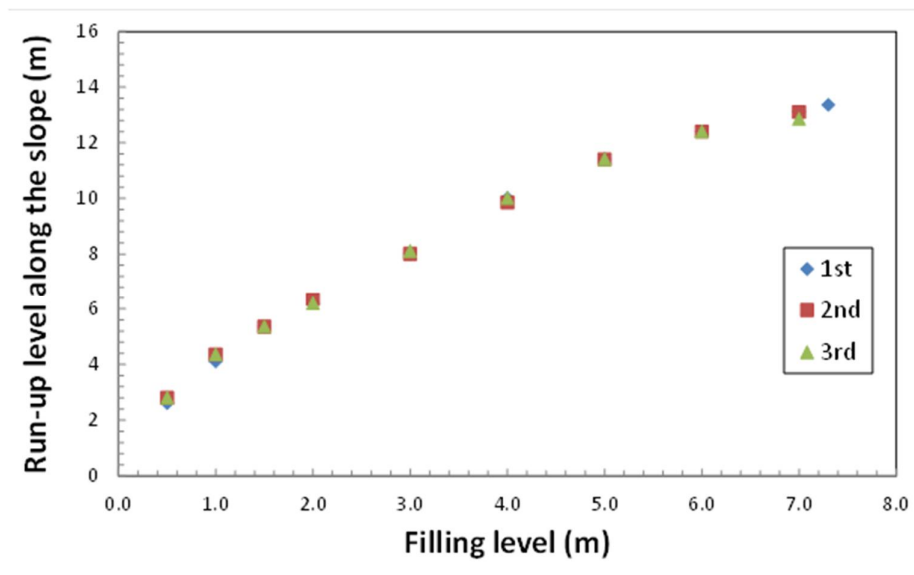


Figure 2.4. Relationship between filling level and run-up level along the slope

In fact the information in Table 2.1 and Figure 2.4 is enough to create a steering file for actual testing, which was one of the objectives of the calibration. A whole measuring campaign on run-up velocities and run-up flow thicknesses was not foreseen. Mainly because setting up and calibration of the surfboards takes quite some time. But by omitting the measurement of flow thicknesses, and therefore the surfboards, it is also possible to place the available paddle wheels directly on the grass. It is quite fast and easy to install eight paddle wheels and measure run-up velocities on the slope.

The set-up is shown by pictures in Appendix C and records of measured velocities in Appendix D. Two paddle wheels were placed every time next to each other in order to give an idea of accuracy of the measurements. The distance between the paddle wheels was 0.67 m. The first pair of paddle wheels was placed 1.6 m from the outflow of the simulator (originally 1 m, but after the described displacement this became 1.6 m). Then every 3 m another pair was installed, covering an area of 9 m along the slope (at 1.6 m, 4.6 m, 7.6 m and 10.6 m from the outflow).

Small filling levels reached only the lowest pair of paddle wheels. The largest filling levels went well over all paddle wheels. Figure 2.5 gives an overall view of all the measured velocities. It seems that the maximum velocities (the peaks in Figure 2.5) increase linearly to a certain filling level and then remain more or less constant.

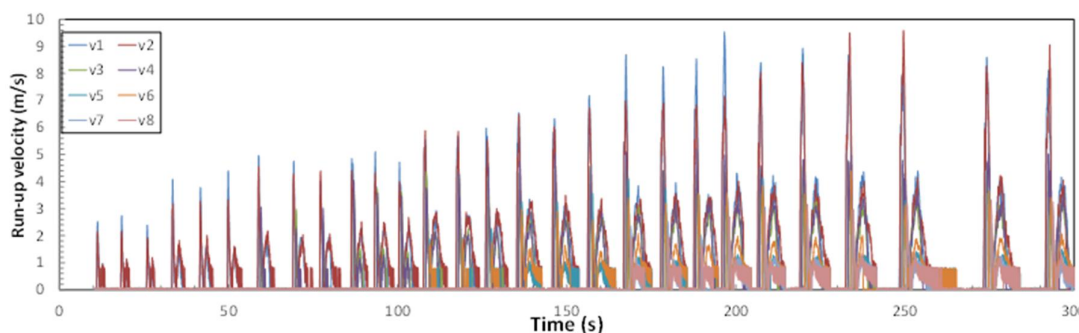


Figure 2.5. Overall picture of the measured velocities along the slope

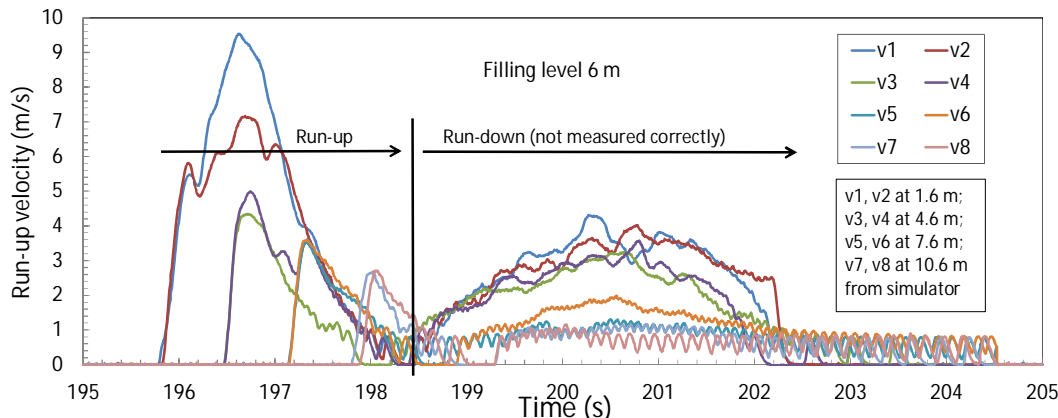


Figure 2.6. Detailed record of all velocities for a filling level of 6 m

Figure 2.6 shows in more detail the measured velocities for a filling level of 6 m (almost full box). The overall picture is that the maximum run-up velocity is reached quite quickly, in tenths of seconds for the higher placed paddle wheels and about one second for the lowest pair, and the velocity then reduces to zero. This is the moment that the water that was running up along the slope comes to a full stop. This zero-point is quite similar for all paddle wheels (around 198.5 s) and indicates that the water over the whole run-up length comes to a stop at the same time. The second part of the record shows the run-down. As the paddle wheels measure velocities correctly in only one direction (upwards along the slope), the actual values of the run-down velocities might not be correct. But still it shows how long the run-down takes place. Figure 2.6 shows that a box with a filling level of 6 m empties

within about 2.5 s (from 195.8 s to 198.5 s), which is at least two times faster than during the pilot test at Tholen. The run-up simulator empties very fast.

The first analysis of the measurements was performed on the maximum run-up velocities. Table 2.2 gives all these maxima and Figure 2.7 shows the maximum run-up velocities as a function of the filling level. There is a fair amount of scatter. Each location has six measurements (pair of paddle wheels and three times repetition of the filling level). Maximum velocities measured (at the lowest location) exceed 9 m/s! This is significantly more than maximum velocities from the wave overtopping simulator at the crest of a dike (around 6 m/s). Within the six measurements a difference of 2 m/s is easily found for the highest filling levels and 1 m/s for the lower ones. This is about the accuracy of measurements of maximum velocities.

Number	Time (s)	Filling level (m)	Velocity v1 (m/s)	Velocity v2 (m/s)	Velocity v3 (m/s)	Velocity v4 (m/s)	Velocity v5 (m/s)	Velocity v6 (m/s)	Velocity v7 (m/s)	Velocity v8 (m/s)
1	10.9	0.5	2.52	2.16						
2	18.1	0.5	2.74	2.17						
3	25.7	0.5	2.39	1.93						
4	33.2	1.0	4.08	3.18						
5	41.5	1.0	3.78	3.28						
6	49.6	1.0	4.40	3.33						
7	58.6	1.5	4.97	4.56	2.17	3.06				
8	68.9	1.5	4.76	4.29	2.97	2.26				
9	76.9	1.5	4.03	4.40	2.54	3.03				
10	86.2	2.0	4.85	4.41	3.67	4.05				
11	93.1	2.0	5.11	4.34	3.73	3.59				
12	100.3	2.0	4.73	3.99	3.61	3.48				
13	107.6	3.0	5.55	5.89	4.35	3.77	1.87	1.68		
14	117.2	3.0	5.68	5.86	4.22	4.28	1.92	1.90		
15	125.9	3.0	5.98	5.55	4.24	4.54	2.27	1.76		
16	135.2	4.0	6.55	6.48	4.32	4.75	3.26	2.97		
17	145.7	4.0	6.33	6.03	4.55	5.02	3.26	2.91		
18	156.1	4.0	7.18	6.73	4.58	4.56	3.56	2.57		
19	166.6	5.0	8.69	6.98	4.49	5.10	4.10	3.40	2.37	1.92
20	177.8	5.0	8.26	6.92	4.39	4.41	3.73	3.19	2.54	1.93
21	187.5	5.0	8.54	6.84	4.28	5.20	3.50	3.55	2.02	1.64
22	195.8	6.0	9.54	7.17	4.34	4.99	3.53	3.59	2.68	2.71
23	206.3	6.0	8.41	8.03	4.49	4.59	4.13	3.85	3.06	2.91
24	218.9	6.0	8.93	8.41	4.58	4.82	3.45	3.53	2.89	3.17
25	232.4	7.0	8.69	9.50	4.72	4.98	3.49	4.40	2.95	2.96
26	248.4	7.0	8.01	9.59	4.59	4.79	3.30	3.13	2.77	3.20
27	273.3	7.0	8.60	8.26	4.41	5.05	3.73	3.66	2.90	3.33
28	291.5	7.3	8.12	9.06	4.38	5.03	3.23	3.41	2.93	3.26

Table 2.2. Maximum run-up velocities in each record

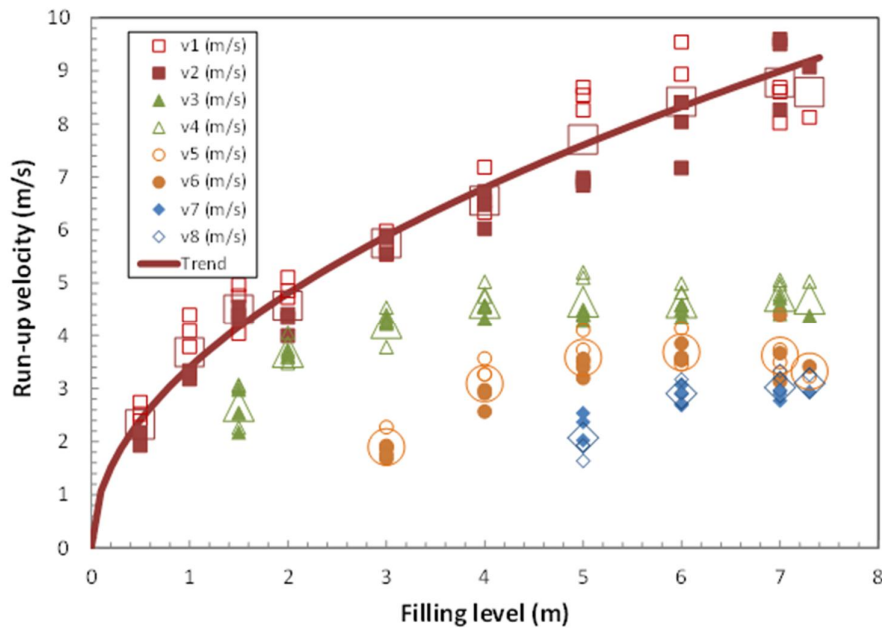


Figure 2.7. Maximum run-up velocities in each record versus the filling level

The small symbols in Figure 2.7 show the individual measurements, the large symbols the average value. Trends for increasing filling levels are clear and an average trend is given for the lowest location at 1.6 m from the outflow of the simulator. Maximum velocities at 4.6 m are lower than 3 m lower and are more or less constant for filling levels of 4 m and higher. Maximum velocities at 7.6 m and 10.6 m are again lower than at lower locations, but for the maximum filling levels the velocities are quite close, between 3-5 m/s. It can be concluded that the maximum velocities in a run-up record decrease with run-up level.

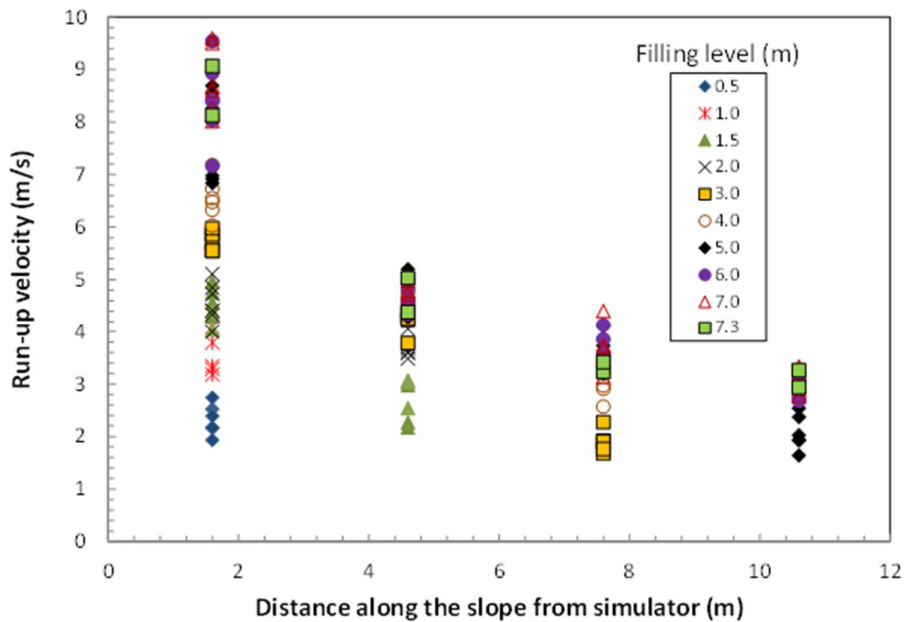


Figure 2.8. Maximum run-up velocity of each record versus the location on the slope

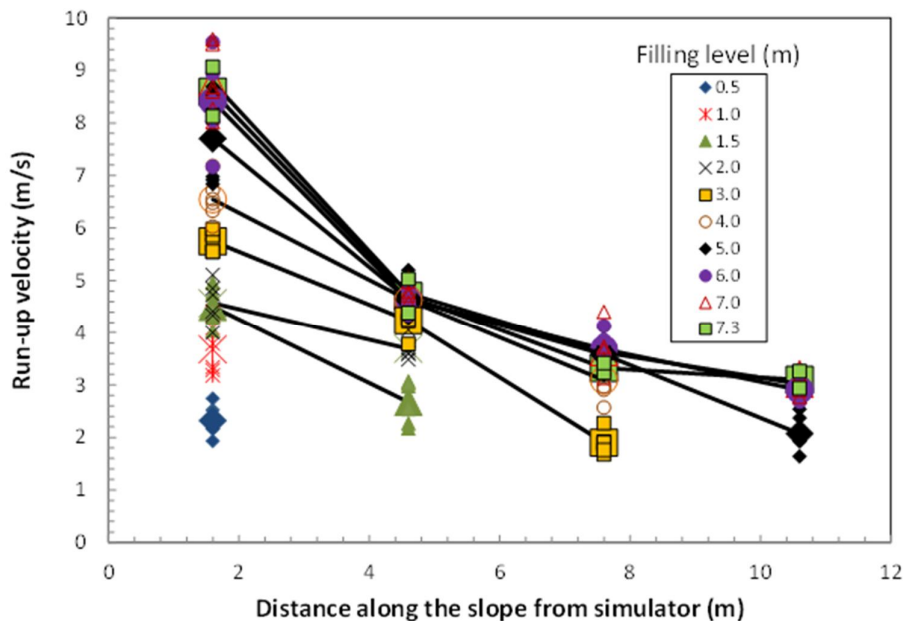


Figure 2.9. Similar to Figure 2.8, but including averages (large symbols) and trends

Figures 2.8 and 2.9 show the same maximum velocities in another way than Figure 2.7. The velocities are now shown versus the location on the slope. Figure 2.8 shows each measurement and the picture is not easy to analyse due to the scatter of the measurements. In Figure 2.9 the averages are given too by large symbols and these averages have been connected by a line. The conclusion is similar as from Figure 2.7: the maximum velocity decreases with increasing run-up level.

At first sight this was not expected. In the extensive analysis that was performed to come to a good description of the whole wave run-up process (Van der Meer, 2011), it was concluded that the velocity of the wave run-up front was quite similar to at least 75% of the maximum individual run-up level. The analysis and conclusion was based on records of the wave run-up front, not by velocity measurements at a certain location. Also the observations indicated that the front of the run-up was quite fast and did not reduce much, certainly not to a degree as indicated in Figures 2.7-2.9.

This discrepancy seems strange, but can possibly be explained by the difference in definition of velocity. The paddle wheels measure the velocity during run-up at a certain location and from the record the maximum value was taken. This might be different from the velocity of the wave run-up front. Actually, the velocity of the wave run-up front was not measured, but still the measurements on the slope include the possibility to re-construct the front velocity along the stretch from 1.6 m to 10.6 m from the outflow of the simulator.

Filling level m	Front velocities		
	v0-3 m/s	v3-6 m/s	v6-9 m/s
7.3	4.42	4.26	4.18
7.0	4.47	4.07	4.72
7.0	4.35	4.20	4.52
7.0	4.56	4.18	4.54
6.0	4.77	4.11	4.47
6.0	5.07	4.11	4.52
6.0	4.51	4.46	4.33
5.0	5.06	4.37	4.35
5.0	5.04	4.13	4.17
5.0	4.47	4.49	4.13

Table 2.3. Front velocities measured between the various locations and for filling levels larger than 5 m

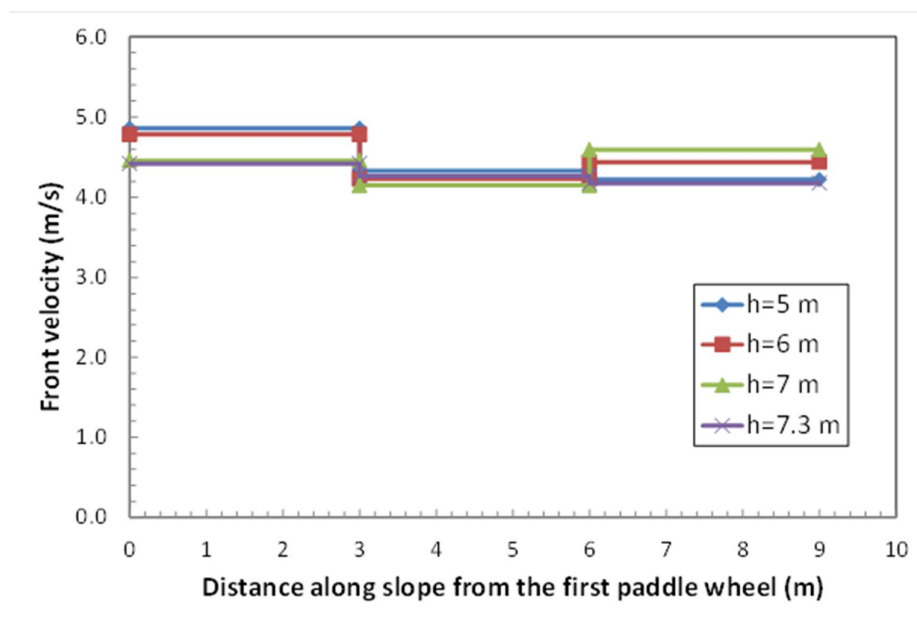


Figure 2.10. Trend of front velocities between 1.6 m and 10.6 along the slope. The zero-point is given at 1.6 m from the outflow of the simulator

Figure 2.6 can be used as an example. It is quite clear for each pair of paddle wheels when the up-rushing water reaches the instrument. Then a fast increase from zero velocity is observed. The time difference between this onset of velocity between the various locations can be used to calculate the average front velocity over 3 m. The onset of velocity for each paddle wheel and for each location was determined from the records for filling levels of 5 m and higher. From a filling level of 5 m and higher all 8 paddle wheels were reached during run-up. Then the onset of velocity was averaged between each pair of paddle wheels and the average velocity over the 3 m along the slope was calculated. These average front velocities are given in Table 2.3 and in Figure 2.10.

The trend is completely different for the front velocity than for the maximum velocity from a record! There is a slight tendency that the front velocity decreases, but Figure 2.10 also shows that the front velocities over the first 3 m are larger for filling levels of 5 m and 6 m than for filling levels of 7 m and more. This could be explained by the fact that for the highest filling levels a little damage was observed at the grass slope, just in front of the simulator. This might have had effect on the measurements at the first measuring point 1.6 m away. A fair conclusion is that the front velocity is about 4.5 m/s over the whole range of 9 m and more or less regardless of the filling level (but 5 m or higher). This conclusion agrees with the conclusion in Van der Meer (2011) about the front velocity.

The two conclusions about maximum velocity and front velocity lead to an interesting discussion. It was (personally) observed in various Delta flume tests that after wave breaking on a slope, the wave is “pushed” up the slope and that there is hardly a reduction in front velocity over a large part of the run-up area. This observation was validated by the analysis of the wave run-up front in Van der Meer (2011). Velocities on an upward slope have been measured in quite some investigations. The general trend is that the maximum velocities decrease with higher run-up levels (although this conclusion was not checked here).

An explanation might well be that the maximum velocity occurs later than when the front has passed and that this larger velocity indeed gives an extra push to the water upwards, resulting in a more or less constant and not decreasing front velocity.

With respect to analysis of test results on grass strength this gives an interesting observation. During the wave overtopping testing it was concluded that especially the front velocity was the governing factor for damage to grass, more than a velocity itself or the duration of the velocity. For this reason the duration of an overtopping event is not part of the model on cumulative overload. It means that for run-up one should indeed concentrate on the front velocity and not too much on the very high maximum velocities at the onset of wave run-up.

Overall it seems that the new wave run-up simulator works very well and can produce (vertical) run-up levels up to 5 m and in a way quite close to real wave run-up.

2.1.4 Observations on the machine and possible improvements

The calibration of the wave run-up simulator and certainly the observations with a complete filling of the machine showed a few points that preferably should be improved before the actual testing in Zeeland should start. The list of items follows below.

1. The original idea was to use the crane to support the high simulator against wind forces. A hydraulic crane, however, has not a fully stable support due to the hydraulic system that often has some leakage. This lowers the support at the simulator and is not allowed. Better is to fix 4 steel cables from the top of the simulator to poles at four edges in the ground. These poles should be equipped with plates that fix these poles sufficiently in place. What is needed are connecting eyes, cables and supporting plates.
2. The original idea was to have one gauge along to simulator to watch the filling level of the machine. This gauge was dismountable and can be placed at front as well at the rear side. Experience shows that actually two gauges are needed as often people are at the back and rear side (possibly in the crane or in the measuring cabin) as well as at the front side (watching the run-up). One extra gauge should be made.
3. It appeared that it is quite difficult to place the upper modules exactly on top of each other. The idea is to make four stainless steel guiding pens, which enable an easier connection of modules.
4. The footplates of the adjustable legs are flat with 4 pens to connect them to hard superstructure, like asphalt. For placing on grass, however, the plates should have skirts underneath, like with the wave overtopping simulator. These plates with skirts have to be manufactured.
5. A module has been made which is connected to crane or fork lift truck and enables lifting of the simulator models in an easy way, see picture 31 of Appendix A. This module consists of only steel and it appears that the steel damages the paint of the simulator. A solution is to place rubber at the contacting points.
6. Four girders strengthen the horizontal box with valves with the simulator at a height of 1.5 m above the horizontal box, see picture 32 of Appendix A. The simulator is very high (8 m from the ground) and should also be fixed with an extra set of girders at a level of 3 m above the horizontal box.
7. Two plastic bars should be mounted on the front side in order to place a large 1.5 m by 2 m information board.
8. The bend was already strengthened, but it was observed that the water pressures are so high that it needs to be strengthened even more. Also the outflow direction has to be made flexible, from 90°-110°, to enable simulation from a horizontal berm or directly on a slope.

9. Filling of the simulator can best be done at the top of the simulator. This needs a spread plate, similar to the one in the wave overtopping simulator.
10. The tests in Zeeland will be performed with salt water. The simulator consists of three metals, steel, aluminium and copper. In order to avoid erosion due to salt water zinc anodes have to be mounted.
11. During the calibration it appeared that the hydraulic cylinders loosened a little. This could be concluded from some observed leakage between the two valves (the pressure was not high enough anymore to close the valves completely). Now the whole horizontal box has to be dismantled to check and fix the system. This can be avoided to construct two dismantlable panels in order to check and fix the cylinders.
12. With wave overtopping the guiding plates, which create the “flume” are placed beside each other. With wave overtopping the flow goes only one direction, but with run-up the flow also runs down. This run-down meets the front side of the plates and gives irregularities in the run-down pattern. It is better to place the heads of the plates against each other and fix them with thin steel plates. These plates have to be manufactured.
13. The simulator modules have been painted ones. When above modifications have been made, the simulator should be painted in the yellow colour of the Rijkswaterstaat.

All these improvements were performed before the actual tests in Zeeland near the Zeelandbrug started.

2.2 Hydraulic measurements near the Zeelandbrug

2.2.1 Calibration for steering files

This section will describe the calibrations that were performed to enable the production of steering files. The wave run-up simulator generates the up-rushing waves by releasing a certain amount of water given by the filling level of the simulator. The calibration determines the relationship between the filling level and the wave run-up level on a certain geometry of the dike. These wave run-up levels are determined visually and are often given in m up-rush along the slope, starting from the outlet of the simulator. Section 2.1.3 and Figure 2.4 gave the calibration for a straight 1:2.7 slope at the Vossemeerdijk.

Figure 2.11 is similar to Figure 2.4, but now a fit has been shown:

$$Ru_{\text{along slope}} = 4.2 h_v^{0.6} \quad (2.1)$$

where h_v is the filling level in m.

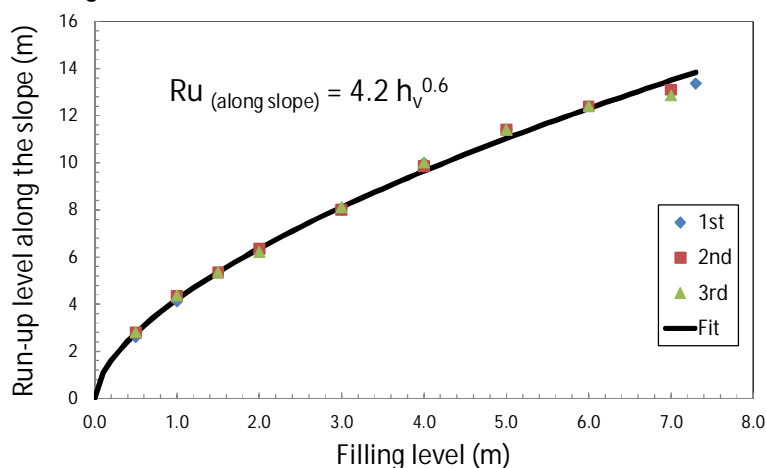


Figure 2.11. Calibration of wave run-up on a 1:2.7 slope (Vossemeerdijk) with fit

The geometries of the dike tested near the Zeelandbrug were significantly different from a straight 1:2.7 slope as for the Vossemeerdijk. Figure 2.12 shows the geometry of the Vossemeerdijk and two geometries at the Zeelandbrug. The geometries at the Zeelandbrug both have a long nearly horizontal berm before the upper slope starts. At one situation the run-up simulator was placed 0.4 m (vertically) below the start of the berm (section 1) and at the other situation the simulator was placed on the berm and 3 m before the start of the upper slope. This location is given with a light brown square in Figure 2.12.

The (long) berm has influence on the run-up. Figure 2.13 shows the wave run-up measured along the slope. Due to the long flat berm the distance of the run-up along the slope is much larger than for a straight 1:2.7 slope. But run-up is defined as a vertical distance from a certain level and not along a slope or geometry. Figure 2.14 shows this wave run-up for the Vossemeerdijk and section 1.

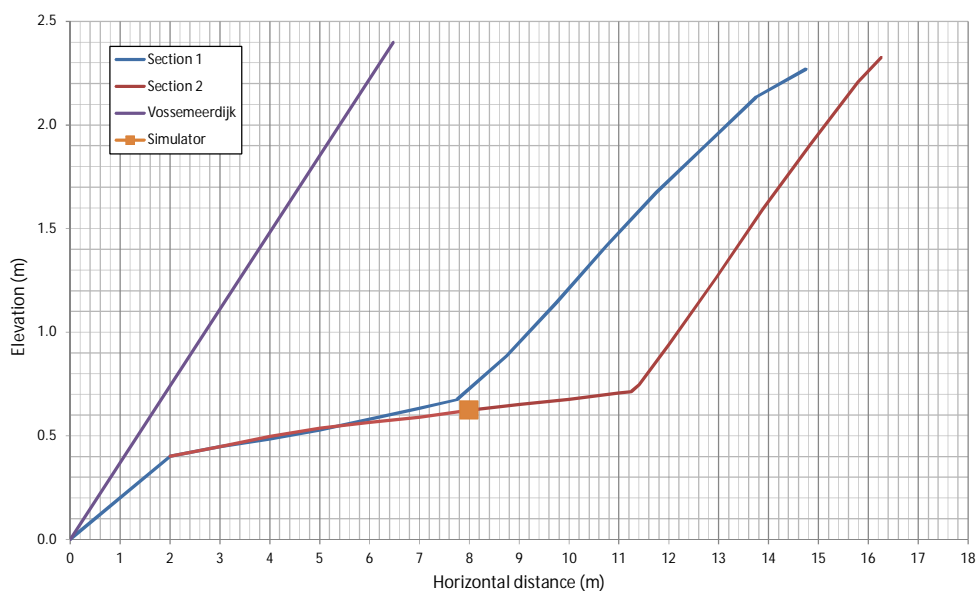


Figure 2.12. Geometries of the Vossemeerdijk and two sections near the Zeelandbrug

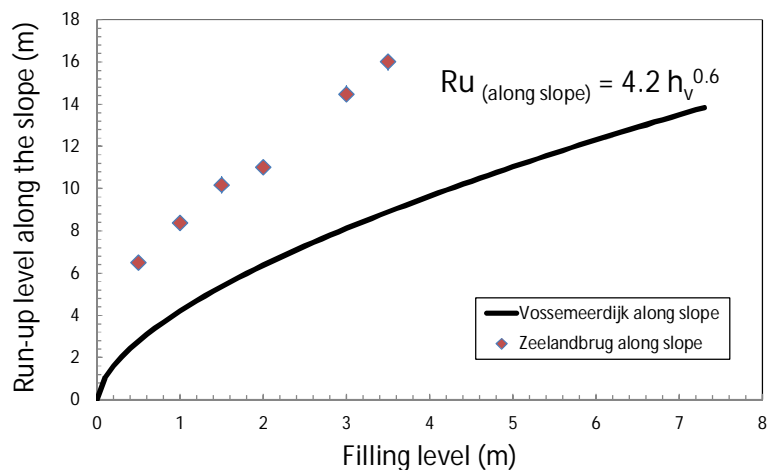


Figure 2.13. Measured run-up along the slope as function of filling level for the Vossemeerdijk and section 1 at the Zeelandbrug

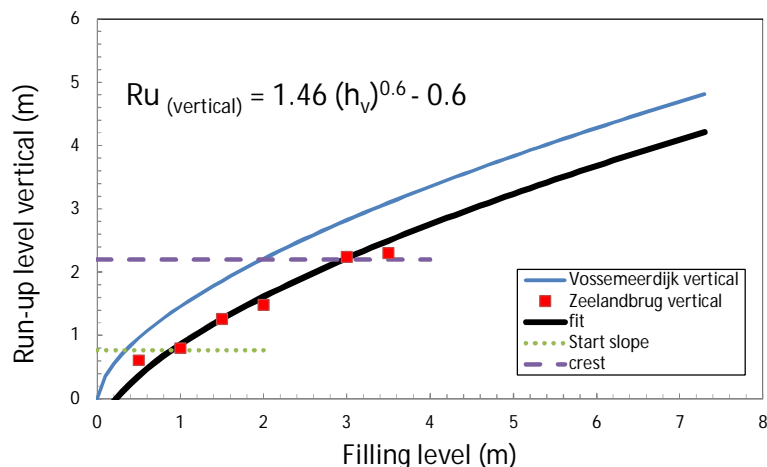


Figure 2.14. Calibration run-up and filling level for section 1, measured vertically

Due to energy dissipation over the long berm the wave run-up at section 1 is lower than at the Vossemeerdijk. Figure 2.14 shows two horizontal lines indicating the start of the upper slope and the crest of the dike. Wave run-up could not be measured higher than the crest of the dike, about 2.2 m above the outlet of the simulator. A filling level of 4 m and more will give overtopping. Still the required “run-up” from the calculated run-up distribution has to be simulated in a correct way. The only way to achieve this is to combine the calibration results at the Vossemeerdijk (over the full range of filling levels) with the measurements for section 1.

Equation 2.1 can be re-written to vertical run-up and is given in Figure 2.14 with the blue line. It is valid for the full range of filling levels between 0.5 m and 7.3 m.

$$Ru_{\text{vertical}} = 1.46 h_v^{0.6} \quad (2.2)$$

The dissipation of energy over the berm takes place below the lowest horizontal line in Figure 2.14. Above that line the upper slope starts, which is not so far from a 1:2.7 slope as at the Vossemeerdike. The calibration points at the upper slope follow the same trend as for the Vossemeerdike, but the trend is lower due to energy dissipation before reaching the upper slope. A correct way to come to a good calibration curve is to lower the curve given by equation 2.2. A good fit is given by:

$$Ru_{\text{vertical}} = 1.46 h_v^{0.6} - 0.6 \quad (2.3)$$

This is the calibration that has been used to produce the steering files for test 1 at section 1.

At test 2 the simulator was placed on the berm 3 m before the start of the upper slope. In this situation the energy dissipation will be much smaller than for section 1. It was assumed that the calibration curve could be described by equation 2.4, which would be quite close to equation 2.2. This equation was used to produce steering files for section 2.

$$Ru_{\text{vertical}} = 1.46 h_v^{0.6} - 0.1 \quad (2.4)$$

2.2.2 Set-up for the hydraulic measurements

The section where hydraulic measurements were performed was quite similar to section 1 and is given in Figure 2.15. The geometry was measured in two ways: by measuring the inclination of the slope over every 1 m and by measuring individual points directly. Both ways gave similar results in Figure 2.15.

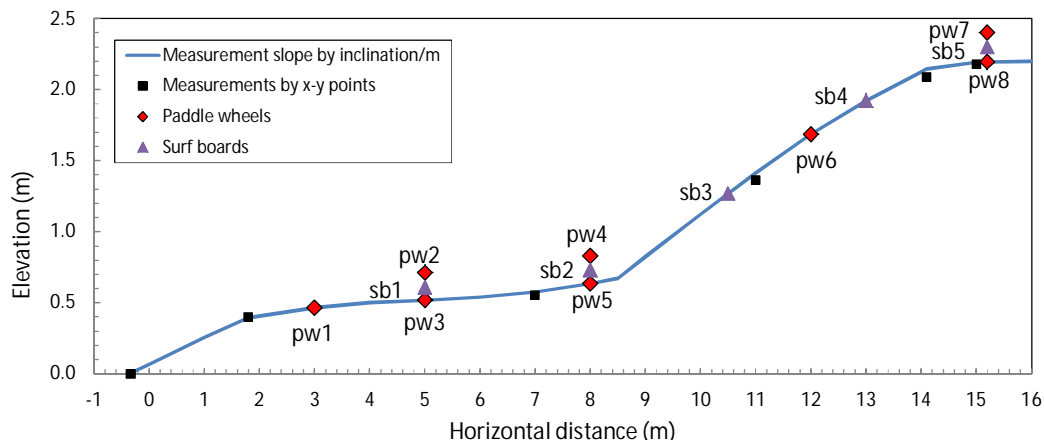


Figure 2.15. Geometry of the dike for hydraulic measurements and locations of instruments

Figure 2.15 also shows the locations of the instruments. In total eight paddle wheels (velocity meters) were used and five surf boards (flow thickness). Three of the surfboards had a paddle wheel, which measures the velocity on top of the up-rushing layer. The other five paddle wheels were mounted in the concrete or grass in such a way that the velocity was measured 3 cm above the soil level (to avoid boundary layer effects). At three locations the velocity was measured at the soil level and on top of the layer (in the surf board). The exact measurements of the geometry and locations of instruments is given in Table 2.4.

The hydraulic measurements were performed by releasing pre-defined filling levels and each level was repeated three times. Filling levels of 0.5 m; 1 m; 1.5 m; 2 m; 3 m; 4 m; 5 m; 6 m; 7 m; and 7.3 m were released. The performance and recording was done by two separate records, one for filling levels from 0.5 m to 4 m and one for 5 m and higher. An overall view of the recorded measurements is given in Figure 2.16, first for the velocities and then for the flow thicknesses.

One detailed measurement is given in Figure 2.17 for flow velocities and Figure 2.18 for flow thicknesses, both for a filling level of 5 m. In this example the wave run-up reaches the first paddle wheel after 24.5 s and the run-up finishes about between 27 and 28 s. After that the run-down starts of the water that had not flowed over the crest. The records after 28 s show the run-down velocities (but not measured correctly as the paddle wheels measure then in the wrong direction). This run-down also causes forces on the surfboard, which eventually could break this instrument. Therefore, after the run-up was finished the surfboards were lifted manually to avoid damage. In Figure 2.16 this lifting can be observed, but in Figure 2.18 the record was terminated just before the lifting. Records like Figures 2.17 and 2.18 are shown in Appendix E for all other records.

x (m)	y (m)
-0.4	0.000
0.0	0.069
1.0	0.256
1.8	0.395
2.0	0.407
3.0	0.465
4.0	0.503
5.0	0.517
6.0	0.540
7.0	0.577
8.0	0.634
8.5	0.672
9.0	0.825
10.0	1.123
11.0	1.415
12.0	1.685
13.0	1.923
14.0	2.126
14.1	2.147
15.0	2.194
16.0	2.201

Geometry by inclination

x (m)	y (m)
-0.33	0.000
1.80	0.400
7.00	0.553
11.00	1.363
14.10	2.089
15.00	2.179

Geometry by points

	x (m)	y (m)
pw1	3.0	0.465
pw2-sb1	5.0	0.710
pw3	5.0	0.517
pw4-sb2	8.0	0.830
pw5	8.0	0.634
pw6	12.0	1.685
pw7-sb5	15.2	2.400
pw8	15.2	2.195
sb1	5.0	0.610
sb2	8.0	0.730
sb3	10.5	1.269
sb4	13.0	1.923
sb5	15.2	2.300

Locations of instruments

Table 2.4. Data for geometry and locations of instruments

Records like in Figures 2.7 and 2.18 were analysed to find the maximum values of each record. These maximum values of flow velocity and flow thickness during run-up were summarized in Table 2.5. This table shows that low filling levels only reached the lowest instruments and that for a filling level of 4 m and higher all instruments were reached (also overtopping occurred then). These are the open cells at the right upper part of the table.

There are also open cells for paddle wheels 1 and 6 for filling levels of 5 m or 6 m and higher. Possibly these instruments were blocked by some dirt or grass which made them to fail to give a good record. Also paddle wheel 4 shows strange values. Until the second release of a filling level of 5 m the velocity increases gradually. But by and after the third release of this level, the velocity dropped to a more or less constant value of around 4 m/s, where about 6 m/s was expected. Probably also here the instrument was blocked to some extent and these measurements should not be considered as reliable.

The flow thickness records of surfboards 1 and 4 show some offset or bias for filling levels of 4 m or 5 m and larger. The value of the bias (the value just before a wave reached the surfboard), was distracted from the maximum value, to obtain the true maximum in Table 2.5.

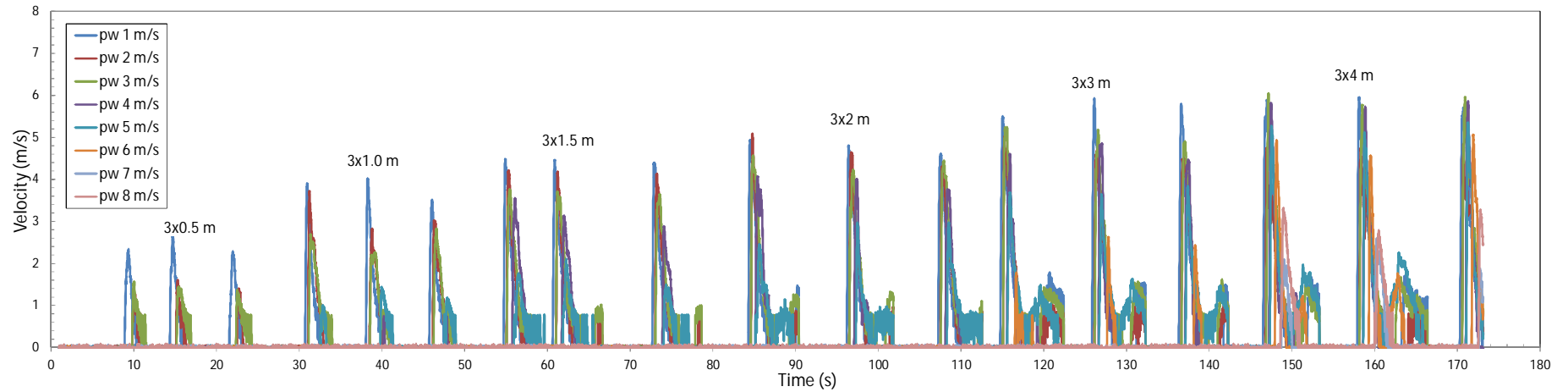


Figure 2.16a. Measured record of flow velocities for filling levels from 0.5 m to 4 m.

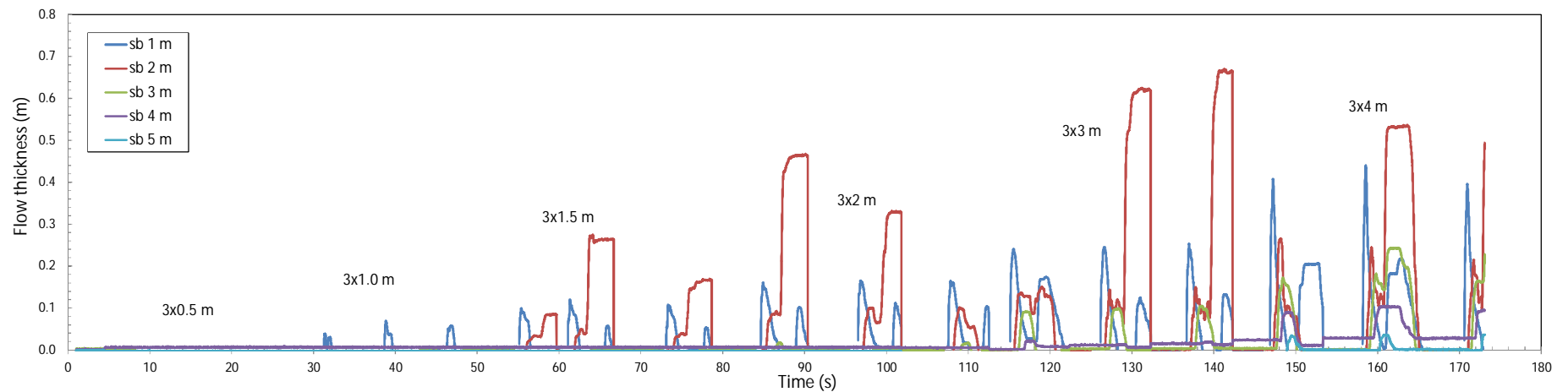


Figure 2.16b. Measured record of flow thicknesses for filling levels from 0.5 m to 4 m

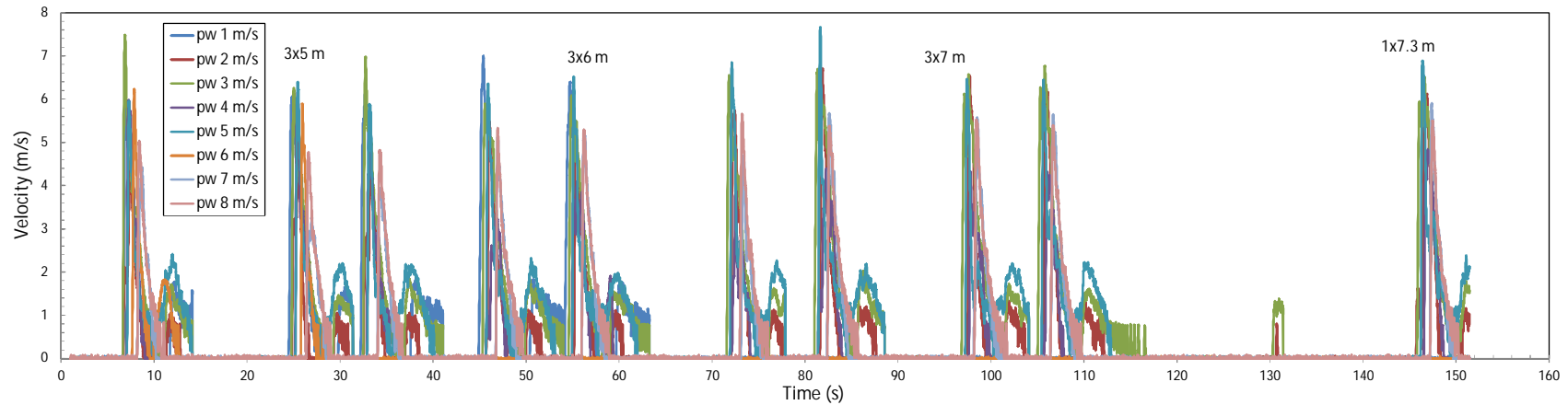


Figure 2.16c. Measured record of flow velocities for filling levels from 5 m to 7.3 m

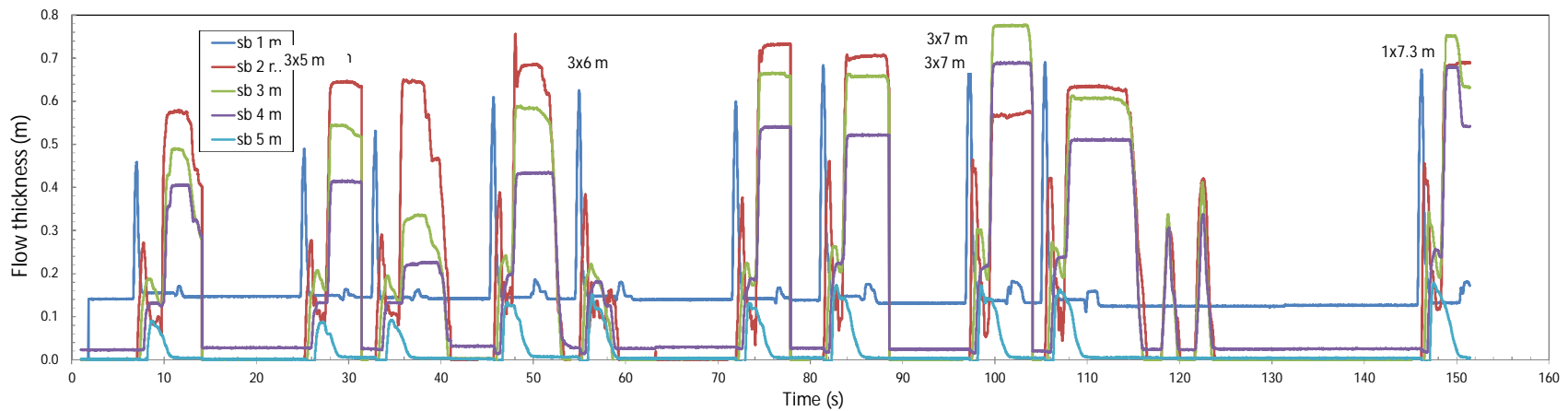


Figure 2.16d. Measured record of flow thicknesses for filling levels from 5 m to 7.3 m

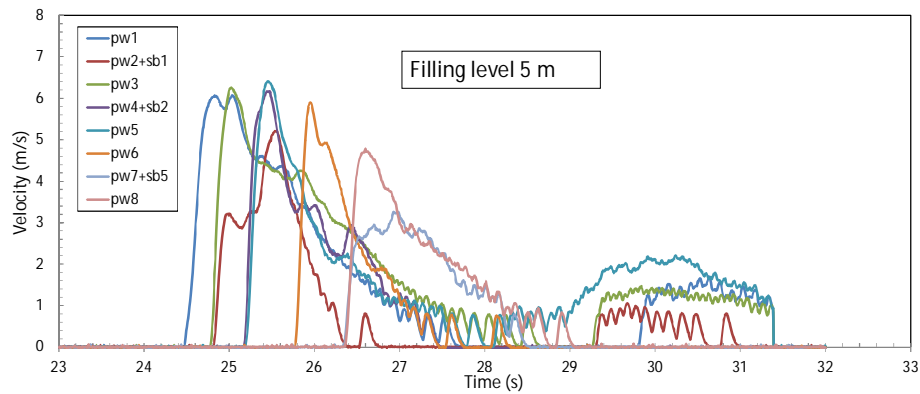


Figure 2.17. Records of flow velocities for a filling level of 5 m

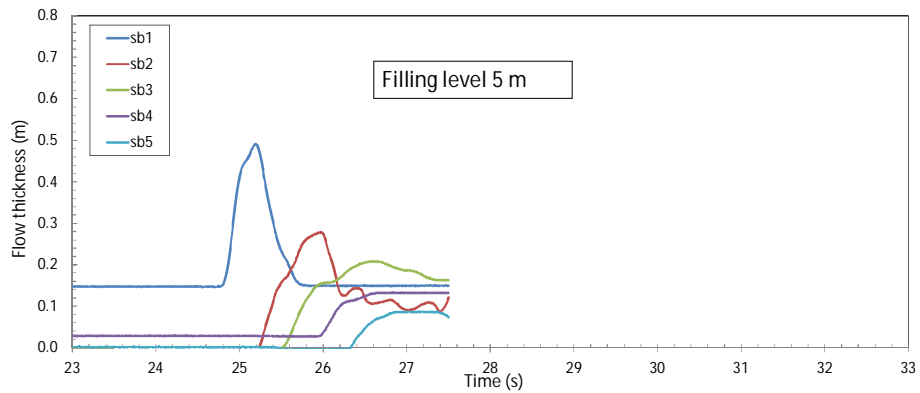


Figure 2.18. Records of flow thickness during run-up only, for a filling level of 5 m

Time s	Fill level m	Pw1 m/s	Pw2 m/s	Pw3 m/s	Pw4 m/s	Pw5 m/s	Pw6 m/s	Pw7 m/s	Pw8 m/s	Sb1 m	Sb2 m	Sb3 m	Sb4 m	Sb5 m
8.3	0.5	2.34	1.28	1.57										
13.5	0.5	2.71	1.61	1.45										
21.4	0.5	2.29	1.41	1.37										
30.0	1.0	3.91	3.73	2.70		1.00				0.039				
37.5	1.0	4.03	2.83	2.27	0.75	1.44				0.070				
45.4	1.0	3.52	3.03	2.83	0.75	1.17				0.058				
54.5	1.5	4.50	4.21	3.76	3.56	1.76				0.099	0.035			
60.0	1.5	4.46	4.19	3.71	3.14	2.11				0.120	0.050			
73.1	1.5	3.99	4.13	3.65	2.89	1.51				0.108	0.040			
84.0	2.0	4.94	5.10	4.57	4.07	2.46				0.162	0.093	0.018		
95.5	2.0	4.81	4.65	4.23	4.01	2.97				0.166	0.101	0.002		
107.1	2.0	4.62	4.42	4.45	3.76	2.97				0.165	0.102	0.016		
114.0	3.0	5.51	5.02	5.24	4.61	3.69	1.78			0.242	0.151	0.093		
125.0	3.0	5.93	4.73	5.18	4.86	3.65	2.63			0.247	0.145	0.100		
136.0	3.0	5.81	4.50	4.91	4.48	3.84	2.44			0.254	0.150	0.105		
146.1	4.0	5.90	4.76	6.05	5.82	5.27	4.94	2.10	3.33	0.408	0.266	0.172	0.062	0.035
157.0	4.0	5.96	4.75	5.78	5.73	5.12	4.57	2.60	2.80	0.441	0.245	0.208	0.075	0.036
170.0	4.0	5.71	4.84	5.96	5.86	5.36	5.07	1.88	3.28	0.396	0.215	0.165	0.014	0.037
6.0	5.0	6.18	4.56	7.49	5.98	5.97	6.24	4.43	5.04	0.318	0.272	0.188	0.111	0.091
23.5	5.0	6.07	5.21	6.26	6.17	6.41	5.90	3.26	4.78	0.312	0.278	0.208	0.105	0.087
32.1	5.0	6.49	4.74	6.98	4.78	5.89		3.95	4.82	0.385	0.291	0.195	0.110	0.093
44.0	6.0	7.00	5.49	5.90	3.23	6.36		5.07	5.23	0.468	0.389	0.245	0.170	0.133
54.0	6.0	6.41	5.20	6.08	4.10	6.53		5.16	5.30	0.484	0.384	0.223	0.155	0.153
71.1	6.0		5.73	6.55	3.93	6.86		4.69	5.66	0.460	0.377	0.225	0.162	0.132
79.8	7.0		6.71	6.70	4.40	7.67		5.68	5.38	0.544	0.462	0.264	0.196	0.174
96.5	7.0		6.55	6.58	4.33	6.47		5.58	5.53	0.577	0.464	0.304	0.211	0.173
105.0	7.0		6.17	6.77	4.32	6.45		5.65	5.39	0.555	0.423	0.274	0.216	0.163
145.1	7.3		6.13	6.51	4.84	6.89		5.91	5.50	0.547	0.456	0.343	0.233	0.179

Table 2.5. Maximum flow velocities and flow thicknesses

2.2.3 Analysis of measurements

The maximum velocities from Table 2.5 are given together in Figure 2.19 and the maximum flow thicknesses in Figure 2.20. The curve in Figure 2.19 was found for the Vossemeerdijk, see Figure 2.7. This was at 1.4 m after the outlet of the simulator on a slope of 1:2.7. Paddle wheel 1 was situated about 3 m from the outlet, but on the berm and about at the same vertical level as the paddle wheel at the Vossemeerdijk. Due to the longer horizontal distance from the outlet for paddle wheel 1, the results were expected to be similar or slightly lower than for the Vossemeerdijk. Up to a filling level of 3 m this is indeed the case, but for higher filling levels the velocity is a little lower and then the instrument did not function properly anymore. This is certainly the case for the two paddle wheels 7 and 8 at the crest. A further analysis will be made later.

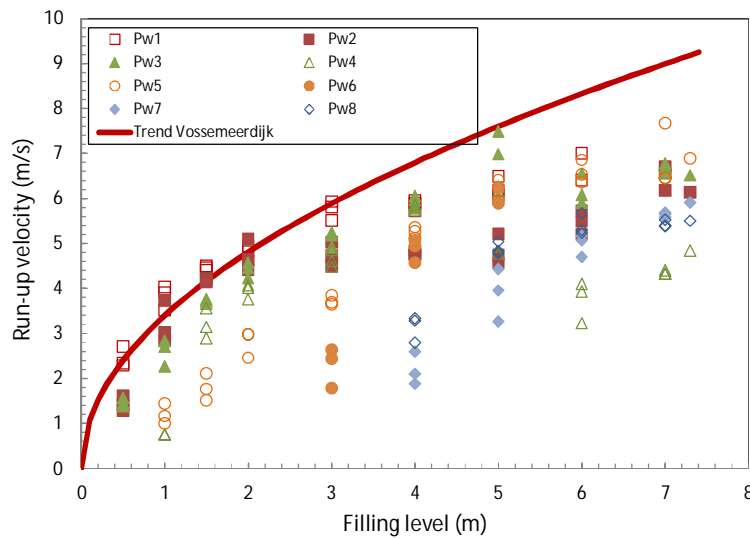


Figure 2.19. Maximum run-up velocities along the dike section

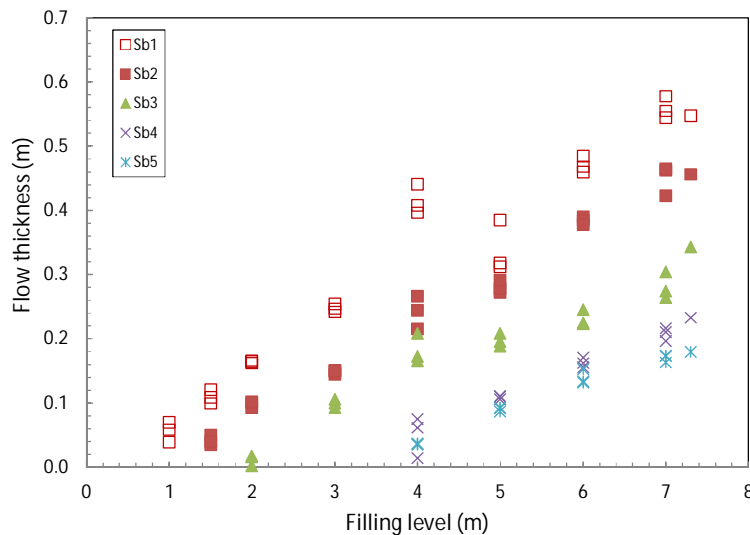


Figure 2.20. Maximum flow thicknesses along the dike section

Figure 2.20 shows a very clear trend that flow thickness increases almost linearly with the filling level and that the maximum thickness reduces with the distance from the simulator.

As a possible decrease of the maximum flow velocities in Figure 2.19 is not easy to observe, the data have been organized differently. Figure 2.21 shows the average of the three measurements for similar filling level and then along the slope. For this graph the paddle wheels mounted on the surface were taken, paddle wheels 1, 3, 5, 6 and 8. These instruments all measure at the same level of 3 cm above the soil. Figure 2.21 shows clearly that the maximum velocity in a record decreases with the distance along the slope. This is similar to the observations at the Vossemeerdijk (Section 2.1).

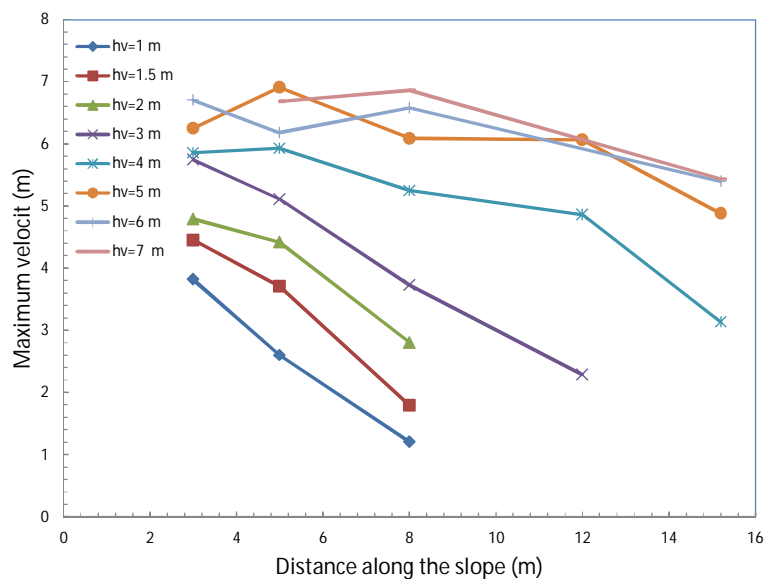


Figure 2.21 Maximum flow velocities as a function of the distance from the simulator. Data points give the average of three measurements for the same filling level

De calibration at the Vossemeerdijk showed that the *maximum* velocities decreased with distance from the simulator, which was validated by the present measurements, but that the *front* velocities remained more or less constant over quite a long distance. This was also investigated for the present tests. Paddle wheels 1, 3, 5, 6 and 8 measured velocities near the surface and 3 cm above it. The time difference between the water reaching two consecutive paddle wheels, combined with the distance between the two instruments, gives the front velocity. All front velocities have been gathered in Table 2.6.

Figure 2.22 shows the front velocities as function of the filling level. Certainly between fillings levels of 3 m to 6 m a lot of data are at the same level. A further analysis is given in Figure 2.23, where the front velocities are given along the slope. For filling levels of 4 m and 5 m it is clear that the front velocity is almost constant over about 9 m. This distance is less for lower filling levels. It is a pity that paddle wheels broke for higher filling levels. But the overall conclusion is that maximum velocities decrease, where front velocities remain constant over quite some distance along the slope. Maximum velocities and flow thickness were measured at some time in a triangular shaped record. It could be that the energy was spent in keeping the front velocity constant: the large velocity and large flow thickness “pushes” the water up

the slope. This is similar to what was found for real up-rushing waves, see Van der Meer, 2011.

Filling level (m)	Front velocity between paddle wheels			
	v1-v3	v3-v5	v5-v6	v6-v8
7.3		7.56		
7.0		7.16		
7.0		7.69		
7.0		7.43		
6.0		8.65		
6.0		7.83		
6.0		7.69		
5.0	7.30	7.04		
5.0	6.60	7.28	6.84	5.60
5.1	7.30			
5.1	6.60			
5.0		6.49	7.59	5.60
4.0	7.30	6.20	6.02	3.99
4.0	7.49	6.40	6.09	4.61
4.0	5.42	6.59	6.68	4.71
3.0	6.02	6.29	4.04	
3.0	5.88	5.86	4.10	
3.0	5.90	5.85	4.33	
3.1	6.02			
3.1	5.88			
3.1	5.90			
2.0	6.60	4.03		
2.0	6.76	3.71		
2.0	6.76	5.32		
1.5	5.43	2.99		
1.5	5.13	3.58		
1.5	5.76	3.32		
1.0	3.80			
1.0	4.19			
1.0	4.61			
0.5	2.20			
0.5	2.43			
0.5	2.52			

Table 2.7. Calculated front velocities between paddle wheels

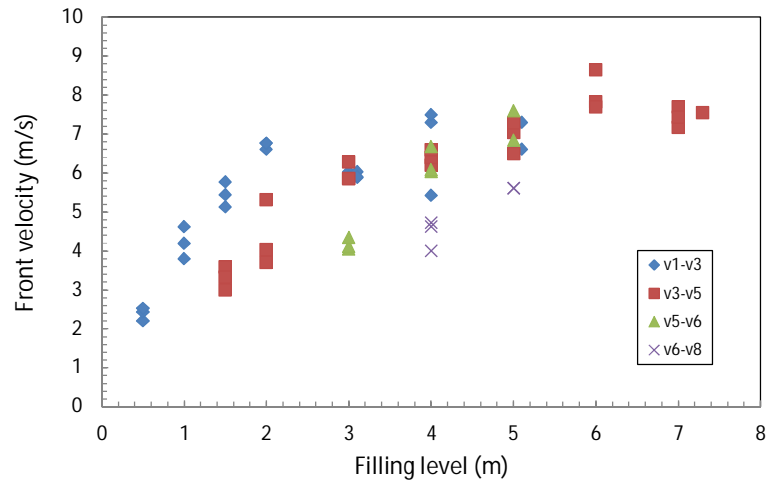


Figure 2.22. Front velocities as a function of the filling level

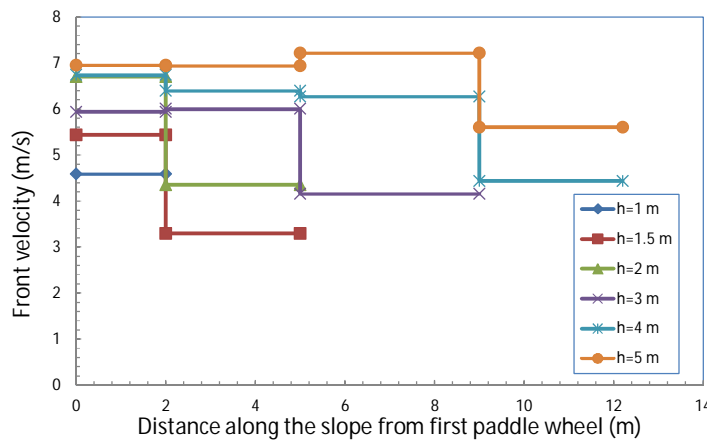


Figure 2.23. Front velocities as a function of the distance along the slope

2.2.4 Wave overtopping by wave run-up simulation

In section 2 the up-rushing waves were able to pass over the crest and generate wave overtopping at the landward side of the dike. It is interesting to compare the generated overtopping discharge with the damage observed. This overtopping discharge has to be calculated from the measurements of flow velocity and thickness at the crest. These are surfboard 5 for the flow thickness and paddle wheel 8 for the flow velocities. For filling levels of 4 m and higher overtopping occurred. Figures 2.24 – 2.28 give the records of surfboard 5 as well as paddle wheel 8.

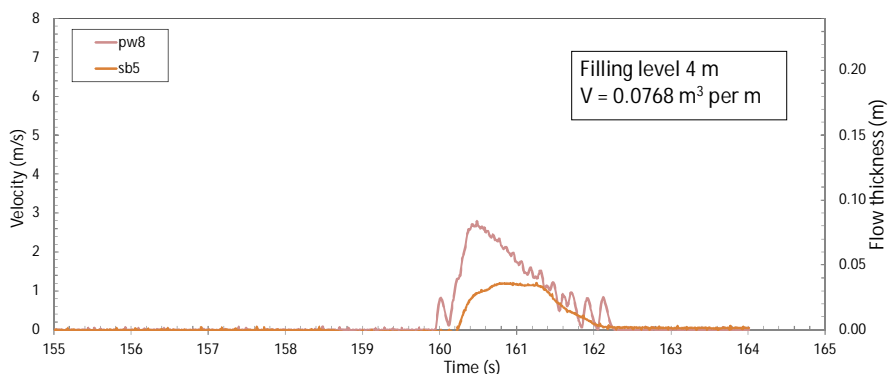


Figure 2.24. Flow velocity and thickness at the crest for a filling level of 4 m

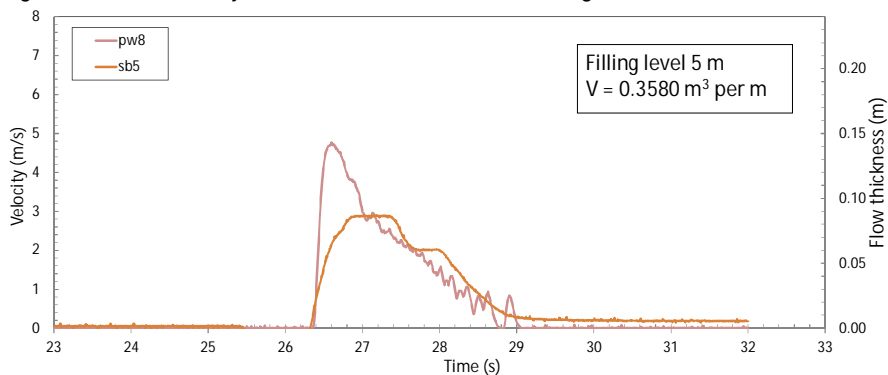


Figure 2.25. Flow velocity and thickness at the crest for a filling level of 5 m

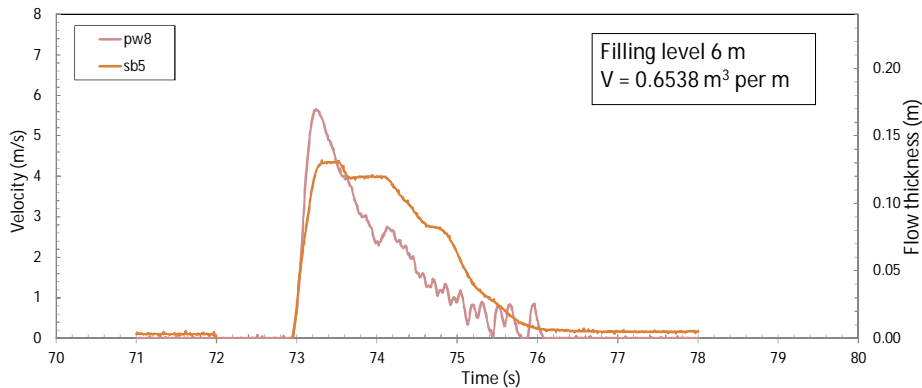


Figure 2.26. Flow velocity and thickness at the crest for a filling level of 6 m

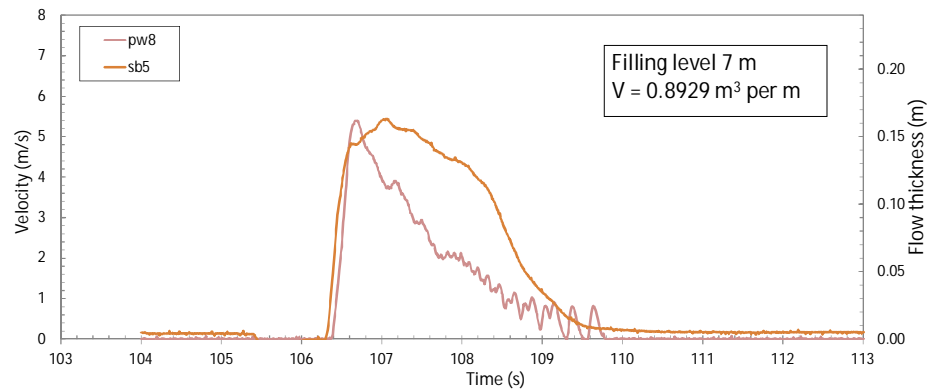


Figure 2.27. Flow velocity and thickness at the crest for a filling level of 7 m

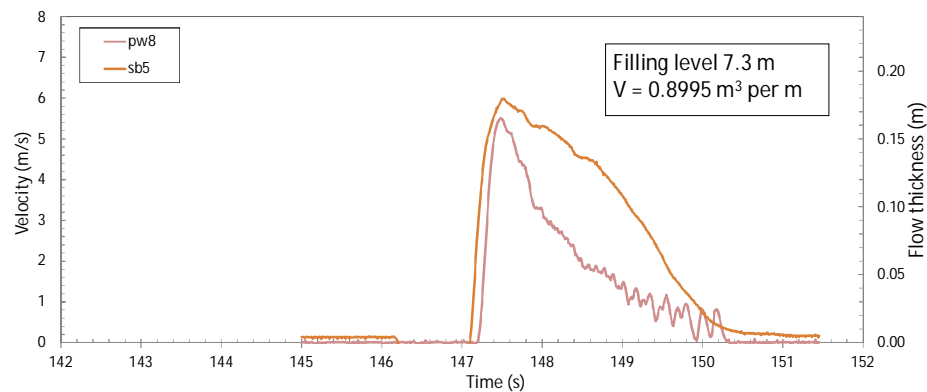


Figure 2.28. Flow velocity and thickness at the crest for a filling level of 7.3 m

The two instruments give records that start and finish more or less at the same time. By multiplying the two records and integrating over the flow duration the volume of the overtopping wave can be calculated. These overtopping wave volumes are given in the graphs and range from 0.08 m^3 per m to 0.9 m^3 per m.

These volumes are for a fixed filling level of the simulator. A real test consisted of a distribution of run-up levels that had to be simulated and this was achieved by the correct filling level for each run-up level. In order to calculate the overtopping discharge during a test a relationship between overtopping wave volume and filling level and/or run-up level has to be established. Figure 2.29 shows the relationship between filling level and overtopping wave volume for section 1 (similar to the section of the hydraulic measurements). By means of equations 2.3 and 2.4 there is a direct relationship between the run-up level calculated (above the crest!) and the overtopping wave volume.

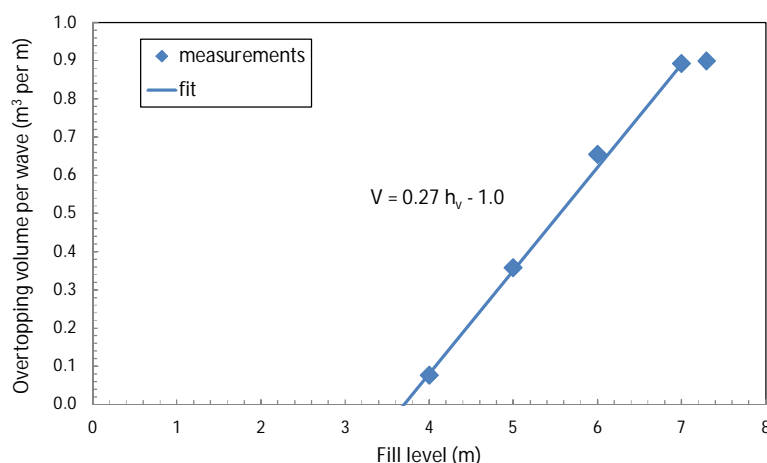


Figure 2.29. Relationship between filling level and overtopping wave volume for section 1

The relationship in Figure 2.29 can be given by:

$$V = 0.27 h_v - 1.0 \quad (2.5)$$

By substitution of h_v from Equation 2.5 in equation 2.3 or 2.4 gives the direct relationship between the calculated run-up level (above the crest) and the overtopping wave volume that will be generated by such a wave, for section 1 and section 2 respectively.

As wave overtopping was generated during the tests at section 2, equations 2.5 and 2.4 were used. This relationship was used to calculate the overtopping wave volume for each calculated run-up level that passed the crest of the dike. Then the total overtopping volumes were added and divided by the simulated storm duration (6 hours for each test). This procedure resulted in wave overtopping discharges for each test performed at section 2. Table 2.8 shows the results. The overtopping discharge amounted to only 0.06 l/s per m for a test condition with the water level 2 m below the front of the berm and went up to 6.25 l/s per m for a condition with the water level equal to the front of the berm. In all conditions the significant wave height was assumed to be 2 m with a wave steepness of 0.04 (using the peak period).

	Overtopping discharge l/s per m
x=0 m	6.25
x=1 m	0.84
x=2 m	0.06
x=3 m	0.00

Table 2.8. Overtopping discharges calculated for the tests at section 2

3 Extension and modification of the database

3.1 Overall view of modifications and extensions

In de Handreiking (RWS, 2012) knowledge on grass erosion by wave run-up and overtopping has been gathered to be used for safety assessments in the Netherlands. In Appendix B en C of that report an extensive summary has been given on characteristic values of all the test locations and damage observations (Appendix B) and a summary of photos of damages at each test location. This Appendix B is called “Samenvatting kengetallen en resultaten golfoverslagproeven”. After an introduction on all the wave overtopping research performed, the Appendix gives a large Excel spreadsheet with the data. These two Appendices have often been called “the Database”.

There are two good reasons to modify and extend this Database:

1. The Database is not up to date anymore as further tests have been performed at Nijmegen and Millingen (river dikes along the Rhine) and Noord-Beveland (wave run-up tests). Furthermore the tests at Tholen in 2012 have been evaluated. The database (spreadsheet and appendix with photos) should be extended.
2. Recent developments on the cumulative overload method have shown that the velocity of overtopping wave volumes should be considered at the location of the damage and not at the crest of the dike. The velocity accelerates at the landward side of dikes due to the steep slope. In the original spreadsheet of the database (RWS, 2012, Appendix B) the cumulative overload for various critical velocities has been calculated by using the velocities of overtopping wave volumes at the crest. All calculations have to be repeated, but now with the velocity at the location of damage.

The first modification, extension of the Database by more recent tests, has been a cooperation between Infram, Van der Meer Consulting, Deltares and Alterra. Infram and Van der Meer Consulting have extended the appendix with photos of damages and have extended the spreadsheet with most recent observations of damages. Deltares has extended the spreadsheet with geotechnical data of recent tests and Alterra did similar work on characteristics of the grass cover and its management at the test locations. The modification under point 2 will be described in more detail in the next section.

The work has resulted in a standalone document (still in Dutch): Samenvatting kengetallen en resultaten golfoverslag- en golfplooppoeven. The document has 137 photos of damages observed or situations after testing when no damages had occurred.

3.2 Recalculation of the cumulative overload for all observed conditions

As described in the previous section, the cumulative overload in the spreadsheet of the database has to be recalculated, but now with the velocity of the overtopping wave at the location of damage, instead of the velocity at the crest of the dike.

Infram has determined the location of damage from Factual Reports of the testing and from photos. The spreadsheet has been extended with a column that gives the distance from crest to the location of damage. Table 3.1 gives a small section of the spreadsheet of the database. After the column with the slope angle of the landward slope (Taludhelling $\cot\alpha$) a column is present with the location of the damage (Locatie schade (m vanaf kruinlijn)).

Proefstrook	Sectie	Observatie	Foto	Belasting (l/s per m)	Taludhelling cotα	Locatieschade (m vanaf kruinlijn)	Versnelingsfactor	Cumulatieve overbelasting $\Sigma (U^2 - U_c^2)$ m ² /s ²				
								3	4	5	6.5	8
Delfzijl	Kale klei	Start head cut erosie mechanisme	B2	na 0,1; 1; 5; 3 uur 10	2.8	7	1.36	5635	2827	958	3	0
Delfzijl	Kale klei	5-10 cm oppervlakte erosie	B4	na 0,1; 1; 5; 10	2.8	7	1.36	8357	4289	1535	5	0
Delfzijl	Gras of gras + geotextiel	Geen schade	B6	na 0,1; 1; 10; 20; 30; 50	2.8	15	1.44	76822	51590	26981	8091	2133
Delfzijl	Gras of gras + geotextiel	Na initieele schade aangebracht	B8	na 50	2.8	7	1.36	29205	20007	10497	3274	686
Boonweg	Sectie 1 talud	Geen schade	B9	na 0,1; 1; 10; 30; 50; 75	2.9	24	1.46	116682	83197	49606	18981	7595
Boonweg	Sectie 2 talud	Geen schade	B10	na 0,1; 1; 10; 30; 50; 75	2.9	24	1.46	116682	83197	49606	18981	7595
Boonweg	Sectie 3 talud	Begin van schade (opbolmechanisme)	B11	na 0,1; 1; 10; 30; 50; 1 uur 75	2.9	21	1.46	74110	50326	29168	10167	3243
Boonweg	Sectie 3 talud	Vrijwel bezweken na opbolmechanisme	B11	na 0,1; 1; 10; 30; 50; 75	2.9	21	1.46	116682	83197	49606	18981	7595
Boonweg	Sectie 4 talud	Begin van schade (opbolmechanisme)	B12	na 0,1; 1; 10; 30; 50; 5 uur 75	2.9	13.5	1.42	100023	68950	39819	14155	5010
Boonweg	Sectie 4 talud	Bezweken na opbolmechanisme	B17	na 0,1; 1; 10; 30; 50; 5:45 uur 75	2.9	13.5	1.42	105963	73435	42532	15261	5504

Table 3.1. Part of the spreadsheet of the database with added column and recalculated cumulative overloads

The acceleration of the velocity of overtopping wave volumes over the landward slope has been predicted, measured and validated in Deltares (2012). The method described in Schüttrumpf and Oumeraci (2005) has been used to calculate the velocity over the slope. In Deltares (2012) a friction coefficient $f = 0.01$ has been validated for grass slopes, which has to be used in the referenced method.

The acceleration of the velocities of overtopping wave volumes depend on the initial velocity at the crest and the slope of the landward side of the dike. In fact the acceleration will be different for each overtopping wave. It is very time consuming (as the method of Schüttrumpf and Oumeraci (2005) is an iterative method) to calculate exactly the acceleration for each overtopping wave. Therefore, a more simplified method has been chosen.

It is mainly the largest overtopping waves, with the largest velocities, that contribute to the cumulative overload. Small overtopping waves will not reach the critical velocity U_c . For this reason initial velocities U_0 at the crest have been chosen of 4 m/s and 6 m/s, which are at the higher end of simulated velocities. These velocities were used to calculate the acceleration over the landward slope for various slope angles. Figure 3.1 gives the result of the calculations.

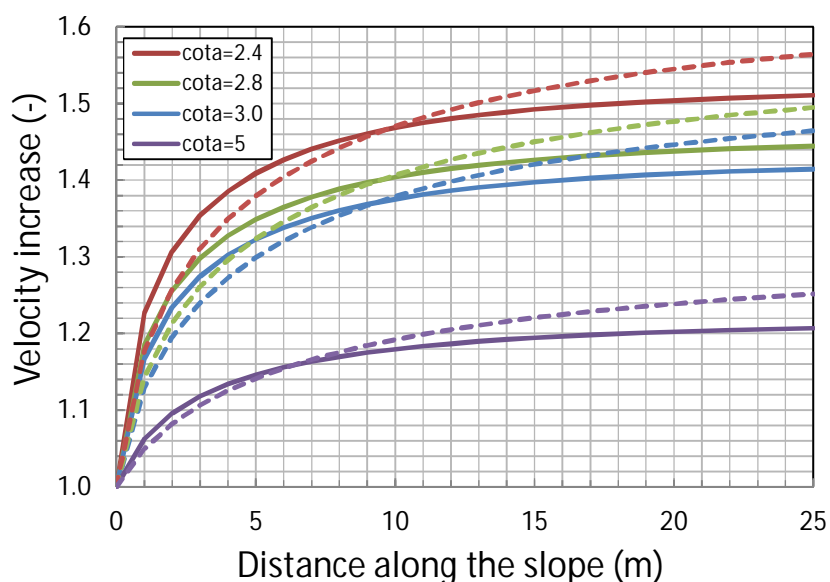


Figure 3.1. Velocity increase over overtopping wave volumes over the landward slope. Solid line: $U_0 = 4$ m/s, dashed line: $U_0 = 6$ m/s

Slope angles of 1:2.4; 1:2.8; 1:3 and 1:5 have been chosen as most of the landward slopes had slope angles between 1:2.4 and 1:3 and the Vechtdijk had a slope of about 1:5. It is evident from the graph that velocities increase fast over the first 5 m and then increase slower. The graph also shows that a steeper landward slope results in a larger acceleration, for a 1:2.4 slope even up to a factor of 1.5 or more. The difference between the two initial velocities of $U_0 = 4$ and 6 m/s is relatively small, less significant than the effect of slope angle or distance. It is for this reason that a fixed acceleration factor was chosen for all velocities in a distribution of overtopping wave volumes, depending on slope angle and location of the damage.

For example, the Boonweg (Table 3.1) had a landward slope of 1:2.9 and damage at 24 m from the crest. Based on Figure 3.1 an acceleration factor of 1.46 was chosen. All chosen acceleration factors, one for each observation in the spreadsheet, are given as an extra column in the spreadsheet, see Table 3.1.

The acceleration factors were used to recalculate the cumulative overload for each observation. The cumulative overload is given by:

$$D = \sum_{i=1}^N (\alpha_1 U_i^2 - \alpha_2 U_c^2) \quad \text{for } \alpha_1 U_i > \alpha_2 U_c \quad [\text{m}^2/\text{s}^2] \quad (3.1)$$

with:

- D = cumulative overload [m^2/s^2]
- N = number of overtopping waves [-]
- i = number of the overtopping wave [-]
- U_i = a characteristic value of the velocity of the overtopping wave [m/s]
- U_c = critical velocity of the grass slope (=strength) [m/s]
- α_1 = influence factor on the velocity U_i by transitions or obstacles [-]
- α_2 = influence factor on the critical velocity U_c by transitions or obstacles [-]

The velocity U_i is the front velocity of the overtopping wave, at the location of the damage. The wave overtopping tests were performed by simulating a distribution of overtopping wave volumes, V . These distributions were the basis of the recalculation of the cumulative overload. From hydraulic measurements, with velocity meters on the slope, the following relationship was established between the overtopping wave volume and the velocity at the crest, U_0 :

$$U_0 = 4.5 V^{0.3} \quad [\text{m/s}] \quad (3.2)$$

This relationship had been used for calculating the cumulative overload in the spreadsheet of the Handreiking (RWS, 2012). But now the actual velocity should be used at the location of damage. This means that U_i in equation 3.1 was calculated by $a \cdot U_0$, where “a” is the acceleration factor. The resulting cumulative overloads per sub test were calculated first. Table 3.2 gives an example, based on the same example at the Boonweg described above, where an acceleration factor of $a = 1.46$ was determined. The tests were based on a significant wave height of 2 m and each sub-test had a duration of 6 hours. Overtopping discharges of 0.1; 1; 10; 30; 50 and 75 l/s per m were simulated (Table 3.2 gives also a discharge of 5 l/s per m, but this was not simulated at the Boonweg).

Critical velocities of 3; 4; 5; 6.5 and 8 m/s were chosen to give various cumulative overloads, depending on the critical velocities. Appendix F gives all tables like Table 3.2 for all hydraulic conditions and acceleration factors used to recalculate the cumulative overload.

Duration <i>hour</i>	Average overtopping discharge <i>l/s per m</i>	$\Sigma (U^2 - U_c^2)$ at $H_s = 2$ m; acceleration factor 1.46				
		$U_c=3$ m/s	$U_c=4$ m/s	$U_c=5$ m/s	$U_c=6.5$ m/s	$U_c=8$ m/s
6	0.1	75	40	14	0	0
6	1	710	342	133	7	0
6	5	3596	1902	779	117	2
6	10	7240	4145	1907	364	29
6	30	21987	14051	7938	2410	451
6	50	35583	25174	15088	5624	1893
6	75	51087	39446	24526	10576	5221

Table 3.2. Cumulative overload for various sub-tests, based on an acceleration factor of 1.46

The cumulative overload for a certain observation depends on when during the testing this observation occurred. For example, start of damage (bulge mechanism) at section 3 of the Boonweg (see Table 3.1) occurred after 6 hours of 0.1; 1; 10; 30; 50 l/s per m and 1 hour of 75 l/s per m. Taking $U_c = 8$ m/s the cumulative overload becomes (see last column of Table 3.2) $0 + 0 + 29 + 451 + 1893 + 5221/6 = 3243 \text{ m}^2/\text{s}^2$ and this is indeed the value that is found in the last column of Table 3.1.

The results of the new cumulative overloads will be analysed in the next Chapter.

4 Re-analysis on cumulative overload

4.1 Summary of original analysis on cumulative overload

The method of cumulative overload, see Equation 3.1 in the previous chapter, has been developed over the years. The critical velocity U_c plays an important role in this method as it describes the strength of the grass cover. The cumulative overload D may give thresholds as a function of the type of damage, like start of damage, several damages or open spots over the slope, and failure of the slope. These thresholds can only be established if the critical velocity of the grass cover is known. The tests at the Vechtdijk in 2010 gave insight in the critical velocity of the grass cover of that dike as well as insight in the thresholds D for various damage types.

This analysis of the Vechtdijk results has been described in the Fase 4D report (in Dutch) "SBW Golfoverslag en Sterkte Grasbekleding. Fase 4D Evaluatie Vechtdijk, 2010". As reference it will be called Fase 4D report (2010). A summary of this work has been given in Handreiking (2012), described in Chapter 3. The basis of the work was an extensive spreadsheet with characteristic values of each test and a document with photos of damages of each tested section. They are given as Appendix B and C in Handreiking (2012). Chapter 3 describes the update (extension) of the document with photos, including the tests up to 2014.

The cumulative overload in the original analysis was based on the velocity of the overtopping wave volume at the crest of the dike. It did not yet recognise that the velocity of overtopping waves may increase significantly down the slope. This was partly due to the fact that at the Vechtdijk only a few velocity meters were present and that the slope at the Vechtdijk was quite gentle, 1:5, which means that the velocity increase over the slope was limited.

The Vechtdijk is the only location with varying hydraulic conditions, allowing for the results to be compared. Tests were performed with assumed wave heights of 1 m (river regime), 2 m (sea regime) and 3 m (severe sea regime). The original analysis, using velocities at the crest of the dike, came to the following conclusions:

- The critical velocity of the Vechtdijk was $U_c = 4$ m/s. This critical velocity can be considered as a minimum as the Vechtdijk was a sand dike with a good grass cover.
- The thresholds for cumulative overload were determined as follows:
 - Start of damage $D = 500 \text{ m}^2/\text{s}^2$
 - Various open spots on the slope $D = 1000 \text{ m}^2/\text{s}^2$
 - Failure of the slope $D = 3500 \text{ m}^2/\text{s}^2$

Chapter 3 describes the update of Appendix B and C of Handreiking (2012), which will here be referred to as Database (2014). The new results in this Database will be analysed in the next section, following similar lines as in the Fase 4D report (2010).

4.2 Re-analysis of various hydraulic regimes at the Vechtdijk

The cumulative overload method, Equation 3.1, has been used to analyse the results of the tests at the Vechtdijk. For the present analysis α_1 and α_2 will be equal to 1, which means that only the results on the grass cover itself will be analysed, not the effect of transitions and obstacles.

The Vechtdijk was a sand dike with grass cover and roots in the first 0.15 m to 0.20 m (in sand). It was expected that this grass cover would be fairly weak in comparison with other dikes with a grass cover on a clay layer. It was therefore expected that a small wave height of 1 m would also lead to damage by wave overtopping. Therefore three test conditions have been used at the Vechtdijk: $H_s = 1$ m (river regime), $H_s = 2$ m (sea regime) and $H_s = 3$ m (severe sea regime). Comparison of damages and hydraulic overload should give a conclusion on the critical velocity (the strength) of the grass cover at the Vechtdijk.

As described in Section 4.1 three damage definitions were used, which actually have been extended with an extra definition if the tests showed no failure at the end:

- Start of damage
- Various open spots on the slope
- Failure of the slope (test terminated due to uncontrolled mechanism)
- No failure at end of test

The cumulative overload for each test situation has been given in the spreadsheet of the Database (2014). Table 4.1 gives a part of this spreadsheet with most relevant data on cumulative overload. Note that the upper block in Table 4.1 is focussed on the undisturbed grass cover itself, not on the effect of the tree or transition. The latter is given in the lowest block, and those results will not be treated in this section. This section concentrates on the grass cover only, although the sections are called “with transition” or “with tree”.

	Belasting (l/s per m)	$\Sigma (U^2 - U_c^2) \text{ m}^2/\text{s}^2$					
		$U_c=3\text{m/s}$	$U_c=3.5\text{m/s}$	$U_c=4\text{m/s}$	$U_c=5\text{m/s}$	$U_c=6.5\text{m/s}$	$U_c=8\text{m/s}$
<i>Rivier regime ($H_s = 1$ m)</i>							
Eerste schade (min. 0,15 m x 0,15 m)	0,1; 1; 10; 1:58 uur 30	3897	1923	840	107	1	0
Meerdere locaties kale plekken (" ")	0,1; 1; 10; 6:00 uur 30	8616	4546	2124	306	2	0
Zand komt vrij (door de afdeklaag)	0,1; 1; 10; 30; 2:00 uur 50	13843	7419	3764	692	17	0
Gestopt: oncontroleerbaar mechanisme	0,1; 1; 10; 30; 2:07 uur 50	14148	7587	3859	715	18	0
<i>Zee regime ($H_s = 2$ m); met overgang</i>							
Eerste schade (min. 0,15 m x 0,15 m)	0,1; 6:00 uur 1	595	405	253	76	0	0
Meerdere locaties kale plekken (" ")	0,1; 1; 5; 3:00 uur 10	6187	4472	3024	1113	120	2
Zand komt vrij (door de afdeklaag)							
Gestopt: oncontroleerbaar mechanisme							
Geen bezwijken talud na:	0,1; 1; 5; 10; 30; 0:23 uur 50	28481	21789	16169	7724	1710	227
<i>Zee regime ($H_s = 2$ m); met boom</i>							
Eerste schade (min. 0,15 m x 0,15 m)	0,1; 1; 5; 4:00 uur 10	3574	2228	1254	277	6	0
Meerdere locaties kale plekken (" ")	0,1; 1; 5; 10; 2:00 uur 30	7725	5156	3180	943	75	1
Zand komt vrij (door de afdeklaag)							
Gestopt: oncontroleerbaar mechanisme							
Geen bezwijken talud na:	0,1; 1; 5; 10; 30; 1:01 uur 50	16970	11862	7817	2755	323	14
<i>Zwaar zee regime ($H_s = 3$ m)</i>							
Eerste schade (min. 0,15 m x 0,15 m)	0,1; 1; 2:00 uur 5	758	581	353	116	7	0
Meerdere locaties kale plekken (" ")	0,1; 1; 6:00 uur 5	1731	1280	822	281	21	0
Zand komt vrij (door de afdeklaag)	0,1; 1; 5; 6:00 uur 10	6172	4806	3466	1541	265	12
Gestopt: oncontroleerbaar mechanisme	0,1; 1; 5; 10; 1:03 uur 30	8187	6449	4762	2251	466	46
<i>Zee regime ($H_s = 2$ m); met overgang</i>							
Begin ondermijning overgang	0,1; 1; 5; 6:00 uur 10	7592	5348	3504	1183	104	0
Gestopt: oncontroleerbaar mechanisme	0,1; 1; 5; 10; 30; 0:23 uur 50	24348	21789	13080	5779	1087	111
<i>Zee regime ($H_s = 2$ m); met boom</i>							
Eerste wortel geerodeerd	0,1; 1; 5; 4:00 uur 10	4315	2813	1674	432	17	0
Grote erosie van wortels, zand zichtbaar	0,1; 1; 5; 10; 2:00 uur 30	9227	6367	4105	1360	139	5
Gestopt: oncontroleerbaar mechanisme	0,1; 1; 5; 10; 5:30 uur 30	15789	11220	7513	2742	340	14

Table 4.1. Cumulative overload for test situations at the Vechtdijk

All tests were terminated due to large and fast expanding damage, but this was not always due to the grass cover. In two cases a transition and a tree were the respective causes of failure of the slope. Therefore the threshold “no failure at the end of the test” has to be used for these two situations, when we consider the grass cover only and not the transition or tree itself. For the tests with the river regime and with the severe sea regime also the undisturbed grass cover failed. There was, however, a difference in condition of the grass slope for these tests, compared to the test with the sea regime and the tree. For the first mentioned tests there was a section, roughly 2-4 m from the crest, with a large activity of moles. Mole activity was everywhere, but here it was concentrated. These sections gave start of damage and eventually failure, although failure was located further down the slope. It means that failure for these sections was probably a little earlier than for a regular slope.

Table 4.1 gives cumulative overloads for $U_c = 3$ m/s up to 8 m/s. It does not give a judgement on what the correct critical velocity for the slope should be. A good way to compare the cumulative overload results is to use a bar graph. The thresholds can be grouped per test:

- start of damage,
- several open spots,
- no failure (at the end of the test) and
- failure.

Figures 4.1-4.6 give the bar graphs, each for a certain critical velocity. No failure at the end of the test actually gives the cumulative overload that was applied to the slope before termination of the test. It indicates that “failure” for that section would have even a larger cumulative overload, but this was not measured as the test was terminated before that state.

The comparison in Figures 4.1-4.6 is theoretically perfect if the level of the bars for each damage threshold is the same. If that is the case, the correct critical velocity has been found. A perfect agreement is not present in any of the graphs and therefore the graph with the best agreement has to be found. From previous tests it has been concluded that the threshold of start of damage is less reliable than several open spots, as start of damage often depends on very local conditions. Note also that the somewhat early failure due to concentrated mole activity occurred for the river regime ($H_s = 1$ m) as well as the severe sea regime ($H_s = 3$ m). Both conditions are the extremes and therefore failure of the slope for these two conditions gives a good impression of the correct critical velocity, although in both cases a slope without the large concentration of mole holes would have given a larger cumulative damage before failure and more comparable to the test with $H_s = 2$ m.

In all graphs the threshold “no failure at the end of the test” of the test with the transition, is much larger than the other tests. This was not really the case in the original analysis. The difference can be explained by the fact that this test was performed at the other side (riverside) of the dike, whilst all other tests were at the landward side. The riverside had a much steeper slope, which gave acceleration on the overtopping wave volumes and now with the new analysis, a much larger cumulative overload. The slope is different as well as the orientation to the sun, which may have had some effect on the grass quality. It might be concluded that the grass cover on the riverside slope might have a different critical velocity from that at the landward slope.

Figure 4.1 shows the results for a critical velocity of $U_c = 3$ m/s. The level of the bars for “several open spots” or “various damages” is more or less similar for three of the four tests at about $6000 - 8000 \text{ m}^2/\text{s}^2$. The level for failure for the river regime is more than 50% higher

than for the severe sea regime. The grass at the tree (green bar), which did not fail, is just a little larger than the level for failure for the river and severe sea regime. It seems that the critical velocity should not be far from 3 m/s.

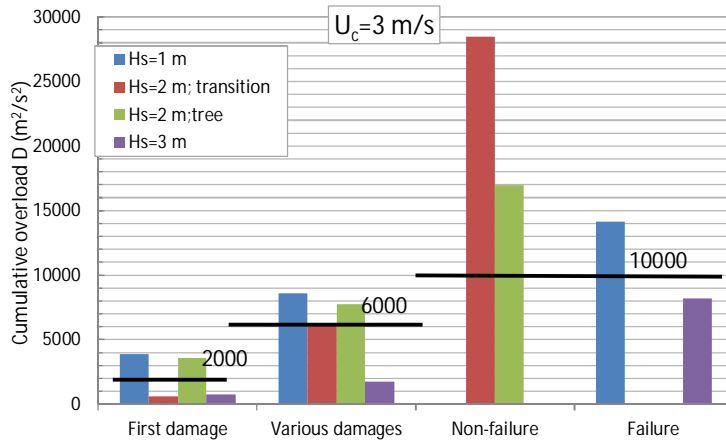


Figure 4.1 Comparison of cumulative overload for various damage thresholds; $U_c = 3 \text{ m/s}$

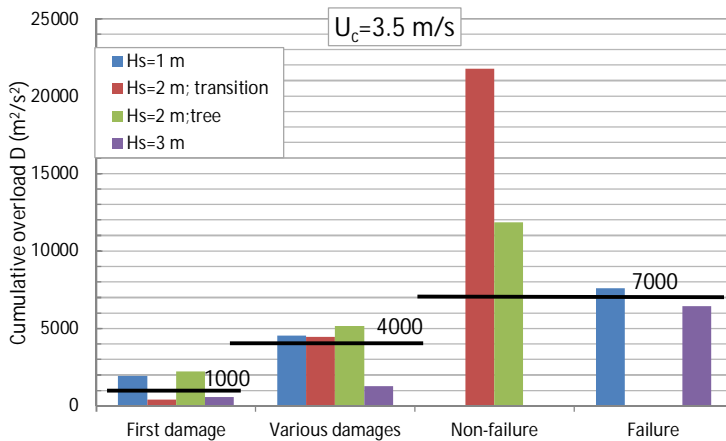


Figure 4.2 Comparison of cumulative overload for various damage thresholds; $U_c = 3.5 \text{ m/s}$

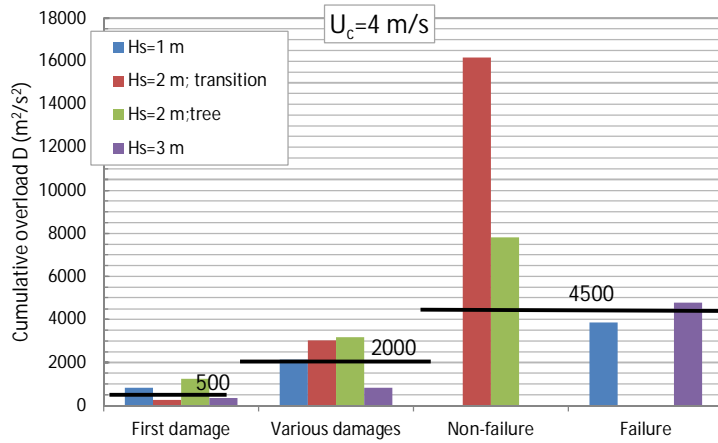


Figure 4.3 Comparison of cumulative overload for various damage thresholds; $U_c = 4 \text{ m/s}$

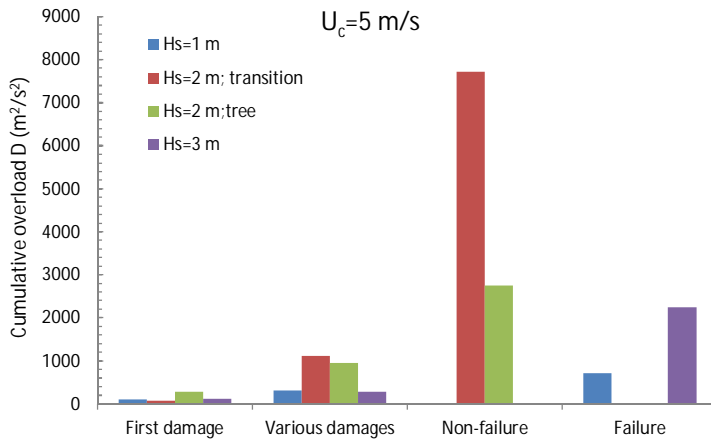


Figure 4.4 Comparison of cumulative overload for various damage thresholds; $U_c = 5 \text{ m/s}$

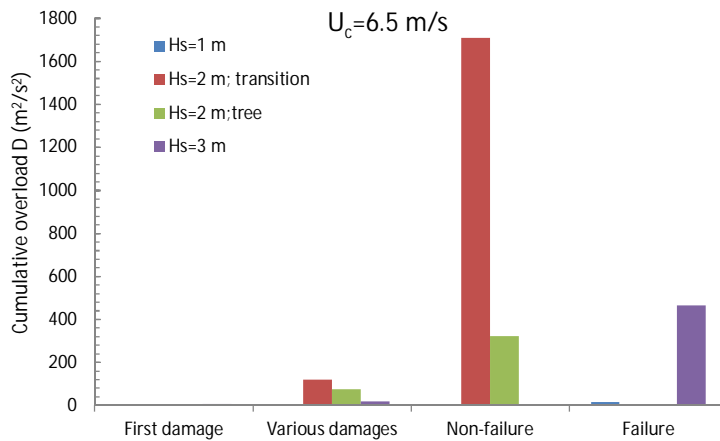


Figure 4.5 Comparison of cumulative overload for various damage thresholds; $U_c = 6.5 \text{ m/s}$

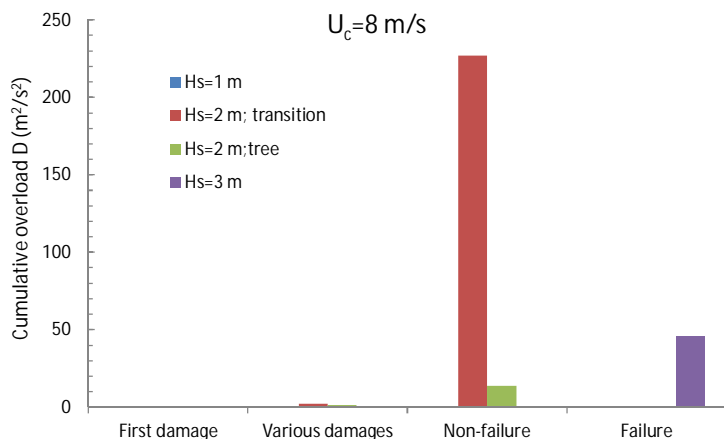


Figure 4.6 Comparison of cumulative overload for various damage thresholds; $U_c = 8 \text{ m/s}$

Figure 4.2 gives the result for a critical velocity of $U_c = 3.5 \text{ m/s}$. Three levels for various damages are now almost equal. The severe sea regime remains lower, but that is the case in all graphs. Also the two failures have similar levels, where the green bar (no failure for the grass with the tree) is about 50% higher. This might well be reasonable as this section had less concentration of mole holes. Overall, this graph shows very good agreement between the various regimes.

Figure 4.3 gives the result for a critical velocity of $U_c = 4 \text{ m/s}$. Again the levels for “failure” are almost equal. The levels at the threshold of several open spots, various damages, are quite close, but not as good as in Figure 4.2. In conclusion, this graph gives also a fair agreement on the most important thresholds, similar to Figure 4.1, but not as good as Figure 4.2.

Figures 4.4-4.6 show an increasing difference for the threshold of failure and later also for other thresholds. The critical velocity should certainly be smaller than 5 m/s .

Based on the analysis above one can conclude that the critical velocity for the grass slope (landward side) of the Vechtdijk will be around $3\text{-}4 \text{ m/s}$. The values of 3 and 4 m/s suit the threshold of failure and lower damage thresholds quite well. But a value in between, a critical velocity of 3.5 m/s , gives the best comparison. Therefore, the choice has been made that the critical velocity for the grass cover of the Vechtdijk is $U_c = 3.5 \text{ m/s}$.

Figure 4.2 gives then the following cumulative overload values for the thresholds:

Start of damage	$\Sigma(U^2 - U_c^2) = 1000 \text{ m}^2/\text{s}^2$
Several open spots	$\Sigma(U^2 - U_c^2) = 4000 \text{ m}^2/\text{s}^2$
Failure (early due to mole holes)	$\Sigma(U^2 - U_c^2) = 7000 \text{ m}^2/\text{s}^2$

The hypothesis of the cumulative overload seems to work: the grass cover under the river regime failed after 2 hours with 50 l/s per m overtopping. For the severe sea regime this was already after 1 hour with 30 l/s per m . The difference in duration is 5 hours with 30 l/s per m plus 2 hours with 50 l/s per m . In both situations the cumulative overload, with $U_c = 3.5 \text{ m/s}$, amounted to about $\Sigma(U^2 - U_c^2) = 7000 \text{ m}^2/\text{s}^2$.

4.3 Re-analysis of all tested locations

4.3.1 Method of analysis

In Section 4.2 values for damage thresholds have been determined, based on the tests with various wave regimes at the Vechtdijk. Given these thresholds for start of damage, several open spots and failure (or non-failure), it is possible to analyse the results of all other test locations and to come up with a value for the critical velocity (= strength) of that location.

The present analysis will only focus on the undisturbed grass cover, not on transitions or objects. The latter will be a separate analysis. In order to analyse all the locations that have been tested, a part of the spreadsheet of the Database (2014) has been taken and analysed further. This selection of the database is given in Table 4.2. First of all only rows with results of the grass cover have been left, results on transitions and objects have been deleted. The left half of the table gives the information on location, damage observation and hydraulic load. The right half gives the cumulative overload for various critical velocities.

What has been added to the table is an indication where a possible damage threshold can be found. Different colours have been used for different thresholds:

	Start of damage ($1000 \text{ m}^2/\text{s}^2$)
	More open spots ($4000 \text{ m}^2/\text{s}^2$)
	(No) failure ($7000 \text{ m}^2/\text{s}^2$)

Often one of the threshold values was between the values in two neighbouring cells. Then both cells were coloured. If the thresholds are more or less correct and they have also been observed during the tests, then the coloured cells for that location should be concentrated around one or two critical velocities (in one or two neighbouring columns). The analysis of the location of the coloured cells gives information on the critical velocity of the tested section. This analysis will be done for all tests performed per location.

4.3.2 Delfzijl

At Delfzijl first bare clay was tested. The clay had a good erosion resistance, category 1. Failure of the clay layer showed that critical velocities around $U_c = 3\text{-}4 \text{ m/s}$ describe the strength of this clay layer.

The grass slopes that were tested showed no damage, giving a critical velocity of at least 8 m/s . Some gullies developed when *initial damage was made*, but only for the grass without geotextile. The test showed that if this damage was made, the gullies were developed for a cumulative overload of $\Sigma(U^2 - U_c^2) = 3274 \text{ m}^2/\text{s}^2$, using a critical velocity of $U_c = 6.5 \text{ m/s}$. This is around several open spots. But it was not yet failure of the slope. The orange colour in Table 4.2 indicates that a *manually damaged grass cover* at Delfzijl, without the geotextile, had a critical velocity of around $U_c = 6.5 \text{ m/s}$.

4.3.3 Boonweg

All four tested slopes at the Boonweg were strong. Two of them did not fail at all, the other two failed in the last sub-test. Almost all green colours are in the last column, all of them had a cumulative overload of around $7000 \text{ m}^2/\text{s}^2$ for $U_c = 8 \text{ m/s}$, indicating very clearly that the critical velocity was around $U_c = 8 \text{ m/s}$.

4.3.4 St Philipsland

Only one section was tested at St Philipsland. The slope failed for a cumulative overload of $14484 \text{ m}^2/\text{s}^2$, assuming a critical velocity of 5 m/s and $4407 \text{ m}^2/\text{s}^2$ for a critical velocity of 6 m/s. A value of $7000 \text{ m}^2/\text{s}^2$ is reached close to a critical velocity of 6 m/s. One may conclude that the critical velocity was $U_c = 6 \text{ m/s}$.

4.3.5 Kattendijke

Section 1 at Kattendijke showed no damage during the test, indicating that the critical velocity was at least $U_c = 8 \text{ m/s}$.

4.3.6 Afsluitdijk

Three sections were tested at the Afsluitdijk, two of them had a staircase or a transition to a parking place paved with clinker bricks. Looking at the grass cover only, failure was not observed. What happened was quite specific for the Afsluitdijk and has not been observed at other locations: thin layers of grass (4-5 cm) were ripped off the slope quite easily, but the remaining clay, which still contained grass roots, was very strong and did not fail. According to the definition of failure (deep holes expanding into the slope) or at the definition of grass cover (at least 0.2 m thick), failure was not observed. The first 4-5 cm showed easily damage, but not the remaining 15 cm of the grass cover.

This somewhat dual behaviour is also present by the coloured cells in Table 4.2. Start of damage and several open holes (rip-off of thin grass layers) with $D = 1000 - 4000 \text{ m}^2/\text{s}^2$ occurred for critical velocities between $U_c = 4-8 \text{ m/s}$. This is quite a large range. The fact that failure was not observed for the grass cover in any of the three tests, indicates that the critical velocity was at least $U_c = 8 \text{ m/s}$ as the value of $D > 7000 \text{ m}^2/\text{s}^2$ without failure.

4.3.7 Vechtdijk

The tests at the Vechtdijk, with the three different hydraulic regimes, were used to establish the values for the threshold. These were based on a critical velocity of $U_c = 3.5 \text{ m/s}$.

The coloured cells in Table 4.2 show indeed that they are mostly present for a critical velocities of $U_c = 3 \text{ m/s}$ or 4 m/s .

4.3.8 Tielrode

The dike of the Controlled Flooding Area at Tielrode (GOG-dike) consisted of poor clayey material and a vegetation cover that was not maintained and had a very rough and ruderal appearance. All damage observations occurred for threshold D-values that belong to a critical velocity of $U_c = 3 \text{ m/s}$ or even quite lower than that. The values are sometimes far below the threshold values, using a critical velocity of $U_c = 3 \text{ m/s}$.

The conclusion in the Handreiking (2012) was that if the grass cover could be described as a ruderal vegetation, the slope should get a critical velocity of $U_c = 0 \text{ m/s}$, meaning hardly any strength. Such a slope should not have an allowable overtopping discharge larger than 0.1 l/s per m. If we assume that the Vechtdijk with a good grass cover, but fully based on sand, would get the lowest critical velocity of $U_c = 3.5 \text{ m/s}$ possible (a clay layer would improve the situation), than the GOG-dike is significantly worse. Which is caused by the lack of a proper grass cover.

4.3.9 Tholen

The tested sections at Tholen show a variety of results. The first test on the seaward side of the dike showed a little different grass quality than on the landward side, which was tested later. The seaward side (section 1) showed first damage and several open spots for a D-values that belong to a critical velocity of $U_c = 5 \text{ m/s}$. The test was terminated as the asphalt slab of the cycle path lifted up, so the damage threshold of failure for the grass was not reached.

The grass slope alongside the staircase had no strength at all. This was due to the fact that a herbicide had been used that had killed the grass along the staircase. No roots were available, which resulted in a critical velocity smaller than $U_c = 3 \text{ m/s}$. A similar conclusion can be given here as for the GOG-dike at Tielrode: this grass cover has no strength and wave overtopping should be less than 0.1 l/s per m.

In section 3 there was very poor maintenance of the grass and extensive grazing by sheep, especially close to a fence running down the landward slope. Also here failure occurred for a critical velocity smaller than $U_c = 3 \text{ m/s}$ and a similar conclusion can be drawn as for the previous section.

Section 4 was a little further away from the fence and although the maintenance was still inadequate, the grass cover was a little stronger, resulting in start of damage and several open spots for D-values belonging to a critical velocity around $U_c = 3 \text{ m/s}$ and failure for D-values with a critical velocity around $U_c = 5 \text{ m/s}$. Overall one could conclude that the critical velocity for this slope should be fixed at $U_c = 5 \text{ m/s}$.

4.3.10 Nijmegen

Also the tests at Nijmegen showed a variety of results, mainly because the first section was along a concrete wall and was partly very steep. This first section shows a critical velocity of $U_c = 4\text{--}5$ m/s. The second section showed no failure. Based on start of damage and on several open spots the critical velocity is around $U_c = 6.5$ m/s.

As concluded in the analysis of the testing at this location, the “fast U_c -test” (only large overtopping wave volumes) resulted in a larger critical velocity of at least $U_c = 8$ m/s. Fast U_c -tests give a too large critical velocity and a direct application of this kind of tests is not possible.

4.3.11 Millingen

The first test at Millingen was a conventional test, the second was a “fast U_c -test”. In the first test only start of damage was observed for the grass cover, which gives a critical velocity between $U_c = 5$ m/s to 6.5 m/s. But this value should not be considered as very reliable as it is only based on one value for start of damage only.

The fast U_c -test showed damage at the crest, which probably could be considered as a transition (from asphalt to crest). The slope itself showed only several open spots and gives a high critical velocity of $U_c = 8$ m/s or even higher.

4.3.12 Noord-Beveland

Wave run-up tests were performed at Noord-Beveland. The crest level was quite low and in most tests the water that appeared at the crest was guided sideways and back to the sea. In one test this was not done and up-rushing waves could flow over the crest and cause wave overtopping at the landward slope. Section 2.2.4 describes the calculation of the wave overtopping discharge that occurred. There was no damage to the slope, which leads to a critical velocity larger than $U_c = 7$ m/s.

4.4 Summary of the re-analysis

Based on the re-analysis of the tests at the Vechtdike, the critical velocity of the grass cover of the Vechtdike (landward side) is $U_c = 3.5$ m/s. This value can be considered as a minimum strength of a well maintained grass cover, as the dike itself was a sand dike without cover of clay or soil. Based on this analysis the following thresholds for damage were established:

Start of damage	$\Sigma(U^2 - U_c^2) = 1000 \text{ m}^2/\text{s}^2$
Several open spots	$\Sigma(U^2 - U_c^2) = 4000 \text{ m}^2/\text{s}^2$
Failure (early due to mole holes)	$\Sigma(U^2 - U_c^2) = 7000 \text{ m}^2/\text{s}^2$

By knowing these thresholds it became possible to analyse the results of all other locations that had been tested and to come up with a fair guess of critical velocities.

The critical velocities considered were $U_c = 3; 4; 5; 6.5$ and 8 m/s. The lower boundary of $U_c = 3$ m/s was chosen to see how far the strength of a poor grass cover could be from the minimum of $U_c = 3.5$ m/s. Some tests showed that even 3 m/s was too high to describe the damages. The observation of test results on poor grass covers has led in the Handreiking (2012) to an important conclusion that these kind of grass slopes have actually no strength and that allowable wave overtopping should be limited to 0.1 l/s per m only (meaning hardly overtopping at all). In contrast to previous guidelines that stated that the quality of a grass cover can be described by a sliding scale (poor, moderate and good), now the definition is: no strength to poor grass (i.e. grass covers with significant presence of ruderal species) and good strength to a well-covered and well-rooted grass slope. A poor grass slope is characterised by inadequate mowing or grazing maintenance or no maintenance at all: ruderal vegetation, open unprotected spots, (private) gardens, etc. Examples of ruderal

species (ruigtesoorten) on Dutch dikes are stinging nettle (*Urtica dioica*), hogweed (*Heracleum sphondylium*), cow parsley (*Anthriscus sylvestris*) or shrubs.

If the minimum critical velocity of a grass slope with adequate maintenance is defined at $U_c = 3.5$ m/s, then slopes that showed a critical velocity less than this value should not be considered to have any strength. On such slopes the allowable wave overtopping discharge should be less than 0.1 l/s per m. As conclusion in the present analysis the strength of such a slope is set at $U_c = 0$ m/s.

The largest critical velocity considered is $U_c = 8$ m/s. Sometimes test results indicate that a slope had even a larger critical velocity. For sake of simplicity and to be a little conservative, a maximum value of $U_c = 8$ m/s is taken for these slopes.

With the remarks and constraints as described above, the testing from 2007 to 2014 with the wave overtopping simulator leads to the following critical velocities for the slopes tested.

Delfzijl, good quality erosion resistant bare clay	$U_c = 3-4$ m/s
Delfzijl	$U_c = 8$ m/s
Boonweg	$U_c = 8$ m/s
St Philipsland	$U_c = 6$ m/s
Afsluitdijk, rip off of thin grass cover	$U_c = 4-8$ m/s
Afsluitdijk, failure	$U_c = 8$ m/s
Vechtdijk	$U_c = 3.5$ m/s
Tielrode, GOG, ruderal vegetation	$U_c = 0$ m/s
Tholen, seaward side	$U_c = 5$ m/s
Tholen, landward side, inadequate maintenance	$U_c = 0$ m/s
Nijmegen	$U_c = 6.5$ m/s
Nijmegen, fast U_c -test (too large U_c)	$U_c = 8$ m/s
Millingen	$U_c = 5-6.5$ m/s
Millingen, fast U_c -test (too large U_c)	$U_c = 8$ m/s
Noord-Beveland, wave overtopping by run-up simulation	$U_c > 7$ m/s

But still it is not easy to establish the critical velocity of a grass slope beforehand, without performing any overtopping tests. The methods described in the Handreiking (2012) may help, but are not yet conclusive. Nevertheless, the tests show a kind of minimum (a grass cover on a sand core), which could be used as a first and (very) conservative value for safety assessment.

4.5 Re-analysis of the graphical method in the Handreiking

Section 6.2 of the Handreiking, RWS (2012) gives a graphical method to calculate the cumulative overload, given the wave height, the overtopping discharge and the critical velocity. The cumulative overload in the Handreiking, RWS (2012) is still given as the basic equation for a grass slope only:

$$D = \sum_{i=1}^N (U_i^2 - U_c^2) \quad \text{for } U_i > U_c \quad [\text{m}^2/\text{s}^2] \quad (4.1)$$

In Equation 4.1 the velocity U_i is taken at the crest of the dike, assuming that this velocity describes what happens at the down slope. In recent years it became clear that the acceleration down the slope is quite extensive and that it depends on the steepness of the slope. Also transitions and objects were taken into account for the method of cumulative overload, using influence factors α_1 and α_2 . The cumulative overload method was extended to Equation 4.2, where for U_i the velocity at the location on the slope that is considered, should be taken into account.

$$D = \sum_{i=1}^N (\alpha_1 U_i^2 - \alpha_2 U_c^2) \quad \text{for } \alpha_1 U_i > \alpha_2 U_c \text{ [m}^2/\text{s}^2] \quad (4.2)$$

Together with a re-analysis of the method of cumulative overload, the damage criteria D were modified for start of damage, several open spots and failure.

Equation 4.2 is an improvement on Equation 4.1, but Equation 4.1 still gives a fair and first indication of damage to be expected. But given Equation 4.2, can the graphical method in Section 6.2 of the Handreiking, RWS (2012) be updated?

The answer is that this is hardly or not possible. There are a few reasons for that. U_i now depends on the steepness of the landward slope and the location on that slope, where in the original method it depended only on the wave conditions and overtopping discharge. It would need tables like Table 6.1 in the Handreiking, RWS (2012) for every acceleration factor (many pages of tables). Another reason is that the influence factor α_1 influences the number of overtopping waves that will be taken into account for the cumulative overload. For every test condition a different number of large overtopping waves have to be taken, which is not possible to fit into tables or graphs.

The overall conclusion is that the graphical method in Section 6.2 of the Handreiking, RWS (2012) gives a first and rough indication of possible damage and that with the recent knowledge and improvement of the method, a procedure has to be followed, which cannot be put in a graphical method. This procedure has been described in Chapter 8.

5 Evaluation of tests near the Zeelandbrug

5.1 Damage development

Five tests were performed with wave run-up simulation at a dike near the Zeelandbrug, see Infram (2014) for the Factual Report. The first three sections were focussed on transitions from asphalt or revetment to a grass berm, and to a transition from a berm to the upper slope. At the fourth section an area of 2 m by 2 m grass cover was removed and testing was on the clay with still remaining grass roots in it. The last test was on a stair case.

A good way to describe the damage to the transitions in the first three tests is to give the measurements of the erosion by the laser equipment (Appendix G in the Factual Report). Figures 5.1 – 5.3 give the measured erosion. Erosion more than 5 cm deep has an orange to red colour, where yellow gives no erosion. In Figure 5.2 also wave overtopping was generated due to up-rushing waves that past the crest, see also Section 2.2.4.

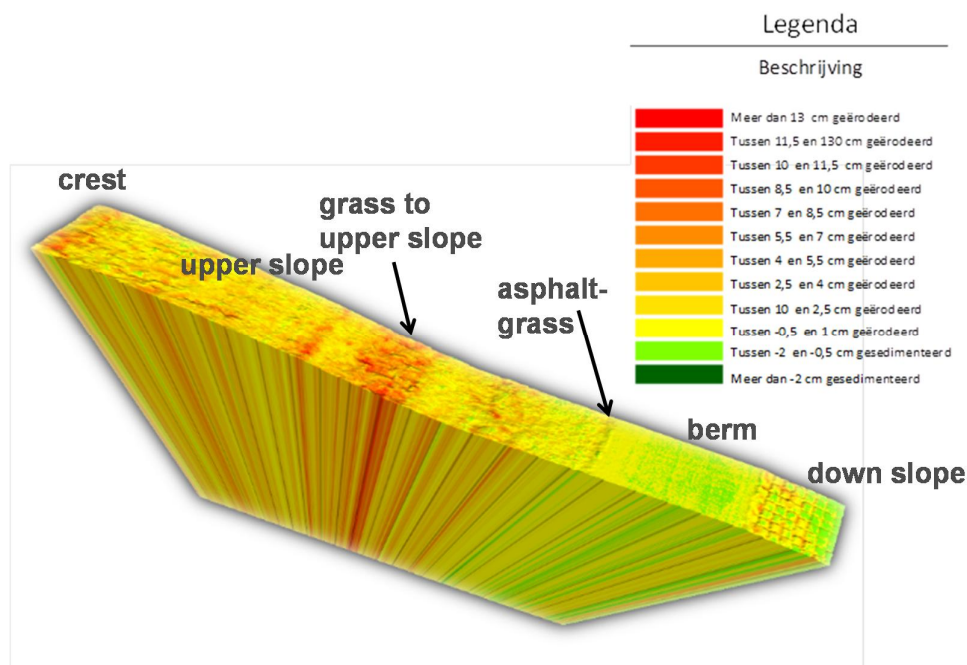


Figure 5.1. Measured erosion for test 1

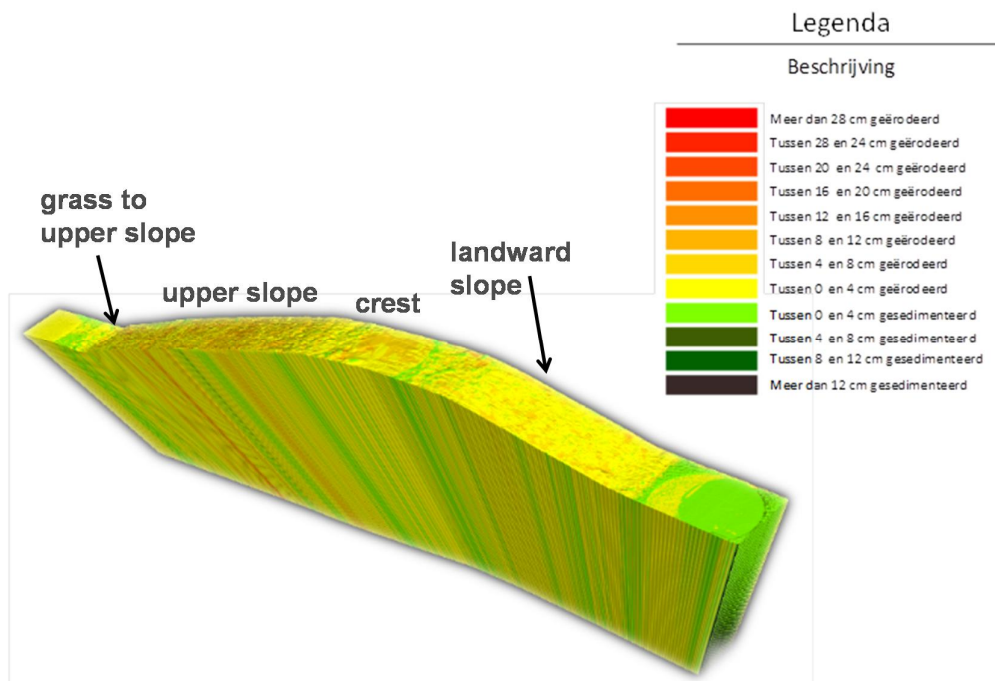


Figure 5.2. Measured erosion for test 2

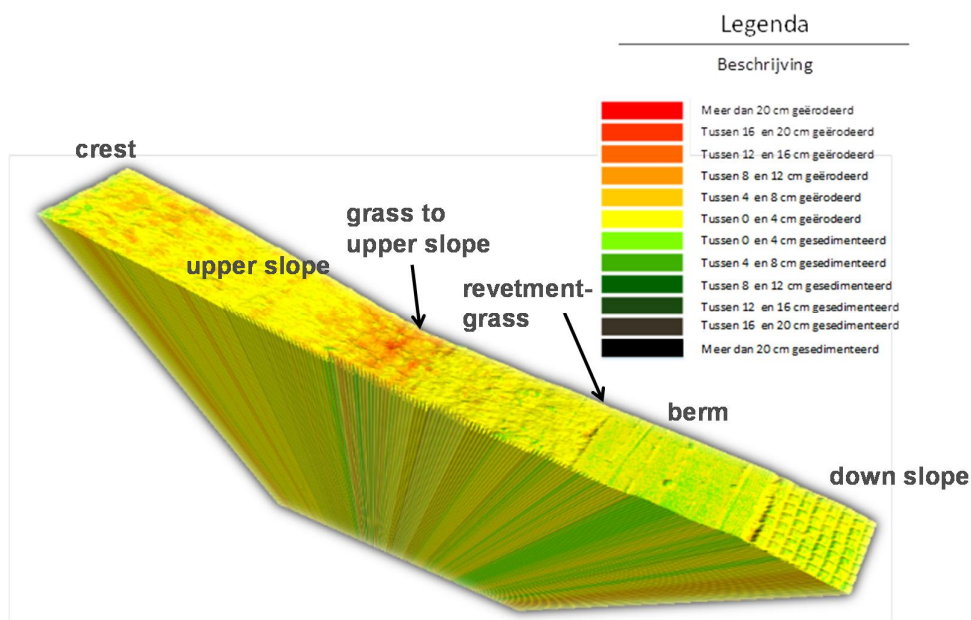


Figure 5.3. Measured erosion for test 3

Figure 5.1 shows that there is no erosion at the transition from asphalt to the grass on the berm. Apparently there was not really a difference in roughness between asphalt and the grass. Limited damage, but clearly visible in Figure 5.1, occurred at the start of the upper slope. This damage/erosion was larger than at the remaining higher part of the upper slope.

Figure 5.2 does not really show the transition from berm to upper slope, as it also gives the landward slope that was subjected to overtopping waves. Upper slope, crest and landward slope show hardly any erosion. Figure 5.4 shows the final situation after test 2. There is slight damage at the transition to the upper slope.

Figure 5.3 shows a similar picture as in Figure 5.1, there is slight erosion at the transition to the upper slope.



Figure 5.4. Slight erosion at the transition to the upper slope, test 2

The overall conclusions on erosion are that the transitions from asphalt or revetment to the grass did not give any erosion, where slight erosion was always found just at the transition from berm to upper slope. But overall the damage was small.

5.2 Front velocities during run-up

Velocities and flow thicknesses were measured during the session on hydraulic measurements (Section 2.2) and from the records also the front velocity between pairs of paddle wheels were derived. Figure 5.5 shows the location of the instruments again, where it can be concluded that the front velocities between pw1 and pw3 (called v1-v3) give the situation at the transition from asphalt to grass and between pw3 and pw5 (called v3-v5) give the situation just before the up-rushing wave arrives at the transition to the upper slope. These two front velocities will be used to calculate the cumulative overload for the two mentioned transitions.

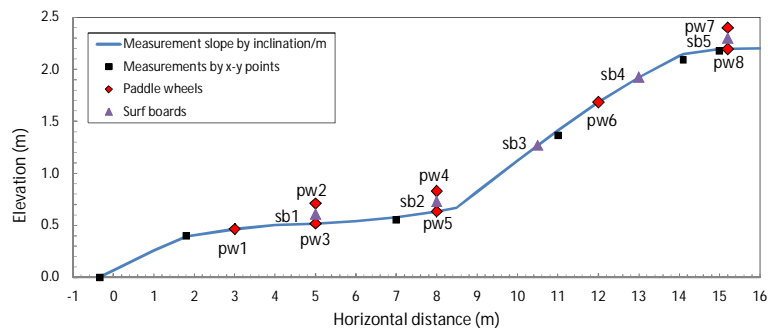


Figure 5.5. Set-up for the hydraulic measurements, with pw's 1, 3 and 5 on the berm

Each filling level of the run-up simulator gives a certain front velocity and the relationship is shown in Figure 5.6. For filling levels of 2 m and higher the front velocities over the whole berm are similar. Only for small filling levels the energy dissipation over the berm plays a role and then the front velocity is a little lower over v3-v5 than over v1-v3. The relationships can be given by:

$$\text{Front velocity } v_{1-v3} = \min[4.5h_v; 0.45h_v + 4.8] \quad (5.1)$$

$$\text{Front velocity } v_{3-v5} = \min[4.5h_v - 3.5; 0.45h_v + 4.8] \quad \text{and } v_{3-v5} \geq 0 \text{ m/s} \quad (5.2)$$

Where h_v = filling level (m) and the front velocity is given in m/s.

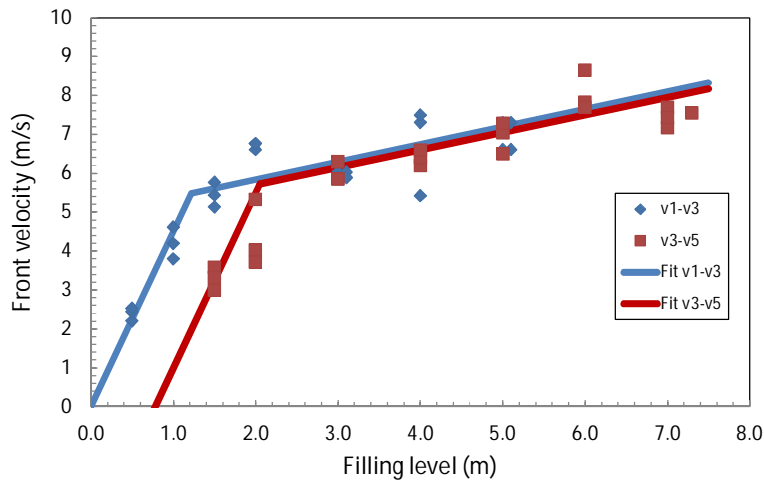


Figure 5.6. Relationship between filling level and front velocity at the berm

During each test the run-up conditions became more severe. A test consisted of four subtests, where the still water level was increased, keeping the assumed wave conditions the same. A subtest is given by the vertical distance between the front of berm and the assumed water level. A test with $x = 3$ m means that the water level for that test was 3 m lower than the front of the berm. Subtests were performed with $x = 3$ m; 2 m; 1 m; and 0 m. The assumed wave height was 2 and the storm duration for each subtest was 6 hours.

Figure 5.7 gives the run-up distributions that were simulated on the berm and the upper slope. The horizontal axis is according to a Rayleigh distribution and as the distribution of wave run-up levels is assumed to be Rayleigh-distributed, the lines are straight. The front of the berm is located at 4.9 m NAP and the crossing of the lines with the y-axis show the distance of the water level to that point.

There are three horizontal lines in the graph, one for the front of the berm, one for the crest level and one for the maximum capacity of the simulator. All wave run-up levels above the crest level gave also wave overtopping (or were re-distributed sideways). All wave run-up levels above the maximum capacity of the wave run-up simulator were kept at the maximum.

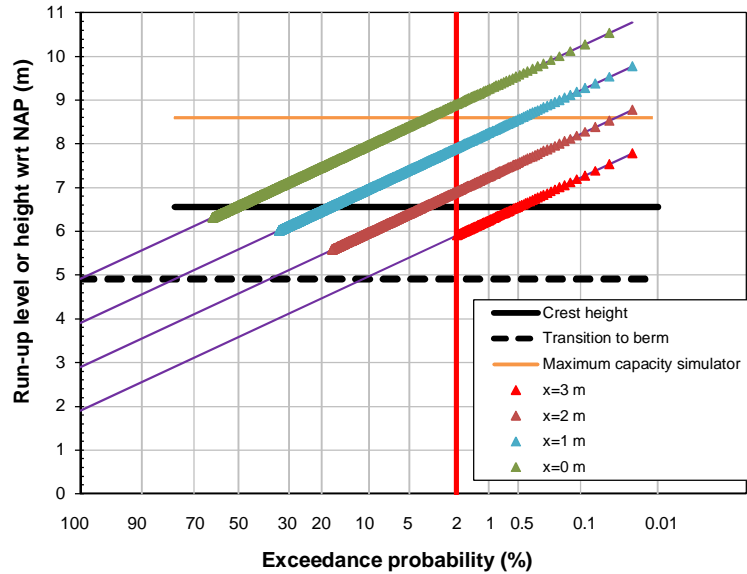


Figure 5.7. Theoretical distributions of wave run-up levels for each subtest. During the tests the run-up levels exceeding the capacity of the simulator were kept at the maximum capacity (orange line)

The relationship between filling level and wave run-up level has been described in Section 2.2.1 and was used to generate the steering files for the subtests. With Equations 5.1 and 5.2 the run-up velocity of the front over the berm can be calculated. Combining the filling levels of the steering files with Equations 5.1 and 5.2 give the distributions of the front velocity. Figure 5.8 shows the distribution of front velocities over v_1 - v_3 .

The basis of Figure 5.8 is the expected front velocity, derived from analysis of wave run-up measurements (Van der Meer, 2011). There is a large scatter between the reached wave run-up level and the maximum front velocity. The graph gives the average line, but also the 80%, 90% and 95% exceedance lines.

The wave run-up simulator produces the same front velocity for the same filling level, or the same run-up level. Figure 5.8 shows that the front velocities that were simulated were always quite high, roughly larger than 5 m/s, which is already the case for filling levels larger than 1 m, see also Figure 5.6. The maximum front velocity was 7.95 m/s, just below 8 m/s.

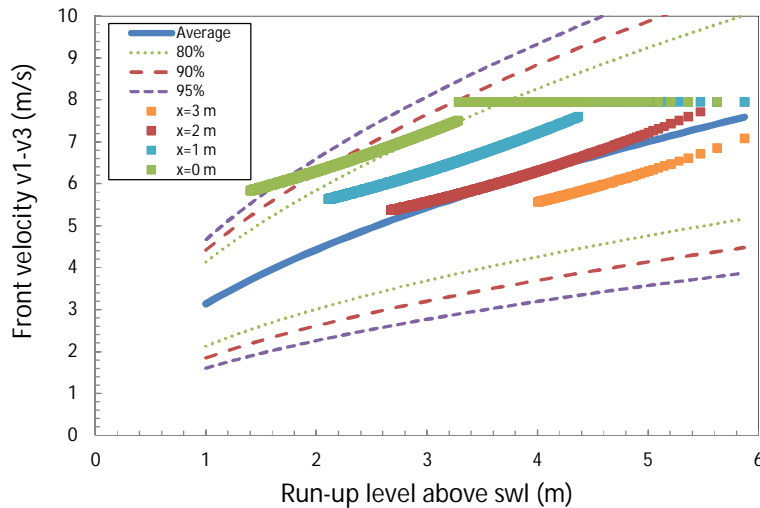


Figure 5.8. Distributions of front velocities v1-v3 for each subtest

Subtest x=3 m is a little lower than the average curve in Figure 5.8, where subtest x=2 m is almost equal to the average. The more severe subtests with x=1 m and 0 m gave front velocities that were higher than the expected average. In that sense it can be concluded that the simulated conditions for the last two subtests were more severe than can be expected in reality.

5.3 Cumulative overload

The method of cumulative overload was developed for wave overtopping, see Chapter 3. The front velocity of the overtopping wave accelerates down the slope and the cumulative overload is then dependent on the location of damage, as well as the steepness of the landward slope. The front velocity for an up-rushing wave does not accelerate. Over about 75% of the run-up height, the front velocity remains almost at its maximum value. Over the last 25% it drops down to zero. The cumulative damage for run-up depends also on the location on the slope. Very often the location of a transition is the most important one. For the tests this is the transition from asphalt or revetment to grass and from berm to upper slope. From Section 5.1 it has become clear that the most severe wave attack was at the transition to the upper slope.

The cumulative overload is given by:

$$D = \sum_{i=1}^N (\alpha_1 U_i^2 - \alpha_2 U_c^2) \quad \text{for } \alpha_1 U_i > \alpha_2 U_c \quad [\text{m}^2/\text{s}^2] \quad (5.1)$$

See Chapter 3 for a further explanation. The front velocities U_i are shown in Figure 5.8 and are mostly between 5 m/s and almost 8 m/s. At first instance the influence factors α_1 and α_2 have been kept at a value of 1. The cumulative overload at the transition from asphalt to berm (using the front velocities v1-v3) for each subtest and for the total test is given in Table 5.1. Table 5.2 is similar, but now for the transition to the upper slope, using the front velocities v3-v5.

Location	$U_c=4$ m/s	$U_c=5$ m/s	$U_c=6.5$ m/s	$U_c=8$ m/s
Asphalt-grass	$\alpha_M=1$	$\alpha_M=1$	$\alpha_M=1$	$\alpha_M=1$
Test	$\alpha_S=1$	$\alpha_S=1$	$\alpha_S=1$	$\alpha_S=1$
x=3 m	1685	875	17	0
x=2 m	13990	6889	302	0
x=1 m	33999	20733	2453	0
x=0 m	79197	53979	12309	0
Total Cum.	128871	82476	15081	0

Table 5.1. Cumulative overload at the transition from asphalt/revetment to grass

Location	$U_c=4$ m/s	$U_c=5$ m/s	$U_c=6.5$ m/s	$U_c=8$ m/s
Grass-slope	$\alpha_M=1$	$\alpha_M=1$	$\alpha_M=1$	$\alpha_M=1$
Test	$\alpha_S=1$	$\alpha_S=1$	$\alpha_S=1$	$\alpha_S=1$
x=3 m	1405	688	17	0
x=2 m	8804	4690	302	0
x=1 m	33473	20207	2453	0
x=0 m	79197	53979	12309	0
Total Cum.	122879	79564	15081	0

Table 5.2. Cumulative overload at the transition to the upper slope

The difference between the two tables is very small for critical velocities of 4 m/s and 5 m/s and non-existent for larger velocities. This is due to the very small difference in velocities for low filling levels, see Figure 5.6. Alpha-values different from 1 will be considered later.

The results in Tables 5.1 and 5.2 are at first sight a little surprising. Very large cumulative overloads are found for critical velocities up to 6.5 m/s. And no cumulative overload is found for a critical velocity of 8 m/s. The explanation is that most velocities are between 5-8 m/s, which means that every simulated up-rushing wave will count for a critical velocity of 4 m/s, almost every up-rushing wave for a critical velocity of 5 m/s and a large part of the up-rushing waves for a critical velocity of 6.5 m/s. As the maximum simulated front velocity is 7.95 m/s, the critical velocity of 8 m/s will not lead to any cumulative overload.

As start of damage should be found for $D = 1000 \text{ m}^2/\text{s}^2$ and this level has hardly been reached during the tests, the critical velocity should be close to 8 m/s or even larger. The conclusion on wave overtopping at the landward slope (see Section 4.4) was that the critical velocity should be larger than at least 7 m/s. These conclusions strengthen each other.

As there was no extra erosion at the transition from asphalt/revetment to grass at the berm, it can be concluded that α_1 and α_2 both remain at a value of 1. There was, however, a concentration of erosion at the transition to the upper slope, see Figures 5.1-5.3, and therefore it is logical that α_1 will be a little larger than 1. Table 5.3 gives the cumulative overload of the total test for critical velocities of 7 m/s, 8 m/s and 9 m/s and for various α_1 -values.

A cumulative overload value of $869 \text{ m}^2/\text{s}^2$, just below the value of $1000 \text{ m}^2/\text{s}^2$ for start of damage, is found for a critical velocity of 8 m/s and $\alpha_1 = 1.05$. If the critical velocity would be 9 m/s then $\alpha_1 = 1.3-1.4$ would be a good value. The upper slope was quite gentle (about 1:5) and the erosion at the transition was more than at the upper slope itself, but not much more.

This all leads to the conclusion that $\alpha_1 = 1.1$ would be a fair estimate with a critical velocity of around 8 m/s.

		$U_c=7$ m/s	$U_c=8$ m/s	$U_c=9$ m/s
α_M	α_S			
1.00	1.00	6773	0	0
1.05	1.00	9440	869	0
1.10	1.00	12710	2034	0
1.15	1.00	16641	3228	0
1.20	1.00	21285	4658	0
1.30	1.00	32895	8558	428
1.40	1.00	47842	14097	2756
1.50	1.00	66014	21561	5317
1.60	1.00	85969	31203	8844

Table 5.3. Cumulative overload for the total test and for various α_1 -values

5.4 Cumulative overload for pilot test at Tholen

In 2011 a pilot test was performed at Tholen on run-up simulation, using the wave overtopping simulator. A similar set-up was used as for the tests at the Zeelandbrug with four test conditions with increasing (assumed) water level. First damage and several open spots occurred quite easily, all on the berm and transition to the upper slope. The grass quality was quite bad in this area, see Figure 5.9. After the test there were three quite deep holes, two at the side walls and one in the middle, see Figure 5.10. Damage was more than several open spots, but certainly less than failure.



Figure 5.9. Quality of the grass berm was bad at Tholen (before testing)



Figure 5.10. Damage at Tholen after the pilot run-up test

From calibration and hydraulic measurements the flow velocities were known and these can be coupled to filling level (or actually fill volume). Cumulative overload can be calculated and the results have been given in Table 5.4.

Location	$U_c=4$ m/s	$U_c=5$ m/s	$U_c=6.5$ m/s	$U_c=8$ m/s
	$\alpha_M=1$	$\alpha_M=1$	$\alpha_M=1$	$\alpha_M=1$
Test	$\alpha_S=1$	$\alpha_S=1$	$\alpha_S=1$	$\alpha_S=1$
x=4.0 m	80	15	0	0
x=3.2 m	607	180	5	0
x=2.4 m	3114	1140	86	0
x=1.6 m	8792	3439	416	0
Total Cum.	12594	4774	506	0

Table 5.4. Cumulative overload for the pilot test at Tholen at the transition to the upper slope

With $D = 4000 \text{ m}^2/\text{s}^2$ for several open spots and $7000 \text{ m}^2/\text{s}^2$ for failure, the cumulative overload after the test should be between these two values. That is the case for a critical velocity of $U_c = 5 \text{ m/s}$ with $D = 4774 \text{ m}^2/\text{s}^2$.

But the grass at the berm was worse than at the slope and there is clearly a transition to the steep 1:3 upper slope. This means that actually α_1 and α_2 both should be different from 1. Table 5.5 gives the cumulative overload for α_1 and $\alpha_2 = 0.9$ and various values for α_1 . For a critical velocity of 6.5 m/s α_1 should be about 1.4, which is a fairly high value. It is more plausible that the critical velocity was around 5.5 m/s or 6 m/s with an $\alpha_1 = 1.1-1.3$. Including the worse grass slope at the berm and the transition to the upper slope, gives a critical velocity of $U_c = 5.5 \text{ m/s}$ to 6 m/s .

α_M	α_S	$U_c=5$ m/s	$U_c=6.5$ m/s	$U_c=8$ m/s
1.00	0.90	6226	944	0
1.05	0.90	7295	1274	33
1.10	0.90	8426	1663	93
1.15	0.90	9833	2114	157
1.20	0.90	11331	2626	237
1.30	0.90	14386	3826	476
1.40	0.90	17512	5254	838
1.50	0.90	20700	6892	1342

Table 5.5. Cumulative overload for $\alpha_2 = 0.9$ and various values for α_1

In Chapter 4 it was concluded that the wave overtopping test on the seaward side of the Tholen dike (which was also tested by the pilot test on run-up) resulted in a critical velocity of 5 m/s. This is a little lower than the 5.5 m/s to 6 m/s concluded on the wave run-up tests. But a closer look at the results of the wave overtopping test shows that all damage was on the berm, actually the transition from the upper slope to the horizontal berm, see Figure 5.11. Also the damage for the wave overtopping test occurred at a transition, not at the slope itself. Actually both $\alpha_2 = 0.9$ and $\alpha_1 = 1.1-1.3$ apply for a critical velocity of 5.5 m/s to 6 m/s, similar to the wave run-up test.

Both tests at Tholen, the wave overtopping test at the seaward side and the pilot test on wave run-up, give a critical velocity of 5.5 m/s to 6 m/s, using $\alpha_2 = 0.9$ and $\alpha_1 = 1.1-1.3$. From this point of view the two tests validate that the method of cumulative damage can also be applied to wave run-up.



Figure 5.11. Damage to the transition from downward on the seaward slope to the berm. Test on wave overtopping at Tholen

5.5 Conclusions on validation cumulative overload for wave run-up

The main reason to perform the wave run-up tests was to validate the method of cumulative overload that was based on wave overtopping tests, for wave run-up. The process to some extent is comparable: the front of an up-rushing or down-rushing wave damages the grass slope. A difference is that overtopping waves accelerate down a slope and that up-rushing waves have a more or less constant front velocity over quite some part of the run-up length.

The method of cumulative overload, however, takes the front velocity at a certain location on the slope, whether it is for waves rushing down or up the slope.

The cumulative overload describes three damage levels, start of damage, several open spots and failure. From the extensive testing with the wave overtopping simulator it is known that failure is the most important damage to establish the critical velocity of a grass slope. The least reliable damage indication is start of damage. Sometimes start of damage occurs quite soon, whilst the slope appears to be very strong, sometimes start of damage occurs just before the slope fails.

In order to make a good validation of the method for cumulative overload for wave run-up it is essential that testing shows the final stage of failure. That did not happen for the pilot test at Tholen, due to problems with large forces on the guiding walls, etc. The test had to be terminated before failure occurred. But the stage of several open spots was reached and even a little more.

The tests at the Zeelandbrug showed that the grass cover was quite strong. With respect to the grass cover the indication on erosion was that start of damage was close, but had actually not fully been reached. The validation had to be done on this criterion.

Analysis of the cumulative overload for the pilot test at Tholen showed that for wave overtopping as well as wave run-up, a critical velocity of 5 m/s described the damage, using $\alpha_1 = \alpha_2 = 1.0$. In both tests the transition in the slope was tested and the α -values should be a little different from 1.0. For both tests $\alpha_2 = 0.9$ and $\alpha_1 = 1.1-1.3$ apply with a critical velocity of 5.5 m/s to 6 m/s. As the outcome for the wave overtopping as well as the wave run-up test was similar, these tests validate to some extent the method for cumulative overload for wave run-up. But it was not based on the criterion of failure.

The tests at the Zeelandbrug only showed erosion close to start of damage. Based on this criterion only, it was concluded that the critical velocity of the grass slope was $U_c = 8$ m/s, using $\alpha_2 = 1.0$ and $\alpha_1 = 1.05$. The run-up test where also overtopping was generated, showed that for the overtopping conditions a critical velocity of at least 7 m/s should be present for the landward slope, as no damage at all was found. The problem is that these critical velocities are only based on no or hardly damage.

The overall conclusion on the pilot test at Tholen and the wave run-up test at the Zeelandbrug is that results show that possibly the method of cumulative overload can also be applied for wave run-up. The analysis did not show contradictions. But the validation is far from conclusive as it could not be based on a damage criterion of failure, but only on no or slight damage.

As it is advantageous to apply a similar method for wave run-up as well as for wave overtopping, a conclusive validation is required. It is therefore recommended to perform again a test series with the wave run-up simulator. With selection of a suitable test location it is necessary to have a steeper transition to the upper slope, a grass cover that is/looks not too strong, and a location that has also objects and/or other transitions. In order to compare directly wave run-up with wave overtopping it is further recommended to do both tests on a similar section. To have both type of tests is very useful for a direct comparison, like at the tests at Tholen.

6 Evaluation of tests with regard to pressure gradients over the grass sod

6.1 General

On both the landward and seaward slopes, the current of overtopping and run-up waves cause pressure fluctuations or pressure gradients near the bed. Both at wave overtopping tests (for instance at Millingen a/d Rijn) and the wave run-up tests near Colijnsplaat, pressure measurements were performed both on the slope surface and just below the grass sod. The difference in pressure over the sod results in a pressure gradient, which acts as a force on a piece of sod which can remove it from the slope surface. Pressure measurements from overtopping tests and wave run-up tests were compared to validate whether the cumulative overload model for grass erosion can also be used for the wave run-up zone. If this is the case the load caused by the up rush of a wave should be comparable to the down rush in case of wave overtopping and the down flow of water (after a run up event) should not produce a significant load, compared to the up-rush.

Figure 6.1 shows a simplification of the hydrostatic and fluctuating pressures as function of time. The soil absorbs over pressures (or pressure gradients directed downward) whereas the roots are mainly loaded by under pressures (or pressure gradients directed upward).

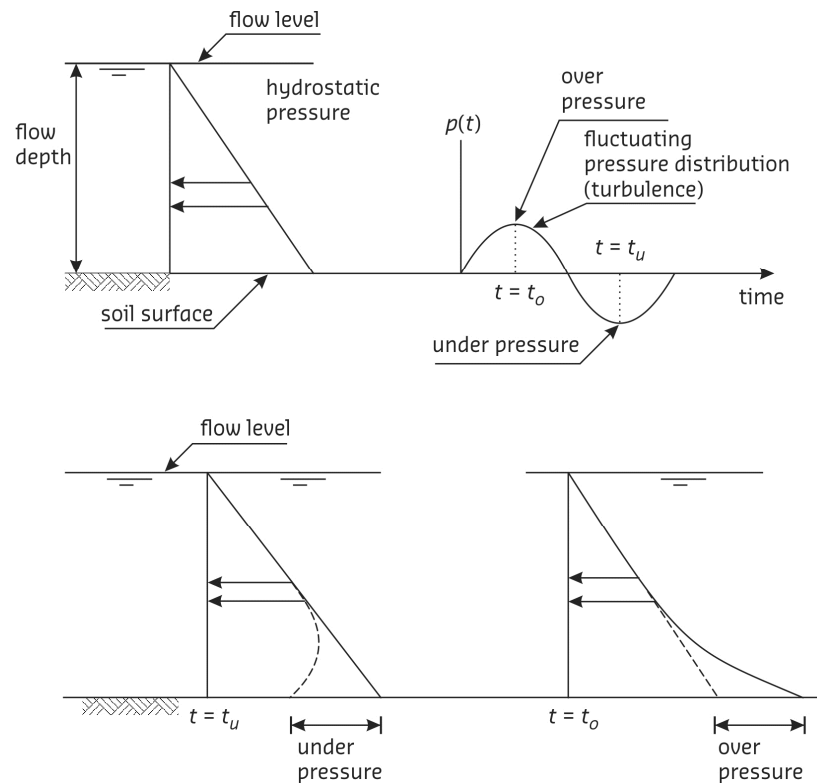


Figure 6.1 Simplification of hydrostatic and fluctuating pressures as function of time

The grass revetment consists of roots, clay and/or sand. As no information is/was available of the load penetration in cohesive soils experimental research and desk studies are carried out. The load on grass revetments and the load penetration in the soil are investigated both in an analytical and experimental way in order to evaluate the assumptions in the turf-element model (WTI-2013).

Sections 6.2 and 6.3 discuss the experimental results of the load penetration owing to bed turbulence in both gravel beds (laboratory tests) and grass revetments (prototype tests). Soil parameters are determined from grass sods taken from the test location in Millingen aan de Rijn. Section 6.4 presents the soil properties which are used as input parameters for the model PLUTO. Section 6.5 gives the results of the computed load penetration with PLUTO and section 6.6 provides conclusions.

6.2 Laboratory pressure measurements

The magnitude of the outward directed pressure gradient represents the measure of grass erosion on a slope, at transitions of revetments and near objects on dikes. The near-bed turbulence energy (k_b) (or turbulent kinetic energy close to the bed) represents the magnitude of the maximum pressure fluctuation (p_m) (or the maximum upward or downward pressure gradient). Emmerling (1973) examined the instantaneous structure of the wall pressure under a turbulent flow in air and found $p_m \approx 6\rho k_b$ (with ρ is the density of water). Following Nezu (1977) this relation is also valid for supercritical flow in water (say Froude number is greater than 2).

Physically, the local turbulence energy (k) is characterized by measured local flow velocity fluctuations (RMS). As pressure fluctuations are related to flow velocity fluctuations they are also correlated to the turbulence energy. Klar (2005) measured the flow velocity fluctuations with a laser Doppler anemometer in the open pores of the filter layer. Figure 6.2 shows that near the bed (at $z/d_{f50} = 0$) the turbulence intensity ($k_b/(u_*^2)$ with u_* is the bed shear velocity) is at maximum (= 100%). For non-cohesive materials the load penetration into the soil decreases significantly with the depth. Measurements of Klar (2005) demonstrate that for gravel with a mean grain size of 1 cm the dimensionless turbulence energy ($k_b/(u_*^2)$) is about 10% at five times the grain size (i.e. at $z/d_{f50} = -5$). Hence, at 5 cm below the ground surface the load acting on gravel may be neglected. This reduction of the pressure fluctuation will probably be even more for sand or clay.

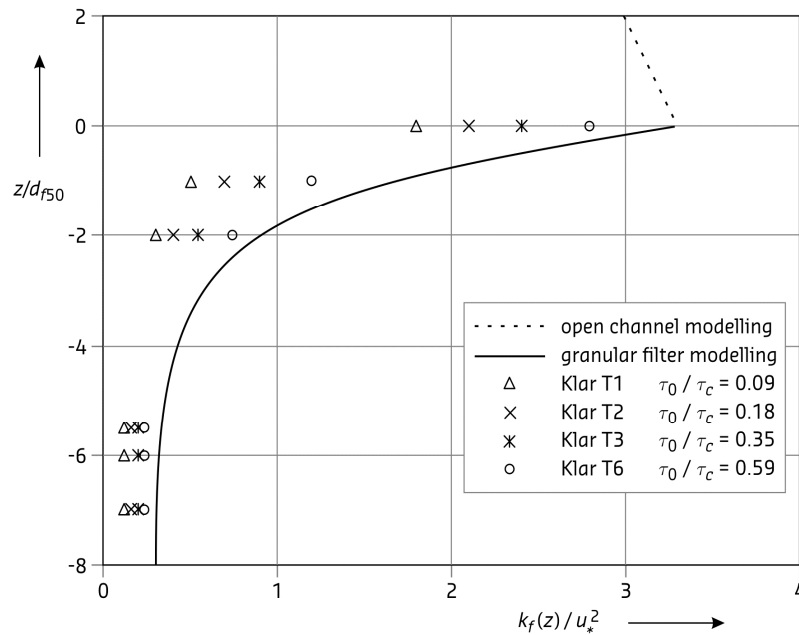


Figure 6.2 Dimensionless load versus relative depth (Klar 2005)
 (τ_0 is the bed shear stress and τ_c is the critical bed shear stress)

6.3 Field pressure measurements

6.3.1 Rivierenland

In Millingen aan de Rijn pressure fluctuations (or pore pressures as function of time) were measured at two locations approximately halfway the landward slope, thus four sensors: two at the surface and two below the surface (at 7 cm and at 11 cm). The distance between the recorder instruments (Fig. 6.3) was about 5 m. At the ground surface and at about 10 cm below, pressure sensors measured signals with a frequency of 100 Hz. As the wave period is about 10 s the total number of samples is 1000 per wave. These tests were carried out for different wave volumes. Before the pressure cell was positioned below the surface the soil in the inclined hole was carefully removed.

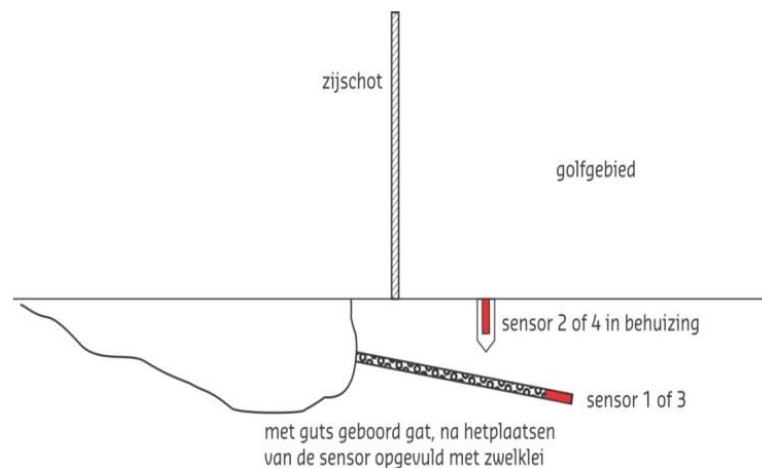


Figure 6.3 Pressure sensors

Figure 6.4 shows the measured pressure fluctuations at the ground level and the measured pore pressures in the soil for an overtopping wave with a volume of $V = 5,000\ell$, see also WTI-2013 where more details of the experimental results are shown.

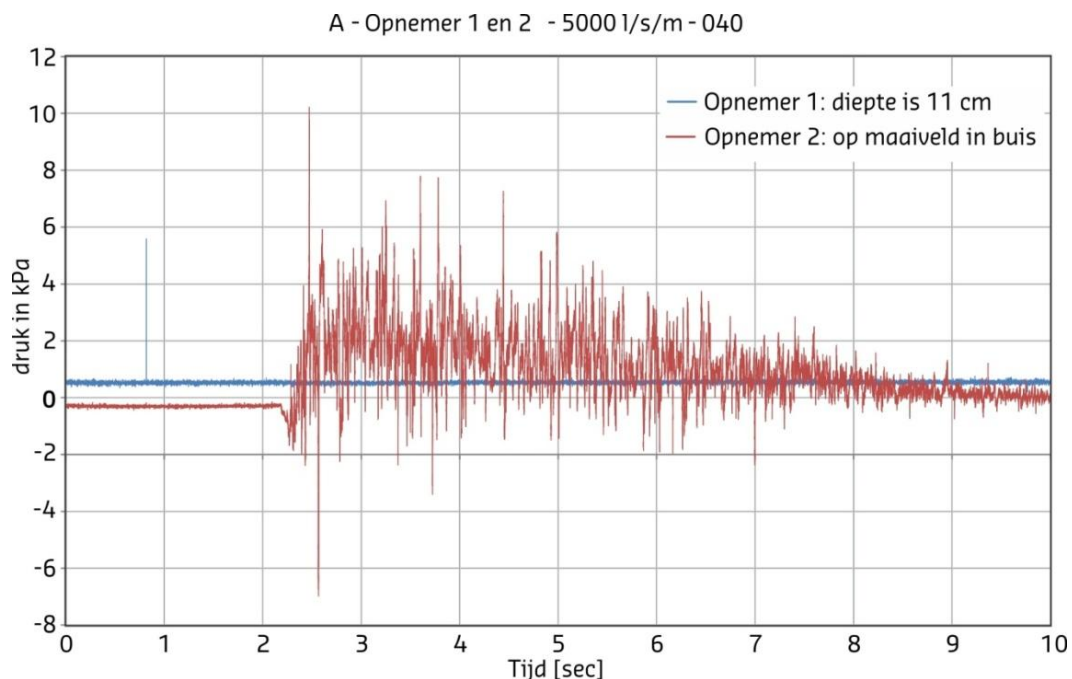


Figure 6.4 Pressure distributions as function of time at the surface and about 10 cm below for $V = 5000 \ell/s$ per m (Location A; series 2; wave overtopping)

At about 10 cm below the surface, the measured pore pressures varied from 0 kPa to -7.5 kPa. When the experiments in Millingen aan de Rijn started the measurements showed that the pore pressures were about -7.5 kPa with a small response. Most likely, the suction pressures were active when the soil was not wet enough. Later, when the soil was saturated (probably fully saturated) the suction pressures increased to zero (thus p_w increased from -7.5 kPa to 0 kPa during the experiment).

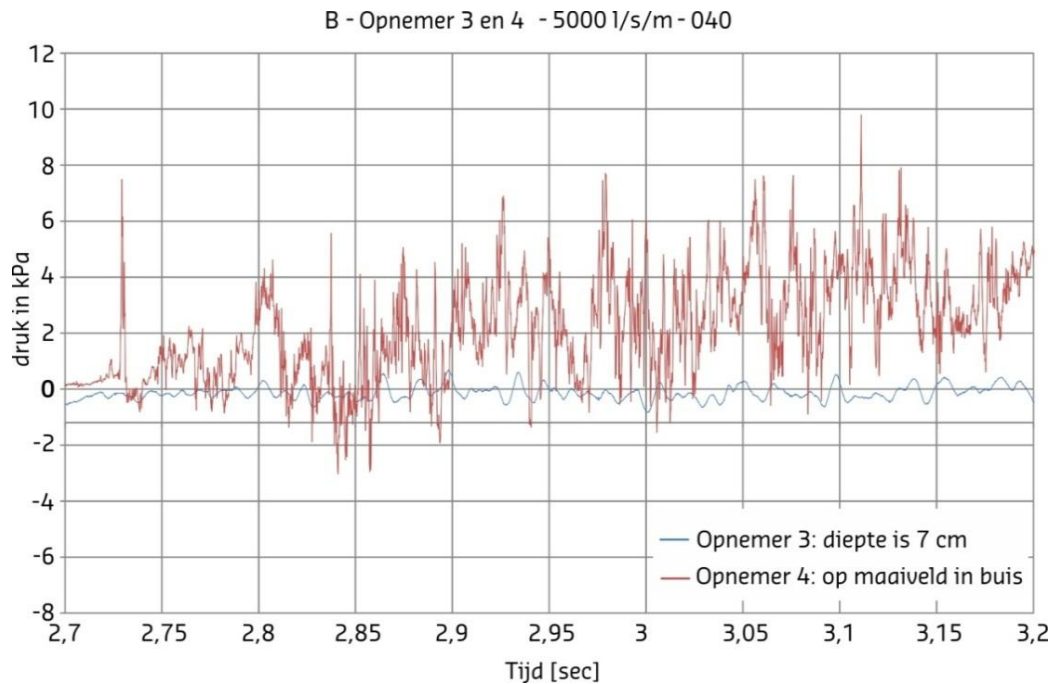


Figure 6.5 Pressure distributions as function of time at the surface and about 10 cm below for $V = 5000 \text{ l/s per m}$ (Location A; series 2)

The measurements also show that there is hardly a correlation between the pressure fluctuations at the ground surface and at 10 cm below (see also Fig. 6.5). Moreover, the amplitude at 10 cm depth is marginal. Hence, the load at this reference level is mainly determined by the suction pressures, which is dependent on the local soil properties and not by the bed turbulence at the ground surface.

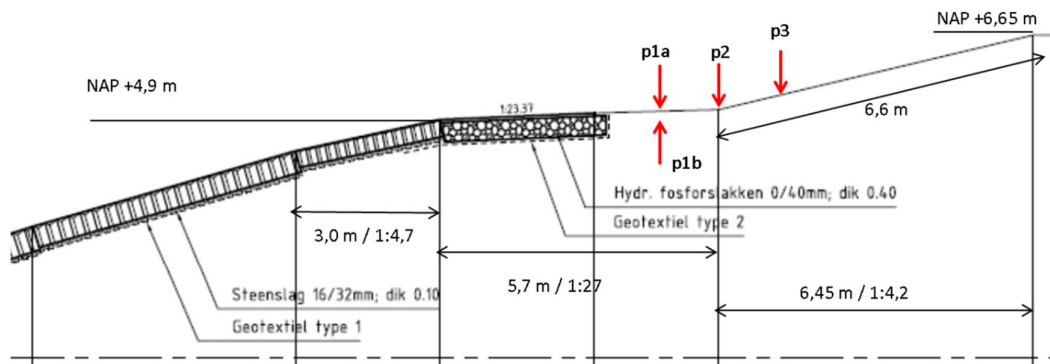
If a wave volume of $V = 5000 \text{ l}$ is considered halfway the landward slope then the flow depth and the flow velocity are about $h = 0.25 \text{ m}$ and $U = 8 \text{ m/s}$ (see also WTI 2013). The pressure period (T) of the largest eddies with the highest energy varies from 0.01 s to 0.05 s for super critical flow as can be seen in Fig. 6.5. Usually such eddies have a length scale which equals the flow depth. Hence, if these eddies are advected with the mean flow, then the time interval for it to pass is given by $T = h/U$. By using $h = 0.25 \text{ m}$ and $U = 8 \text{ m/s}$ it follows that $T = 0.03 \text{ s}$. This value of the pressure period near the bed is used to determine the load penetration with PLUTO (section 6.5).

6.3.2 Noord-Beveland (Colijnsplaat)

In the winter period 2013/2014 the pressures as function of time were measured at four locations due to wave run-up (and wave down-run) on the seaward slope of a dike section near Colijnsplaat. The bed turbulence was determined at three locations (locations p1a, p2 and p3; Fig. 6.6). At one location the over and under pressures were measured at about 10 cm below the surface (location p1b; Fig. 6.6).

Figure 6.7 shows the pressure fluctuations near the surface for a fill level of 7.3 m. The front velocity was about 7 m/s which value is comparable as observed in the wave overtopping tests with $V = 5 \text{ m}^3$. The tests carried out in Colijnsplaat represent the pressure characteristics

of wave run-up. Although there are differences between wave run-up and wave overtopping they are marginal. If the front velocity lies in the range of 7 m/s to 8 m/s then the maximum pressure fluctuation is about 10 kPa in both cases (see also Fig's. 6.4 and 6.7).



p1a, p2 en p3: drukmetingen op het taludoppervlak
 p1b: drukmeting vlak onder het taludoppervlak (ca. 10 cm diepte, geboord vanaf zijkant buiten de strook)
 Vergelijkbaar met metingen Millingen
 Uitvoering Deltares, Enno van Waardenberg

Figure 6.6 Locations of pressure sensors on the seaward slope. Wave simulator is located at horizontal berm

Most likely the measurements at p1a and p1b were influenced by vibrations of the wave overtopping simulator (Fig. 6.7) when the water was released from the reservoir. The pressure periods measured at p1a and p1b are very small (about 2 msec.; Fig. 6.7) with respect to the measured pressure period at p2 (about 30 msec.; Fig. 6.8). If the higher frequencies of the p1-signals are neglected then computational results show that the maximum and minimum values decrease significantly which seems not realistic. Therefore, these signals are not used in the analysis.

At location p2 the pressure period varies from 10 msec to 50 msec which is comparable to the representative period measured in the wave overtopping tests with $V = 5 \text{ m}^3$ (see also Fig. 6.5). There is more to evaluate. The maximum pressure fluctuations are at maximum for the wave run-up. Although a maximum is reached for the wave run-down this maximum is significantly smaller than the peak for the wave run-up. Therefore, the load contribution due to the wave run-down can be neglected (see the green curve in Fig. 6.7).

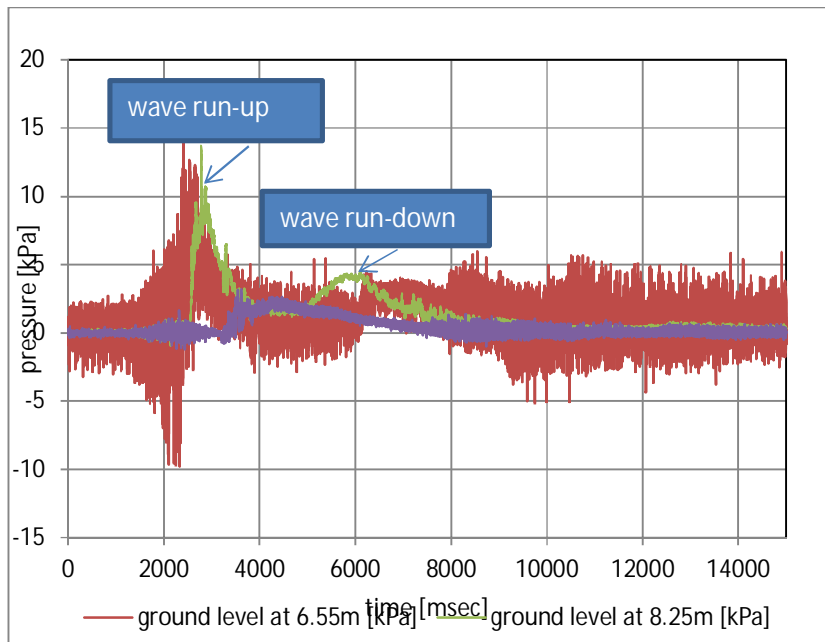


Figure 6.7 Pressure fluctuations at the surface for three locations (p1a, p2 and p3)

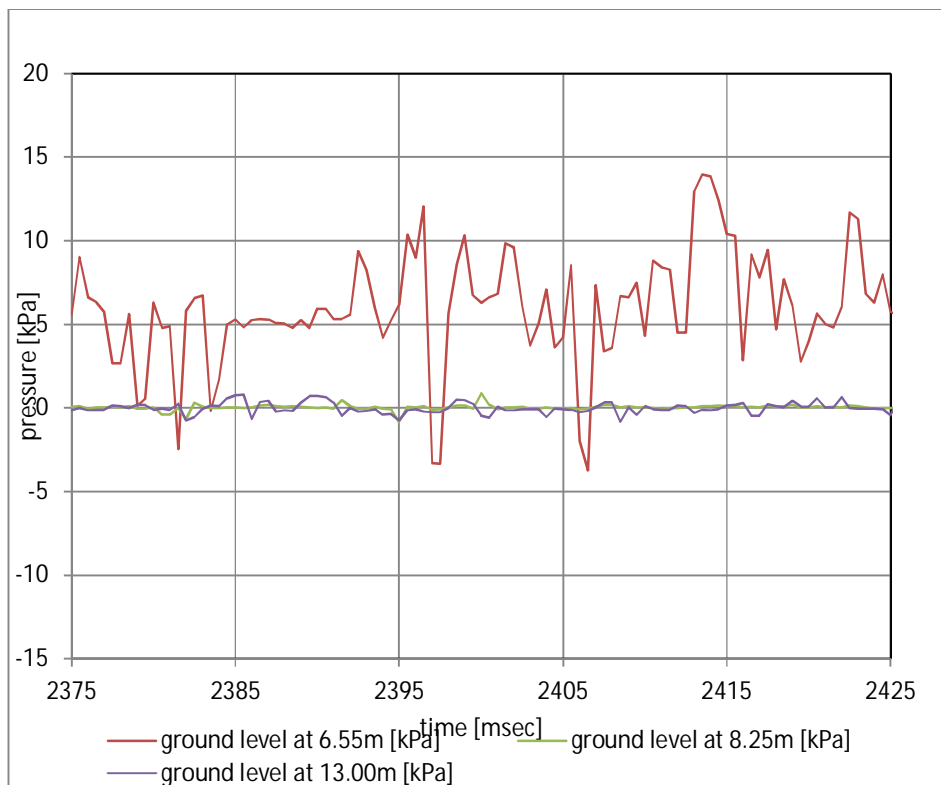


Figure 6.8 Estimated pressure period is about 2 msec at ground level at 6.55 m

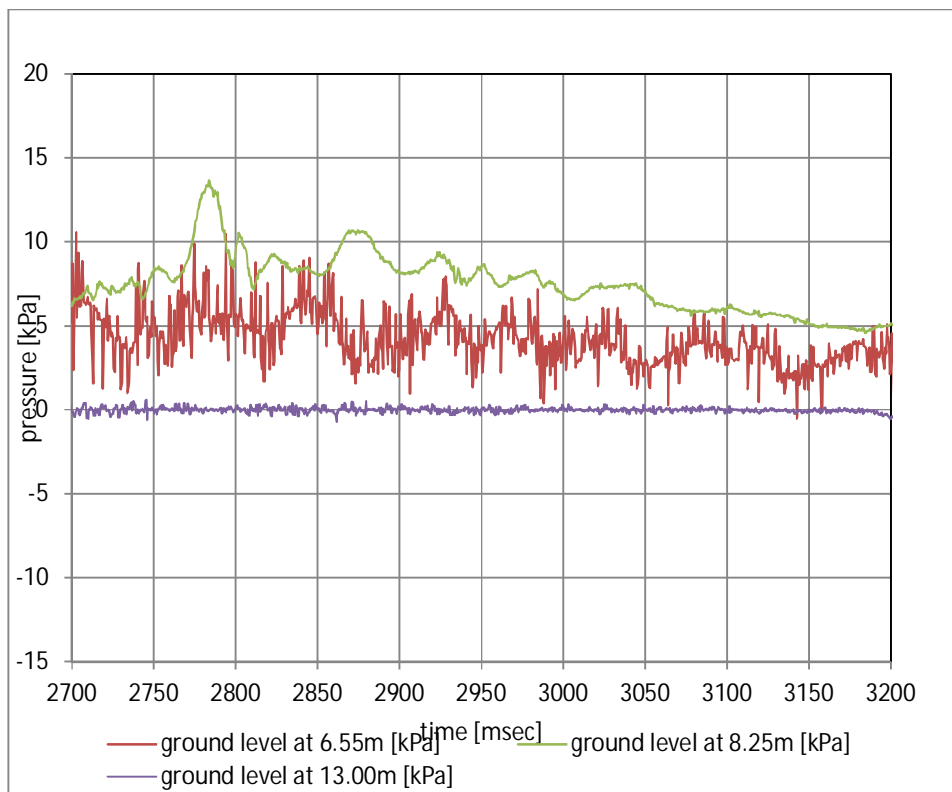


Figure 6.9 Location p2 (ground level at 8.25 m) the pressure period is about 30 msec

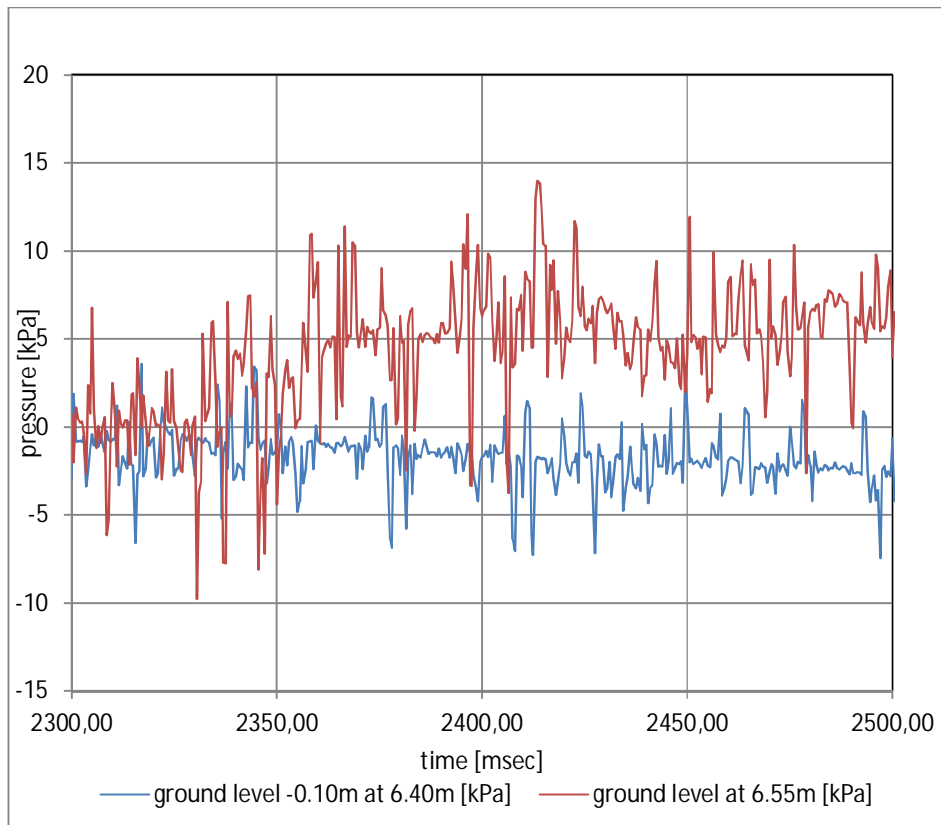


Figure 6.10 Measurements at $p1a$ and $p1b$ are influenced by vibrations of the wave simulator. Therefore, they are not used in the analysis

6.4 Soil properties

The soil properties in the upper 10 cm are characterised by the soil structure, fissures, roots and worm holes. To determine soil parameters just beneath the slope surface, turf samples were taken from a dike along the river Rhine near Millingen (Greeuw 2013). The following soil parameters are experimentally determined, namely the hydraulic conductivity (K), the bulk density of soil (ρ_n), the one-dimensional stiffness parameter (M with dimensions of Pa) ($M = E_{oed}$ is the oedometric modulus of deformation or $M = 1/m_v$ where m_v is the coefficient of volume compressibility). The consolidation coefficient (c_v) is computed by using the Terzaghi formula (e.g. Barends 1992)

$$c_v = \frac{KM}{\rho g} \quad (6.1)$$

where g is the acceleration of gravity. The resulting values of the hydraulic conductivity (20 °C) are $K = 2.1 \cdot 10^{-4}$ m/s (test 1) and $K = 1.7 \cdot 10^{-4}$ m/s (test 2). For a field temperature of 10 °C, a multiplication factor of 0.8 has to be applied as the kinematic viscosity of water is higher and thus the hydraulic conductivity is lower at lower temperatures. After the permeability tests the samples were dismounted and weighed. The bulk densities of the saturated samples are $\rho_n = 1500$ kg/m³ (test 1) and $\rho_n = 1430$ kg/m³ (test 2).

Dynamic load tests were conducted in order to determine the stiffness parameter of turf, see Fig. 7 where the soil sample is shown. Substituting the aforementioned values of K and an averaged value of the stiffness parameter $M = 150$ kPa in Eq. 6.1 yields $c_v = 3.4 \cdot 10^{-3}$ m²/s (test 1) and $2.6 \cdot 10^{-3}$ m²/s (test 2). This range of the consolidation coefficient is used for calculating the load penetration with the mathematical model Pluto (see also Section 6.5).



Figure 6.11 Preparing the bottom side by picking off clay parts and application of gravel layer

Based on a one-dimensional approach, Barends (1992) (see also De Groot et al. 1996) deduced for the characteristic length (L) of the effect of consolidation under cyclic loading

$$L = \sqrt{\frac{c_v T}{2\pi}} \quad (6.2)$$

By using a vertical consolidation coefficient of $c_v = 0.8 \times 3 \cdot 10^{-3} = 2.4 \cdot 10^{-3}$ m²/s (where the factor 0.8 represents a correction for the field temperature 10⁰ C) and a pressure period of $T = 0.03$ s (corresponding to super critical flow) the characteristic length is $L = 0.33$ cm. Hence, the measured pressure variations at 5 cm depth are marginally influenced by the effect of cyclic consolidation and thus one of the assumptions made in the turf-element model is correct, i.e., the load can be considered as acting on the surface (and not on the side walls). This corresponds with measured load penetrations in non-cohesive material (see Section 6.2).

6.5 Pluto calculations

PLUTO is a finite elements program designed for deformation analysis by using non-linear stationary algorithms and consolidation analysis by using quasi-static or time dependent algorithms. The geotechnical problems, which can be solved with this program, include elastic and/or plastic deformation analysis, groundwater flow and the combination of these for consolidation analysis (Teunissen 2010).

For problem schematisation purposes the soil can be constructed by using multiple layers or material groups. Each layer or group can be defined with its own constitutive model and appropriate stiffness and strength parameters. The problem can be defined by either prescribed displacements or by loads. To simulate bed turbulence on the slope of dikes as a result of waves the following starting points are made:

- Grid domain is 0,5 m long and 0,3 m deep.
- Grass shear stresses are excluded (thus the effects of roots along the side walls are neglected). In other words, a free-slip condition is used along the side-walls.
- Horizontal groundwater flow is not modelled.
- Effects of turbulence are modelled by a sinusoidal pressure function with an amplitude of $p_m = 5$ kPa.
- Young's modulus is 200 kPa.
- Hydraulic conductivity (in the vertical direction) is $K = 0.0002$ m/s.
- Front velocity varies from 1 m/s to 10 m/s.
- Pressure period representing the bed turbulence is $T = 0.03$ s.
- Pressure fluctuations caused by the flow act on the soil.
- Bulk density measures $\rho_n = 1500$ kg/m³.
- Porosity is estimated to be $n = 0.4$.
- Compressibility of water (β) is $2.0 \cdot 10^{-4}$ (kPa)⁻¹.
- Poisson ratio (ν) is 0.4.

Figure 6.12 shows computational results of Pluto where the effective fluctuating soil stress is given as function of the vertical coordinate. The maximum value of the effective fluctuating soil stress is 5 kPa and occurs near the surface. At 5 cm depth the effective fluctuating soil stress varies from 0 kPa to 1.5 kPa (for 1 m/s < front velocity < 10 m/s). At 12 cm depth the effective fluctuating soil stress is less than 0.5 kPa. If traveling waves are included in the calculations (thus if the effects of both dp/dx and dp/dt are taken into account) then the load penetration is somewhat faster. Therefore, the decrease of the load penetration at 10 cm is less than 10%. This corresponds with the field test results.

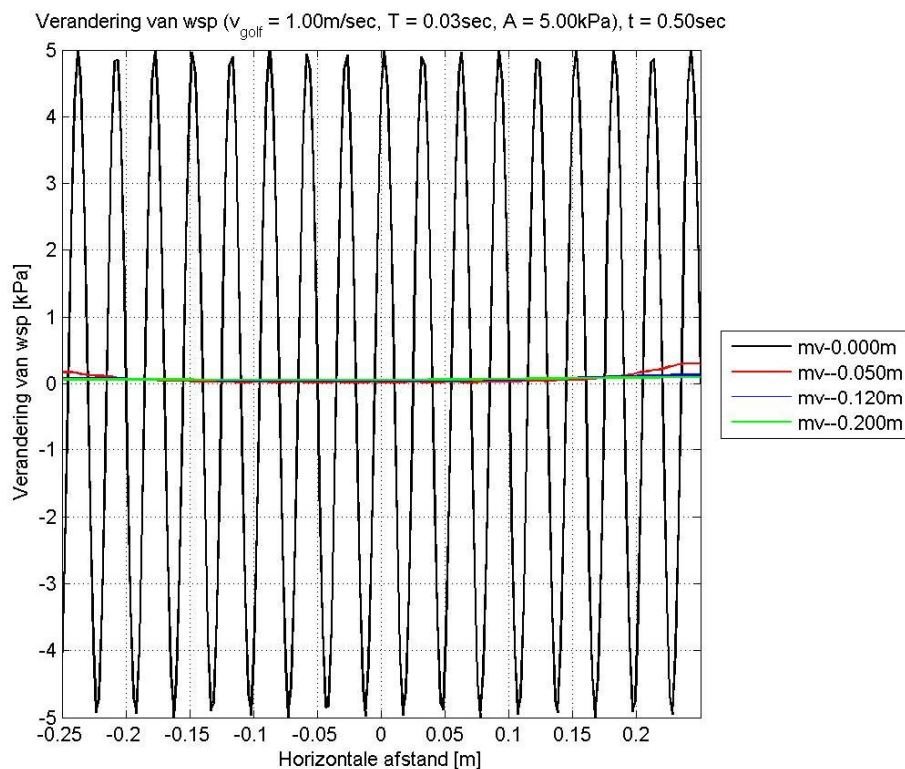


Figure 6.12 Fluctuating pressure as function of time; front velocity is 1 m/s

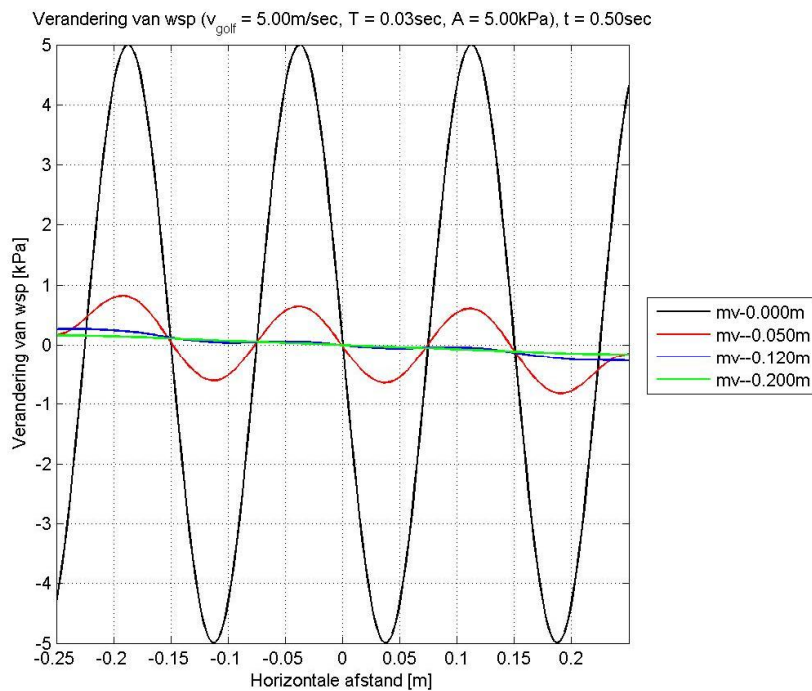


Figure 6.13 Fluctuating pressure as function of time; front velocity is 5 m/s

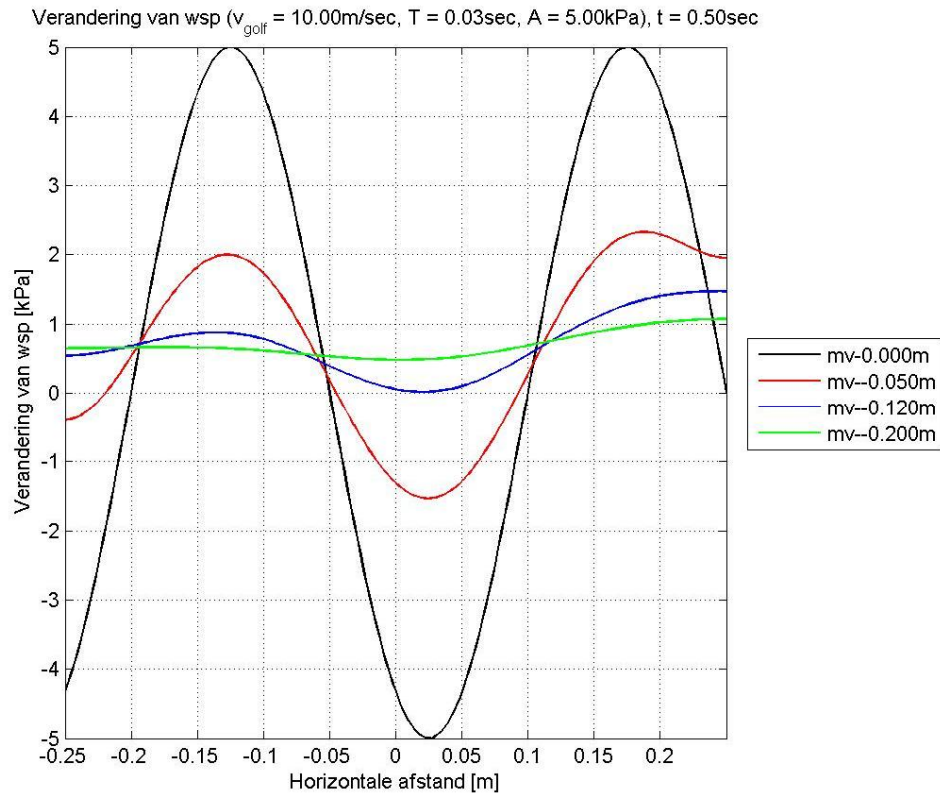


Figure 6.14 Fluctuating pressure as function of time; front velocity is 10 m/s

6.6 Conclusions

Measurements and PLUTO-calculations show that the pressure fluctuations decrease significantly with depth as the bed pressure fluctuations depend on both time and place. If the contribution to the fluctuating soil stresses at about 10 cm below is negligible or if the soil stress is determined by the suction pressures which is dependent on the local soil properties then the damping of the load penetration is very fast. Hence, the starting points made in the Turf-element model are correct, that is the load acts mainly on the top of grass sods (Hoffmans et al. 2008, 2010). The load acting on the side walls is marginal.

This study also shows that the load of the run-down is negligible with respect to the load of the run-up. The relative load is about 30%, thus the load reduction is about 70%.

7 Evaluation of tests with regard to the grass pull out strength versus critical velocity

7.1 Introduction

In February and March 2014, wave overtopping tests (see also chapter 4; section 4.3.12) and turf-tensile tests were carried out in Colijnsplaat to determine the strength of grass revetments. By using the cumulative overload method and the turf-element model (WTI-2013; see also Hoffmans 2012 for more details of the modelling) this strength can be expressed by a critical (depth-averaged) flow velocity.

By applying the cumulative overload method the critical flow velocity can be calculated provided the flow velocities representing the load of the overtopping waves and the definitions of the damage on the grass revetments are known. This critical value is related to a grass area of about 50 m² as the dimensions of the test sections on the slopes of the dikes measured 4 m wide and 10 m to 15 m long. Hence, the critical flow velocity computed with the cumulative overload method represents a lower limit.

If the tensile force is measured then the critical flow velocity can also be calculated by using the turf-element model. This chapter discusses briefly the results of 24 tests in which the tensile force acting on a grass sod with dimensions of 15 cm x 15 cm was measured (see also Infram 2014). Both rapid tests (one load cycle and fatigue tests (about 100 load cycles) were conducted in which the force transmission was determined twofold. The experimental results of the fatigue tests are compared with results obtained from the fatigue curve of pine heartwood. In the analysis the spread of the critical flow velocity is discussed. Moreover, some recommendations are made for future research.

7.2 Performance of turf-tensile tests

On the seaward slope, two test strips were selected with a width of about 5 m. The horizontal distance between strips A and B measured 14 m. These strips were located near dike mark 1791 close to the Zeelandbrug near Colijnsplaat (Fig. 7.1). Before the experiments started, the grass cover was mown and infiltrated with water from the Eastern Scheldt for about one hour. Therefore, cracks in the top layer are considered to be completely saturated.

Up to 8 cm depth the soil was always excavated on two opposite side walls (Fig. 7.2). Pins were inserted through a pull frame at approximately 4 cm below the surface of the turf (Fig. 7.3). The grass sods were tested in two different ways. The soil at the other two sides was either intact (condition-2) or also cut to a depth of 8 cm (condition-4). Consequently, for this type of test the side walls do not contribute to the shear strength (see also Fig. 7.2). The pulling was done with a hydraulic cylinder and a manually operated hydraulic pump with a rotary handle (Fig. 7.4).

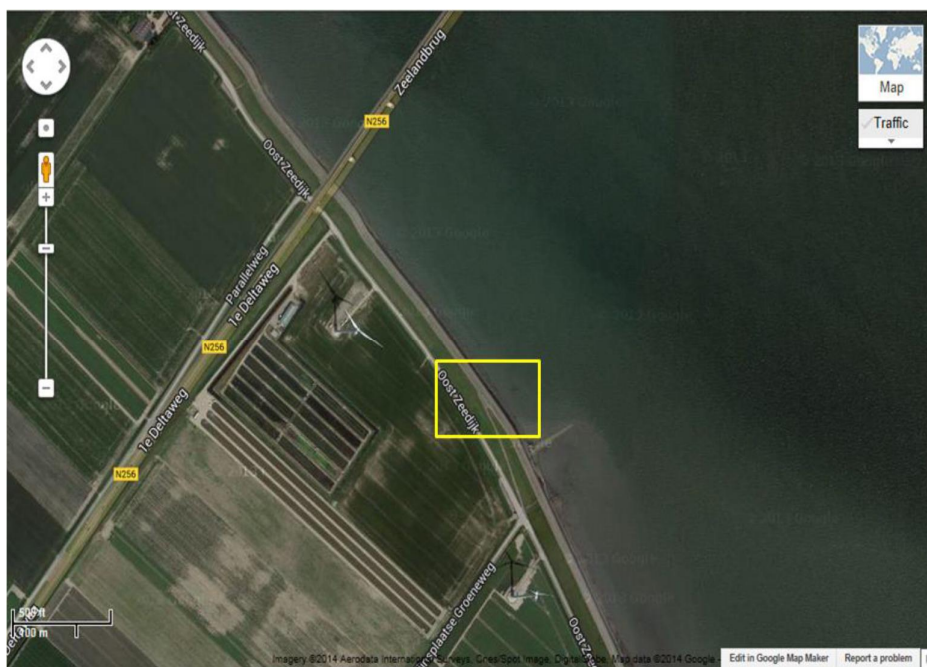


Figure 7.1 Test site of the turf-tensile tests



Figure 7.2 Tested grass sod



Figure 7.3 Pull frame



Figure 7.4 Turf-tensile apparatus (pull frame is inside the apparatus)

Twelve locations were chosen arbitrarily on both strips. At strip A, six locations were located on the slope, two near the toe and four close to the crest. At strip B, twelve locations were selected randomly on the slope and at the berm. At this strip the vegetation varied significantly, i.e. the grass was both short and tall. Occasionally there was locally no

vegetation and sometimes there were individual grass sods with and without moss. At strip B, the grass cover was also damaged by tracks at the toe of the dike which may give a large variation in the tensile strength (see also section 7.4).

On each strip, two different tests were performed 1) rapid tests and 2) fatigue tests. For the rapid tests, the tensile force and the corresponding deformation were measured until all roots failed, i.e. roots could either break or could be pulled up. The rapid tests were used as a benchmark for the fatigue tests. Fatigue tests were performed at ca. 80% of the maximum resistance from the rapid test. Both the rapid and the fatigue test give information about the failure and fatigue characterization of the root-soil system. For both tests the tensile forces and deformations were recorded as function of time by applying a force measuring sensor and a displacement sensor respectively. These experimental results were stored in a data logger. As this device had no monitor function the tensile forces were determined directly from an electronic spring balance, otherwise the fatigue tests could not be performed.

On both strips, eight rapid tests were carried out. In four of the eight tests, the measurement was performed on a grass sod in which two sidewalls (condition-2) were loosened. In the remaining four tests, all sidewalls (condition-4) were cut off. Figure 7.5 demonstrates for Test 3A the force and deformation as function of time respectively. The deformation as function of the force is also shown in Fig. 7.5, see appendix G Experimental results force and displacement (grass sods) where all experimental results are graphically summarized.

In the fatigue tests, the grass sod was pulled up with an imposed tensile force. This force was about 75% of the averaged value of four maximum tensile forces observed from the rapid tests. Subsequently, the imposed tensile force reduced to zero. These loading steps were repeated about 100 times unless the grass sod was torn out (Fig. 7.6). Four fatigue tests were carried out on one strip. Also the fatigue tests consisted of two different conditions (conditions 2 and 4).

To simulate the fatigue of grass the tensile force was reduced by using the material properties of pine heartwood (WTI-2013). Therefore, the chosen factor of 0.75 has to be considered as a first estimation of the reduction for the strength of grass after 100 load cycles and thus it is recommended to validate this factor in greater detail (see also section 7.5). Totally, 24 tests were carried out; see also Table 7.1 where a summary of the tests is given.

Type test	Number of load iterations	4 sides loose	2 sides loose	Number of tests
Rapid test	1	8	8	16
Fatigue test	About 100	4	4	8

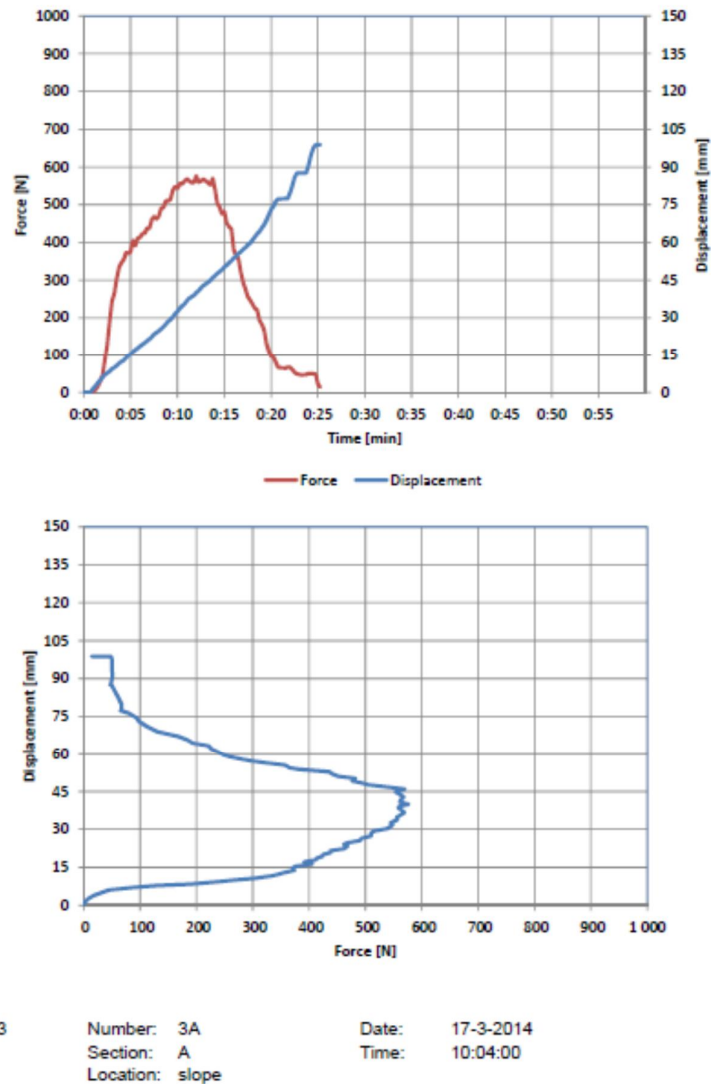
Table 7.1 Overview of the tests

7.3 Root investigation

In February 2014 Alterra investigated the grass quality of some test sections (Fig. 7.1) (see also Infram 2014). The general visual appearance of the grass revetment at the test locations was continuous and slightly tussock, that is, there were no pronounced damages. However, signs of mole and vole activity were observed. Furthermore, many dog excrements were found on the test location. Some mowing litter had remained present on the test location.

The visually estimated sod cover was very high. At the tested sections the sod cover varied from 95% to 98%. Based on the gouge auger method the estimated root density ranged from

moderate to high. According to the so-called spade method the root density of all the test sites was classified as closed. Although the measurements were performed on the visually weakest spots the general conclusion is that the grass revetment at the test location is of good quality. The next section provides more information regarding the calculation method of the critical flow velocity.



3 Number: 3A Date: 17-3-2014
 Section: A Time: 10:04:00
 Location: slope

Figure 7.5 Experimental results of Test 3A; Force and displacement as function of time (above); Displacement as function of the force (below)

7.4 Analysis

The maximum deformation of turf is extremely high, which lies in the range of 5 cm to 10 cm. The measured tensile force reaches its maximum value after 2 cm to 3 cm. In the rapid tests the grass sod was deformed gradually until the grass sod failed completely. In these tests the grass sod was pulled up with a constant speed of order 0.5 cm/s (see also Fig. 7.5).

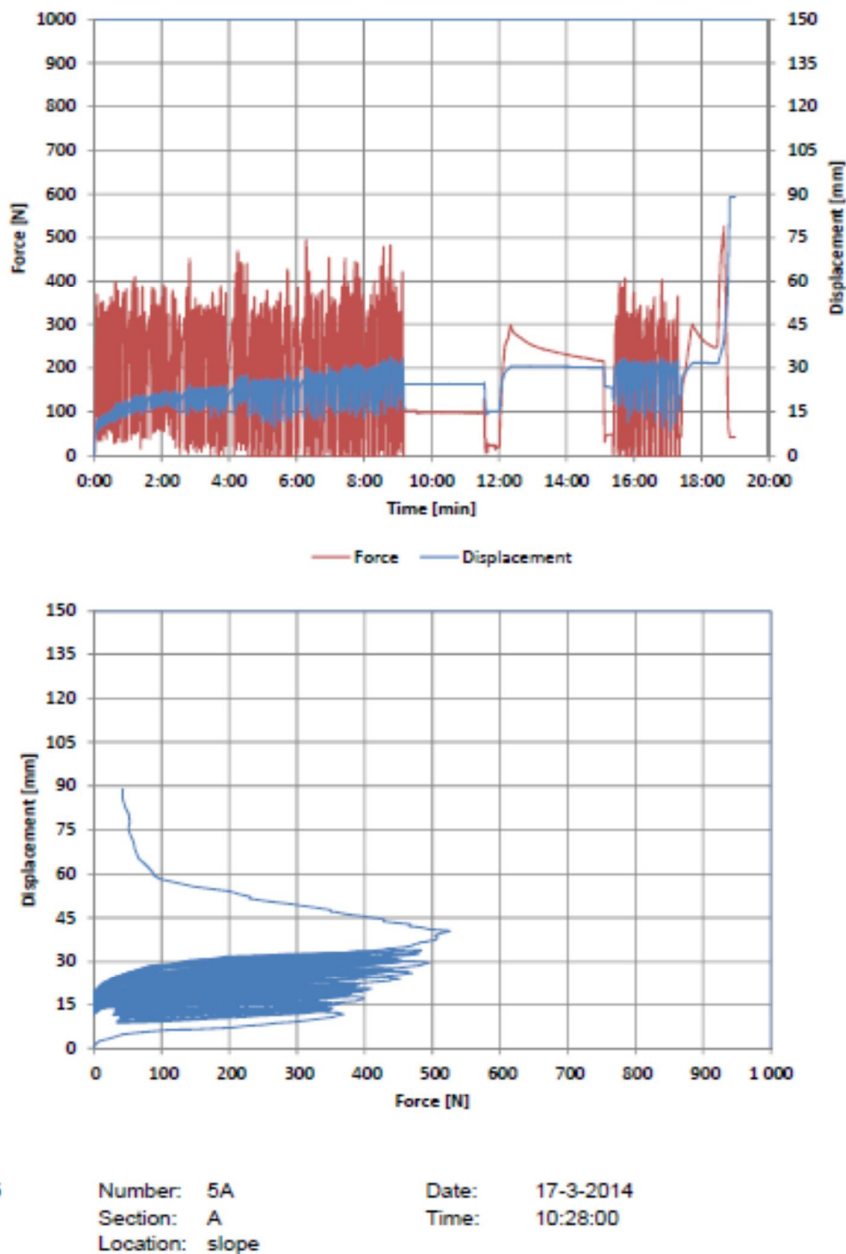


Figure 7.6 Experimental results of Test 5A; Force and displacement as function of time (above); Displacement as function of the force (below)

Also fatigue tests were performed to analyse the elastic and plastic behaviour of turf (see also Fig. 7.6). In these experiments the loading and unloading were repeated about 100 times. Based on the fatigue curve of pine heartwood (Fig. 7.7), which is the material close to grass roots on which fatigue tests are reported, failure of the grass sod is expected to occur if the

strength is reduced with a factor of approximately 0.75. However, measured and predicted tensile forces are not always in agreement. The differences are discussed below.

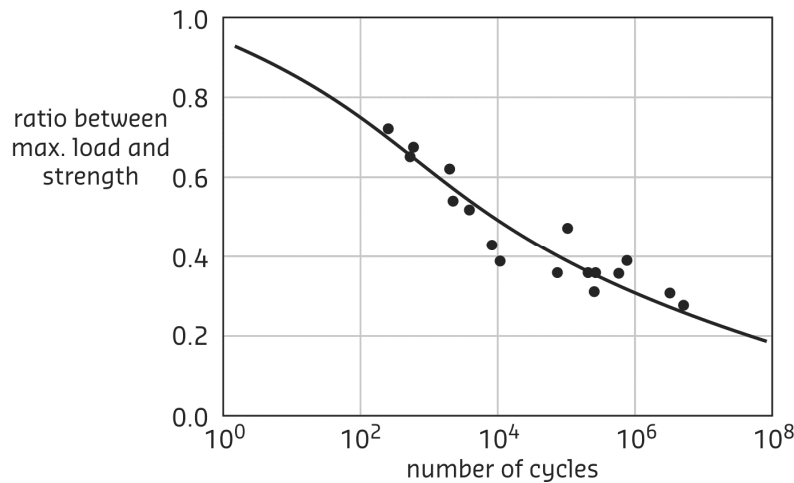


Figure 7.7 Fatigue curve of pine heartwood (Kollman and Côté 1968)

During the testing of the individual grass sods both small and large tensile forces were observed. Figures 7.8 and 7.9 show the measured tensile forces of both the rapid and fatigue tests. In addition, three curves are drawn representing the upper limit, the best guess value and the lower limit of the reduction strength of pine heartwood. Note that at present no fatigue curve for grass or roots is available (see also section 7.5).

For the condition-4 tests (no side walls) the mean value of the measured tensile force is 455 N (Table 7.2). The lower and upper limits were 380 N and 640 N respectively. Hence, the standard deviation is 96 N and thus the coefficient of variation is about 0.2 (= 96/455). When two side walls were cut off (condition-2) the averaged measured tensile force is higher and measures approximately 670 N (Table 7.2). The lower and upper limits measured 550 N and 1000 N respectively yielding a standard deviation of about 145 N and a coefficient of variation of 0.2 (= 145/670). Consequently, in both series the spread of the experimental results is identical.

Usually for nearly uniform distributed sand the coefficient of variation varies from 0.2 to 0.3. For example, consider fines with a mean particle diameter of $d_{50} = 0.2$ mm and a lower limit of $d_{15} = 0.15$ mm the coefficient of variation is $(0.2 - 0.15)/0.2 = 0.25$. Consequently, the heterogeneity of grass covers and the non-uniformity of sand beds/ripples are comparable. Note that the critical bed shear stress related to sandy beds without dunes/ripples is proportional to the particle diameter (Shields 1936).

On the berm, the difference between the lower and upper boundaries of the measured tensile force is relatively high. These measured forces lie in the range of 291 N (test 24B) to 1320 N (test 11A) as the vegetation on the berm varied extremely. The mean value of the measured tensile force is about 800 N and thus comparable with the mean values as discussed above. However, the coefficient of variation is significantly larger and equals about 0.6.

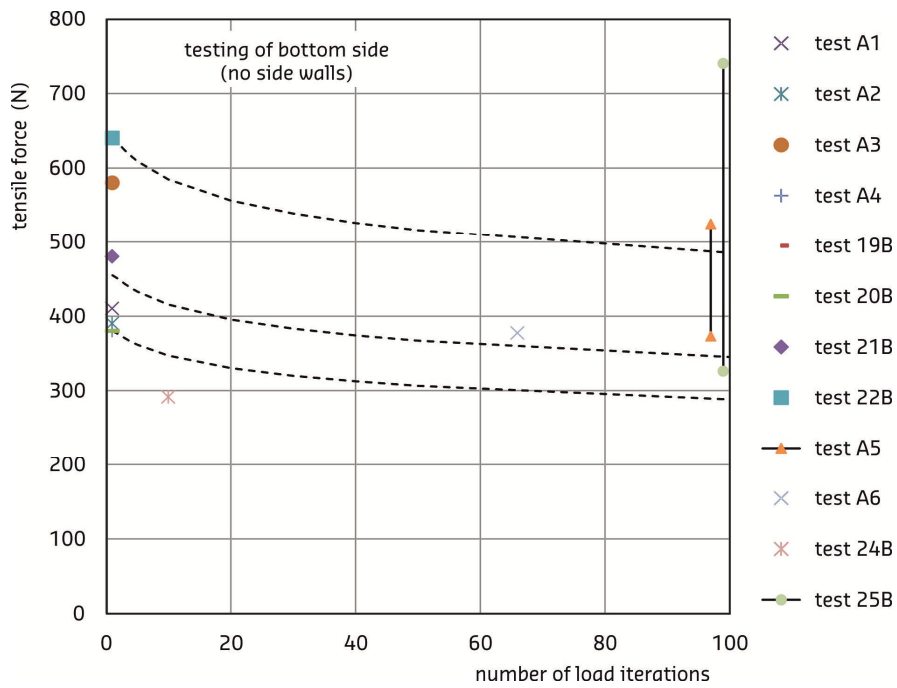


Figure 7.8 Experimental results of the rapid and fatigue tests (two sidewalls were cut off) rapid tests after one load cycle; fatigue tests after about 100 load cycles

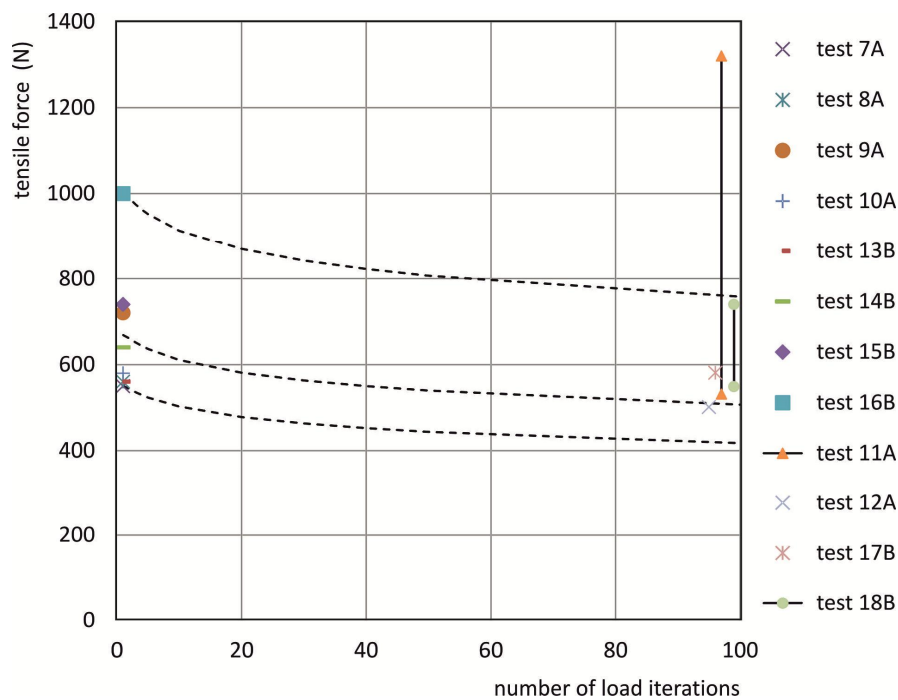


Figure 7.9 Experimental results of the rapid and fatigue tests (two sidewalls were cut off) rapid tests after one load cycle; fatigue tests after about 100 load cycles

Test	Number of cycles	F_{max} (N)		Test	Number of cycles	F_{max} (N)	
Condition-4				Condition-2			
1A	1	410		7A	1	550	
2A	1	390		8A	1	560	
3A	1	580		9A	1	720	
4A	1	380		10A	1	580	
19B	1	380		13B	1	560	
20B	1	380		14B	1	640	
21B	1	480		15B	1	740	
22B	1	640		16B	1	1000	
	F_{ave}	455			F_{ave}	669	
	σ_F	96			σ_F	143	

Table 7.2 Overview of the experimental results (rapid tests)

Test	Number of cycles	F_{max} (N)	F_{imp} (N)	Test	Number of cycles	F_{max} (N)	F_{imp} (N)
Condition-4				Condition-2			
5A	100	525	373	11A	100	1320	531
6A	66	-	377	12A	95	-	501
23B	test failed	-		17B	96		581
24B	10		291	18B	100	740	549
25B	100	740	326				

F_{max} is the maximum tensile force obtained from measurements

F_{ave} is the mean tensile force (based on 8 experiments)

F_{imp} is the imposed tensile force (based on measurements and a reduction factor of 0.75)

σ_F is the standard deviation (based on 8 experiments)

Table 7.3 Overview of the experimental results (fatigue tests)

7.5 Critical flow velocity

The critical flow velocity is related to the critical lift force that acts on the surface level. Hence, the maximum values of the measured tensile forces have to be corrected as the root intensity decreases with the depth. Moreover, for the condition-2 tests also a correction has to be made for the influence of the side walls. The computed values of the critical flow velocity are listed in Table 7.4 for two different storms, namely storms with 500 waves and 3000 waves; see also WTI-2013 where the correction-factors are discussed in greater detail. Based on the rapid wave overtopping tests (note that 'rapid test' is also used to describe the grass pull out test where the sod is pulled in one go), the critical flow velocity varies from 4.4 m/s to 6.4 m/s for a storm with 3000 waves. The mean value and its standard deviation of the critical flow velocity are 5.2 m/s and 0.6 m/s respectively (Fig. 7.9). Note that the range of the computed critical flow velocity is based on crest conditions where the turbulence intensity is about 0.2 (20%). The turbulence intensity r_0 is based on the relations between the Chezy coefficient C , flow velocity U , water layer thickness h and slope S_b ($U = C\sqrt{hS_b}$; $r_0 = 1.2g / \sqrt{C}$). As the front velocity on the seaward slope is about constant for up to 75% of the run-up height, below this level the flow can be considered as uniform. In other words, the flow neither accelerates nor decelerates. Assuming that the turbulence intensity is about 0.15 (15%) a correction factor should be used of $0.2/0.15 = 1.3$ resulting in a critical flow velocity of about

$5.2 \times 1.3 = 7 \text{ m/s}$. This value of U_c agrees with the outcome of the cumulative overload method as discussed in the previous chapters.

Because the average bed shear stress ($1/18 * p_{max}$) is small compared to the maximum lift, the bed shear stress is neglected in the analyses. The bed shear stress can cause transport of small soil particles and small clay aggregates, however the grass sod, e.g. rooted soil, will only fail due to lift forces.

7.6 Conclusions and recommendations

The critical flow velocity calculated by using the turf-element model, in which the tensile force is measured, is about 7 m/s and agrees with the value that is computed with the cumulative overload method. It is recommended to determine the turbulence intensity with the mathematical model Open Foam to validate the turbulence intensity of $r0 = 0.15$ on the seaward slope (see Section 7.5).

Furthermore it is recommended to analyse the following subjects/matters

- 1) Investigate the relevant differences between grass/roots and pine heartwood. Discuss the material properties and determine, e.g., the Young's modulus (or the elasticity modulus) of the tested grass sods and compare these values with the Young's modulus of pine heartwood as this result could provide insight in the fatigue curve of grass. If these Young's modulus's have the same magnitude of order then the fatigue curve of pine heartwood (or an adjusted curve) could be a useful engineering tool for predicting the fatigue strength of grass (see also Fig. 7.10).

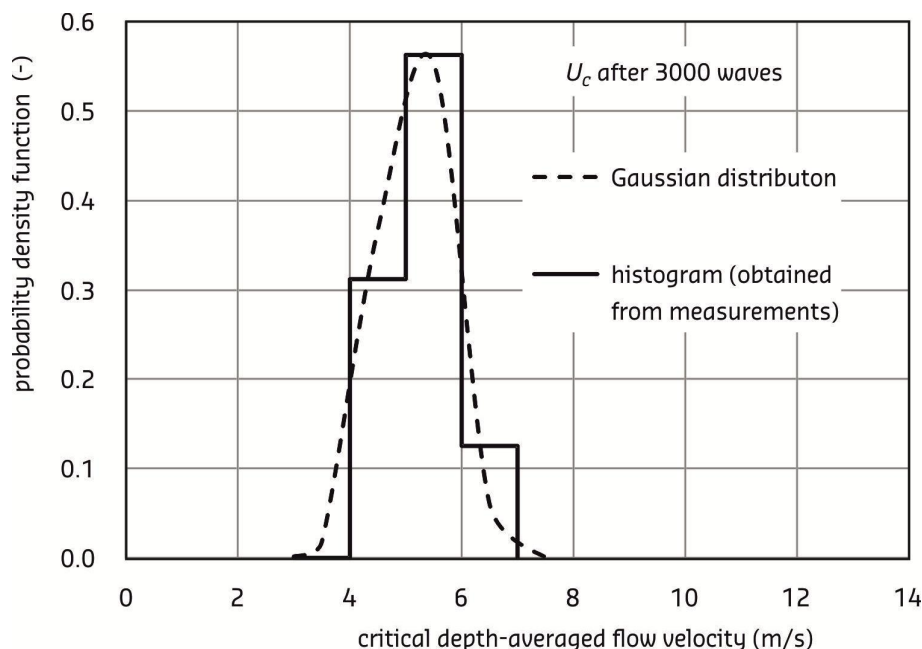


Figure 7.10 Probability function of the critical flow velocity (based on turf-tensile tests)

Test	U_c (after 500 waves) (m/s)	U_c (after 3000 waves) (m/s)
1A	6.0	5.2
2A	5.9	5.1
3A	7.2	6.2
4A	5.8	5.0
7A	5.1	4.4
8A	5.1	4.5
9A	5.8	5.0
10A	5.2	4.5
13B	5.1	4.5
14B	5.5	4.8
15B	5.9	5.1
16B	6.9	5.9
19B	5.8	5.0
20B	5.8	5.0
21B	6.5	5.7
22B	7.5	6.5
Mean value	6.0	5.2
Standard deviation	0.7	0.6

Table 7.4 Critical flow velocity obtained from the turf-element model

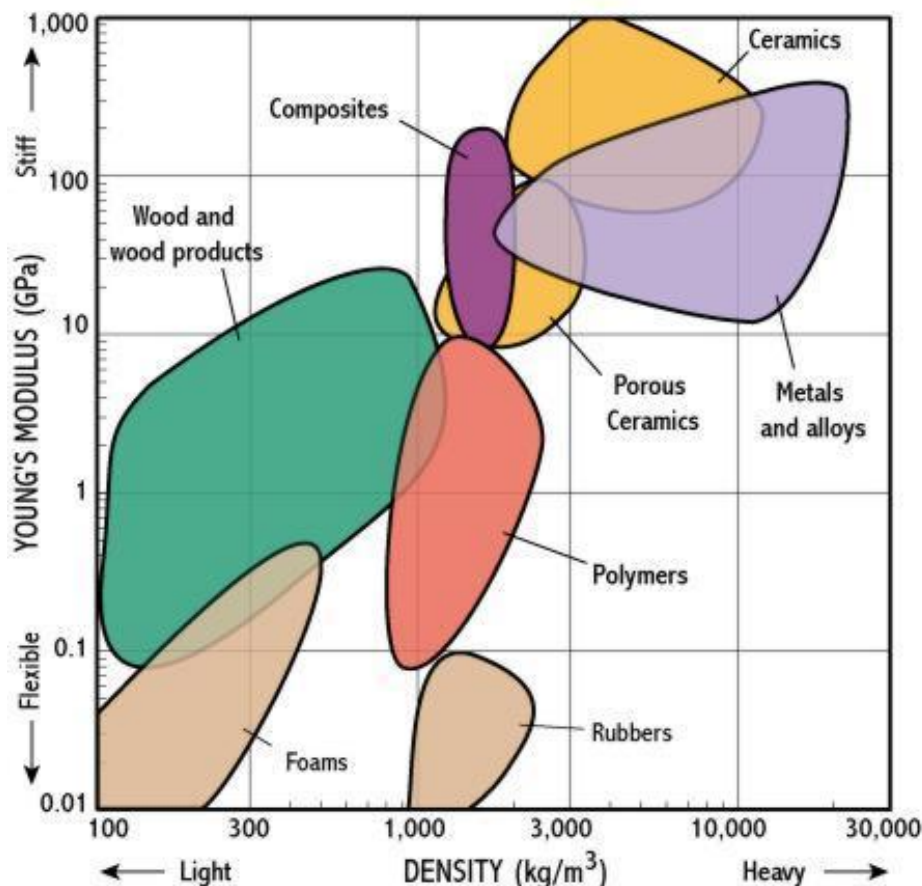


Figure 7.11 Young's modulus as function of the density for various materials (source: http://www-materials.eng.cam.ac.uk/mpsite/interactive_charts/stiffness-density/NS6Chart.html)

- 2) Define a strategy of how the fatigue curve of grass sods could be determined (Figs. 8a and 8b). If known that a correlation can be determined with the CIRIA-diagram in which the critical flow velocity or the permissible flow velocity decreases with time (Fig. 7.12)?
- 3) Investigate both the measured root tensile forces (conducted by Alterra) and the measured grass tensile forces as discussed in this chapter as they are related through the root properties (root intensity, root diameter and critical tensile strength of roots).
- 4) Validate the coefficient of variation by carrying out sufficient tests with the turf-tensile apparatus. For a good grass revetment the coefficient of variation is about 0.2. If there are tracks or irregularities in the grass revetment then the coefficient of variation may reach values up to 0.6 (see also Section 7.4).

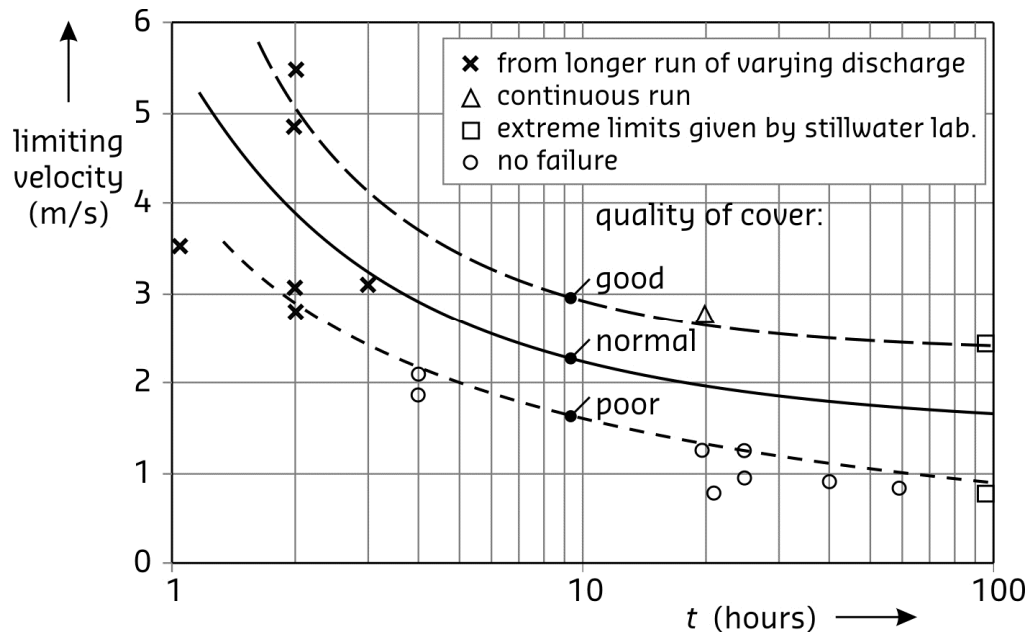


Figure 7.12 CIRIA-curve; Limiting flow velocity (overflow conditions) as function of time

8 Procedures for the cumulative overload method

8.1 Introduction

The cumulative overload can be applied for wave overtopping as well as wave run-up. The procedure, however, is a little different. The next two sections give these procedures. For the WTI2017-process a procedure has to be produced that can be developed and used as semi-probabilistic software. A first set-up is given in the last two sections.

8.2 Procedure for wave overtopping

The geometry of the structure, including the crest freeboard, R_c , and the wave conditions like H_{m0} , $T_{m-1,0}$ and storm duration (or duration of the sea state) determine the overtopping discharge q , as well as the 2%-run-up level, $R_{u2\%}$, the number of overtopping waves, N_{ow} , or the percentage of overtopping waves, $P_{ov\%}$. Pc-overslag or the accompanied dll can be used to calculate q as well as $R_{u2\%}$, N_{ow} or $P_{ov\%}$.

Theory on flow velocities (and flow thicknesses) on the crest is not well established. In Van der Meer (2011) known investigations have been brought together and compared and this resulted in the following conclusion. The 2%-value of the velocity on the crest, $U_{c2\%}$, can be calculated by:

$$U_{c2\%} = c_{u2\%} \sqrt{g(R_{u2\%} - R_c)} \quad (8.1)$$

The coefficient $c_{u2\%} = 1.4 - 1.5$ for slopes between 1:3 and 1:6. It is this coefficient that is not well established. For the time being $c_{u2\%} = 1.45$ will be used, which gives:

$$U_{c2\%} = 1.45 \sqrt{g(R_{u2\%} - R_c)} \quad (8.2)$$

Equation 8.2 gives the velocity on the crest for only the 2%-value, where the velocity of each overtopping wave volume is needed. By assuming a Rayleigh distribution for the wave run-up, the velocities of other volumes can be calculated if Equation 8.2 is transformed to:

$$U_{ci\%} = 1.45 \sqrt{g(R_{ui\%} - R_c)} \quad (8.3)$$

Where i is the exceedance probability. The smallest exceedance probability is given by:

$$P_{ov1} = 1/(N_w + 1) \quad (8.4)$$

Where N_w is the number of waves in the sea state. The largest exceedance probability is given by:

$$P_{ovN_{ow}} = N_{ow}/(N_w + 1) \quad (8.5)$$

A list can be made of probabilities for all overtopping wave volumes. The run-up level $R_{ui\%}$ can be calculated by:

$$R_{ui\%} = R_{u2\%} [\ln(P_{ovi})/\ln(0.02)]^{0.5} \quad (8.6)$$

Combination of Equations 8.3 and 8.6 give a direct calculation of velocities for each overtopping wave volume:

$$U_{ci\%} = 1.45\sqrt{g\{[R_{u2\%}(\ln(P_{ovi})/\ln(0.02))^{0.5} - R_c]\}} \quad (8.7)$$

Equation 8.7 gives the velocities on the crest. These velocities will increase over the landward slope and the velocity is depending on the location on the slope considered. The theory given by Schüttrumpf and Oumeraci (2005), also summarised in Deltares (2012), can be used directly, using a friction coefficient of 0.01 for a grass slope.

Another method is to use a graphical method as was also done in Section 3.2 and given here in Figure 8.1 (copy of Figure 3.1). Depending on the distance on the slope, measured from the inner crest line and the slope angle of the landward slope, an acceleration factor can be determined. All velocities of overtopping wave volumes at the crest should be multiplied with this acceleration factor.

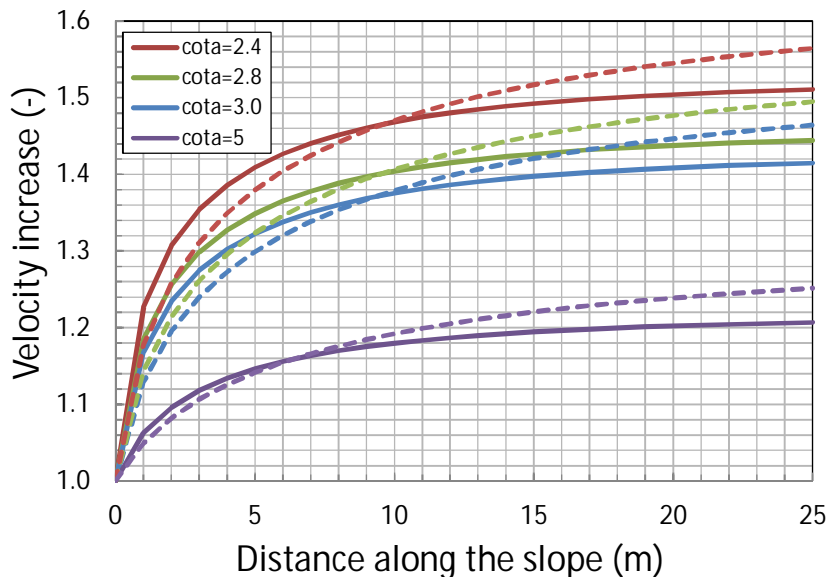


Figure 8.1 Velocity increase over overtopping wave volumes over the landward slope. Solid line: $U_0 = 4$ m/s, dashed line: $U_0 = 6$ m/s

Then the overload for each overtopping volume can be calculated, incorporating α_1 and α_2 if objects and/or transitions play a role, and assuming a certain critical velocity U_c :

$$D_i = (\alpha_1 U_i^2 - \alpha_2 U_c^2) \quad \text{for } \alpha_1 U_i > \alpha_2 U_c \quad [\text{m}^2/\text{s}^2] \quad (8.8)$$

Finally the sum of the overload for all overtopping wave volumes can be calculated:

$$D = \sum_{i=1}^N (\alpha_1 U_i^2 - \alpha_2 U_c^2) \quad \text{for } \alpha_1 U_i > \alpha_2 U_c \quad [\text{m}^2/\text{s}^2] \quad (8.9)$$

The procedure above has not been used when analysing all the results from the wave overtopping tests. The reason is simple, the wave overtopping simulator was designed in such a way that it should give the correct overtopping velocities on the crest. It was designed on Equation 8.3 (although using a coefficient 1.35 instead of 1.45), coupling it with the overtopping wave volume that belonged to the exceedance probability considered. When the overtopping simulator had been constructed and proper ways were found to measure the very turbulent velocities, a direct relationship was found between the simulated overtopping wave volume and the velocity on the crest. All wave overtopping tests were then steered by the

individual overtopping wave volumes. The distribution of overtopping wave volumes that had to be simulated, was given by:

$$P_{V\%} = P(V_i \geq V) = \exp \left[- \left(\frac{V}{a} \right)^b \right] \cdot (100\%) \quad (8.10)$$

where P_V is the probability that an individual wave volume (V_i) will be less than a specified volume (V), and $P_{V\%}$ is the percentage of wave volumes that will exceed the specified volume (V). The two parameters of the Weibull distribution are the non-dimensional shape factor, b , that helps define the extreme tail of the distribution and the dimensional scale factor, a , that normalizes the distribution.

$$a = \left(\frac{1}{\Gamma(1+\frac{1}{b})} \right) \left(\frac{qT_m}{P_{ov}} \right) \quad (8.12)$$

where Γ is the mathematical gamma function and T_m is the average period. The shape factor b for relatively smooth dike type structures can be described by:

$$b = 0.73 + 55 \left(\frac{q}{gH_{m0}T_{m-1,0}} \right)^{0.8} \quad (8.13)$$

With the number of overtopping waves and above distribution the overtopping wave volumes, each overtopping wave volume can be calculated.

In the first years of testing a fixed value of $b = 0.75$ was used, as the theory above had not yet been developed. Tests since 2011 (Millingen and Nijmegen) were performed with the theory above.

As the relationship between simulated overtopping wave volume and velocity on the crest had been established, this relationship was directly used to calculate the cumulative overload. It replaced Equation 8.7 when the cumulative overload for wave overtopping tests was analysed. The part after Equation 8.7 (the acceleration factor and influences factors) was the same.

8.3 Procedure for wave run-up

The geometry of the structure and the wave conditions like H_{m0} , $T_{m-1,0}$ and storm duration (or duration of the sea state) determine the 2%-run-up level, $R_{u2\%}$. Pc-overslag or the accompanied dll can be used to calculate q as well as $R_{u2\%}$, N_{ow} or $P_{ov\%}$. Also the EurOtop Manual (2007) can be used.

With the 2%-run-up level known, all run-up levels on the seaward slope can be calculated with Equation 8.6. The front velocity of an up-rushing wave is more or less constant over the first 75% of the run-up height. In the remaining 25% the velocity reduces quickly to zero. The calculation of the cumulative overload has to be done for a certain location on the seaward slope. Only run-up levels that come a factor $1/0.75 = 1.33$ higher on the slope than the point of interest (measured from the still water level) count for the cumulative overload. Lower run-up levels have reduced velocities at the point of interest and can be neglected.

The relationship between run-up level and front velocity has been described by Van der Meer (2011) or Van der Meer et al. (2012). Figure 8.2 shows the relationship and this can be described by:

$$U/(gH_s)^{0.5} = c_u (Ru/H_s)^{0.5} \quad (8.14)$$

with c_u as stochastic variable with $\mu(c_u) = 1.0$ and a normal distribution with $V = 0.25$.

It is clear that in reality there is not a fixed relationship between run-up level and maximum front velocity, there are run-up events with a fairly high level and low velocity, as well as low run-up levels with quite high velocities. In principle the scatter in Figure 8.1 should be taken into account when coupling wave run-up levels to up-rushing front velocities. An easier and more practical approach is to use the average curve with $c_u = 1$.

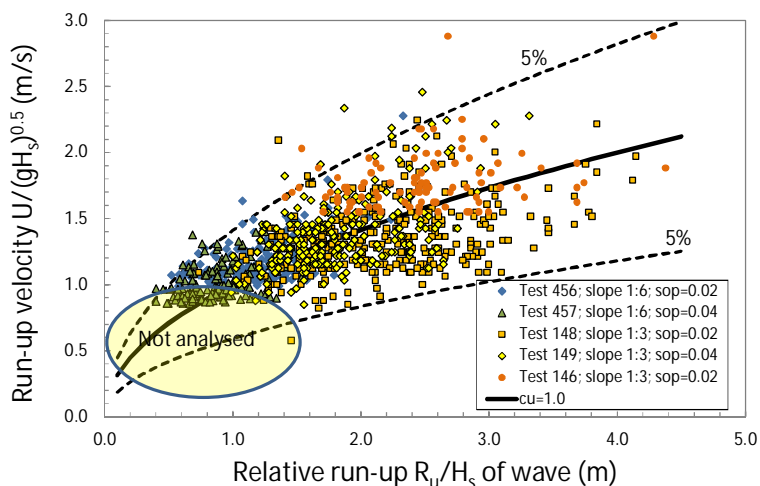


Figure 8.2 Run-up velocity (maximum) versus relative run-up level

With known velocities the cumulative overload can be calculated by Equations 8.8 and 8.9.

When analysing the tests with the wave run-up simulator Equation 8.14 was not used, but the relationship between filling level, run-up level and front velocity as found during calibration and hydraulic measurements for the particular section under investigation, see Section 5.2.

8.4 Procedure wave overtopping in WTI2017

The short term procedure in WTI2017 (ontwerpinstrumentarium korte termijn, OITK) is based on a critical overtopping discharge. The method of cumulative overload does not directly play a role. What has changed with earlier overtopping models is that the influence of the wave height has been taken into account. The critical overtopping discharge depends on the wave height and on the condition of the grass. The critical discharges have been given for a minimum critical velocity of 4 m/s.

The method has been described in Jongejan (2013).

8.5 Procedure wave run-up in WTI2017

The original assessment method for wave run-up was to calculate a characteristic velocity for the wave run-up that lasted for a period that the slope was “wet” (no flow over the grass). It was assumed that this characteristic velocity remained as a constant flow for the wet period, which is a part of the storm duration. The well-known CIRIA curves were used to make the assessment.

If possible, a new method should be based on the cumulative overload method, although it still has to be validated more in depth. The wave height also plays a significant role for wave run-up. A larger wave height gives larger front velocities.

To get an idea of cumulative overload in wave run-up situations a few characteristic situations have been worked out according to the method in Section 8.3. The following situation was assumed:

- Slope angle seaward slope (no berm): 1:4.
- Wave steepness: $s_{op} = 0.04$, $T_m = T_p/1.1$.
- Wave heights 0.5 m; 1 m; 2 m; and 3 m.
- Duration of the sea state: 1 hour.

This gives 2%-run-up values of 1 m; 2 m; 4 m and 6 m, respectively. The cumulative overload was calculated for $U_c = 4$ m/s; 5 m/s; 6.5 m/s and 8 m/s and for various locations on the slope, given as the vertical distance to the still water level. Figures 8.3 – 8.5 give the results.

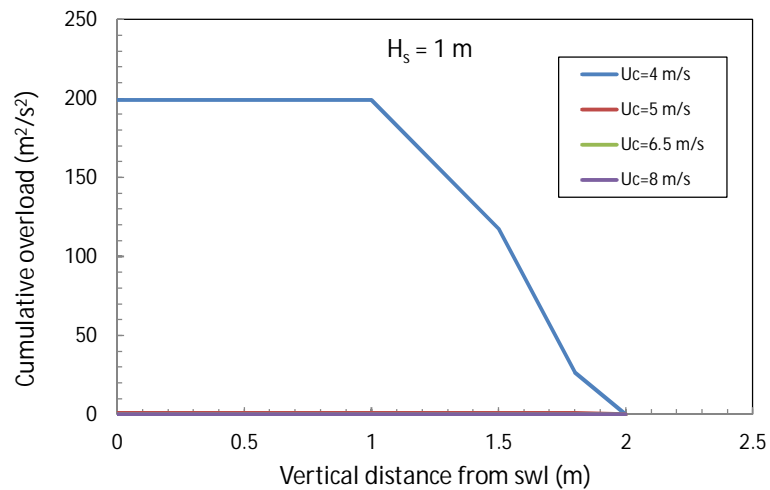


Figure 8.3. Cumulative overload as a function of location on the seaward slope, for $H_s = 1$ m

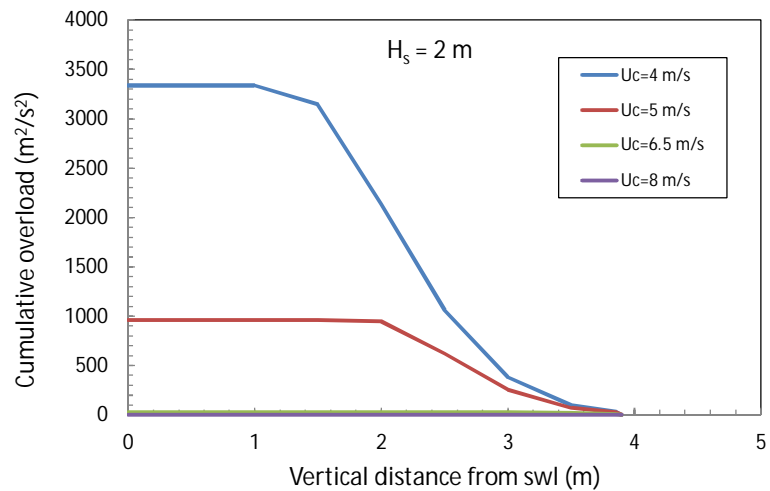


Figure 8.4. Cumulative overload as a function of location on the seaward slope, for $H_s = 2$ m

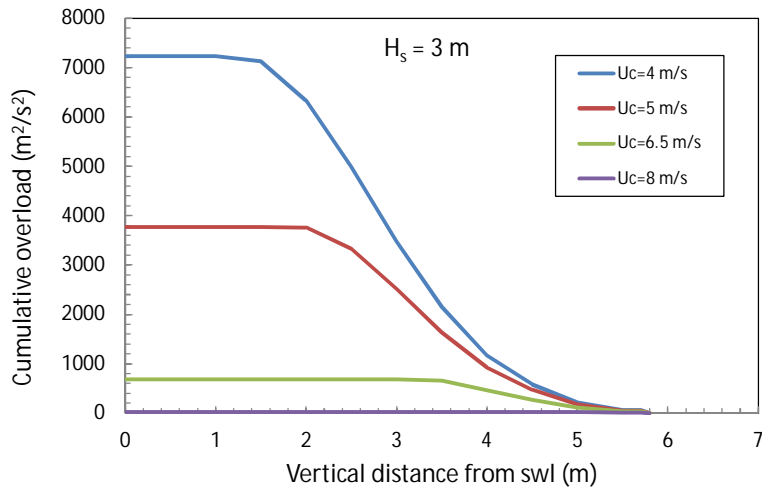


Figure 8.5 Cumulative overload as a function of location on the seaward slope, for $H_s = 3$ m

Figures 8.3-8.5 show that there is a large influence of the critical velocity. With larger critical velocity the cumulative overload decreases fast. The graphs also show that the cumulative overload is more or less similar for the lowest half of the run-up area and then decreases rapidly to zero over the upper half of the run-up area. The cumulative overload is zero for locations higher than the 2%-run-up value.

Another way of presenting the results is to give the cumulative overload for one critical velocity only ($U_c = 4$ m/s) and for various wave heights. This has been done in Figure 8.6. Figure 8.6 shows that also the wave height has a large influence on cumulative overload. The cumulative overload for a wave height of $H_s = 0.5$ m is zero. It is quite small for $H_s = 1$ m and becomes large for a wave height of $H_s = 3$ m. A cumulative overload of $D = 7000$ m²/s² on the lower half of the run-up area and for a wave height of 3 m means that this area should fail after one hour, assuming a critical velocity of 4 m/s. For a wave height of 2 m it would take 2 hours before failure.

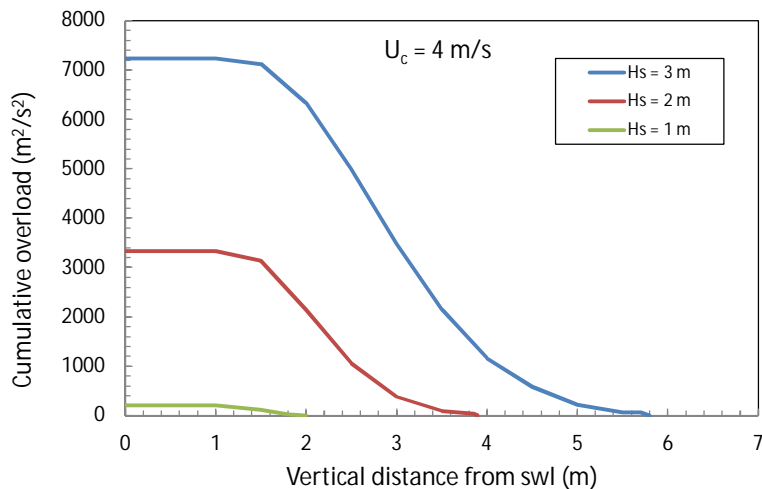


Figure 8.6 Cumulative overload as a function of location on the seaward slope, for $U_c = 4$ m/s

A similar picture appears for the critical velocity, see Figure 8.5. For a wave height of 3 m and a critical velocity of 4 m/s the slope will fail after 1 hour. For a critical velocity of 5 m/s this will be about 2 hours. A critical velocity of 6.5 m/s gives a cumulative overload of $690 \text{ m}^2/\text{s}^2$, which gives about 10 hours before failure. A critical velocity of 8 m/s gives no cumulative overload and will not fail.

In contrast to wave overtopping one may say that a critical velocity of “only” 4 m/s or 5 m/s for wave run-up may already give quite some problems for wave heights of 2 m and more and the point of observation at the lower half of the wave run-up area. And this is still for a straight slope and not for a transition like a berm to an upper slope.

The development of a further method for WTI2017 should be discussed with people involved.

9 Conclusions and recommendations

9.1 Conclusions

The overall conclusion on the pilot test at Tholen and the wave run-up test at the Zeelandbrug is that results show that possibly the method of cumulative overload can also be applied for wave run-up. The analysis did not show contradictions. But the validation is far from conclusive as it could not be based on a damage criterion of failure, but only on no or slight damage.

Evaluation of a comparison of pressure measurements at wave overtopping tests and the wave run-up tests at Colijnsplaat also supports the use of the overload model for wave run-up. The load on the sod for overtopping waves and for wave run-up are comparable if the front velocity is comparable and the load caused by the wave run-down is negligible compared to the wave run-up.

It is possible to compare results from the sod pull out device with the critical velocity on the slope. Both the run-up tests and the results from the device give a critical velocity in the order of 8 m/s or somewhat larger for location Colijnsplaat. More analyses will however be required to obtain a procedure to get a design value of U_c , from the field (see recommendations).

9.2 Recommendations

As it is advantageous to apply a similar method for wave run-up as well as for wave overtopping, a conclusive validation is required. It is therefore recommended to perform again a test series with the wave run-up simulator. With selection of a suitable test location it is necessary to have a steeper transition to the upper slope, a grass cover that is/looks not too strong, and a location that has also objects and/or other transitions. In order to compare directly wave run-up with wave overtopping it is further recommended to do both tests on a similar section. To have both type of tests is very useful for a direct comparison, like at the tests at Tholen.

To obtain a procedure to get a (design) value of U_c from field tests with the sod pull out device the following subjects/ matters should be investigated:

- 1) Investigate the relevant differences between grass/roots and pine heartwood. Discuss the material properties and determine, e.g., the Young's modulus (or the elasticity modulus) of the tested grass sods and compare these values with the Young's modulus of pine heartwood as this result could provide insight in the fatigue curve of grass. If these Young's modulus's have the same magnitude of order then the fatigue curve of pine heartwood could be a useful engineering tool for predicting the fatigue strength of grass.
- 2) Define a strategy of how the fatigue curve of grass sods could be determined. For example is there a relation between the fatigue curve and the CIRIA-diagram in which the critical flow velocity or the permissible flow velocity decreases with time?
- 3) Investigate both the measured root tensile forces (conducted by Alterra) and the measured grass tensile forces as discussed in this chapter as they are related through the root properties (root intensity, root diameter and critical tensile strength of roots).
- 4) Validate the coefficient of variation by carrying out sufficient tests with the turf-tensile apparatus. For a good grass revetment the coefficient of variation is about 0.2. If there are tracks or irregularities in the grass revetment then the coefficient of variation may reach values up to 0.6 (see also Section 7.4).

References

Deltares (2012). Evaluation and Model Development. Grass Erosion Test at the Rhine dike. Draft report.

Jongejan, R. (2013). De ontwikkeling van een voorlopig ontwerpinstrumentarium (OIKT). Overloop en golfoverslag

RWS (2012). Handreiking Toetsen Grasbekledingen op Dijken t.b.v. het opstellen van het beheerdersoordeel (BO) in de verlengde derde toetsronde. Rijkswaterstaat, Ministerie van Infrastructuur en Milieu.

Schüttrumpf, H.; Oumeraci, H. (2005). Layer thicknesses and velocities of wave overtopping flow at seadikes. Amsterdam, The Netherlands: Elsevier, Coastal Engineering, Vol. 52, No. 6, 473-495 (PIANC award for PhD thesis 2004).

Van der Meer, J.W., Y. Provoost and G.J. Steendam (2012). The wave run-up simulator, theory and first pilot test. ASCE, Proc. ICCE 2012, Santander, Spain.

Van der Meer, J.W. (2011). The Wave Run-up Simulator. Idea, necessity, theoretical background and design. Van der Meer Consulting Report vdm11355.

Infram, 2014. Factual report: Golfplooppoeven Noord-Beveland. Authors: Jan Bakker, Roy Mom, Gosse Jan Steendam, Wing Hong Wong en Jentsje van der Meer, Projectnummer 13i084, Marknesse.

Hoffmans, G.J.C.M., 2012. The Influence of Turbulence on Soil Erosion. Deltares Select Series Vol. 10, Deltares, Delft.

Hoffmans, G., G.J. Akkerman, H. Verheij, A. van Hoven and J.W. van der Meer. 2008. The erodibility of grassed inner dike slopes against wave overtopping. ASCE, Proc. ICCE 2008, Hamburg, 3224- 3236.

Hoffmans, G.J.C.M., Van Hoven, A., Verheij, H.J., 2010. Instability of grass caused by wave overtopping, Proc. of ICSE-6, San Francisco, 1023-1033.

Kollman, F.F.P., Wilfred A. Côté, W.A., 1968. Principles of wood science and technology: Solid wood, Springer-Verlag, 592 pages.

Shields, A., 1936. Anwendung der Aehnlichkeitsmechanik und der Turbulenzforschung auf die Geschiebe-bewegung, Mitteilungen der Preussischen Versuchsanstalt für Wasserbau und Schiffbau, Heft 26, Berlin NW 87.

WTI-2013. Evaluation and model development, Grass erosion test at the Rhine dike, authors: Andre van Hoven, Henk Verheij, Gijs Hoffmans en Jentsje van der Meer, report 1207811-002, Deltares, Delft.

Barends, F.B.J., 1992. Personal communications, Delft University of Technology, Delft.

De Groot, M.B., Andersen, K.H., Burcharth, H.F., Ibsen, L.B., Kortenhaus, A., Lundgren, H., Magda, W., Oumeraci, H., Richwien, W., 1996. Foundation design of caisson breakwaters, Publication 198, Norwegian Geotechnical Institute, Oslo, Norway.

Emmerling, A., 1973. Die momentane Struktur des Wanddruckes einer turbulenten Grenzschichtströmung, Max-Planck-Institut für Strömungsforschung, Bericht 9.

Greeuw, G., 2013. Dynamic load tests on two sods from Millingen, (project number 1206016-008), Deltares, Delft.

Klar, M., 2005. Design of an endoscopic 3-D particle-tracking velocimetry system and its application in flow measurements within a gravel layer, Doctoral Thesis, University of Heidelberg, Germany.

Nezu, I., 1977. Turbulent structure in open-channel flows, (*Translation of Doctoral Dissertation in Japanese*), Kyoto University, Kyoto, Japan.

Teunissen, H., 2010. PLUTO 4.3 (Version 3) Manual, Deltares, Delft (E:\pluto\manuals\pluto-manual-new-1.doc).

WTI, 2013. Evaluation and model development; grass erosion test at the Rhine dike, Authors: Van Hoven, A., Verheij, H.J., Hoffmans, G.J.C.M., Van der Meer, J.W., Deltares report: 1207811.

A Pictures of the construction stages of the wave run-up simulator



Picture 1. Front side of frame



Picture 2. Foot plates



Picture 3. Upper modules



Picture 4. Upper modules and frame for valves



Picture 5. Valves closed



Picture 6. Valves open



Picture 7. Ready for testing with water



Picture 8. Valves with a few centimetres water



Picture 9. Valve system without cover



Picture 10. Valve system with cover



Picture 11 Transition module



Picture 12. Inner part with guiding plates



Picture 13 Curved guiding plates at transition



Picture 14 Frame for transport of modules



Picture 15. Placing the first module 0.4 m x 2.0 m



Picture 16. Transporting uppermodule



Picture 17. Placing upper box on transition



Picture 18. Transporting transition with upper box



Picture 19. Placing three boxes together



Picture 20. Frame and three boxes



Picture 21. Frame in more detail



Picture 22. Frame with three modules



Picture 23. Inlet for pump on upper module



Picture 24. Situation without pump inlet



Picture 25. Placing frame for testing



Picture 26. Placing two modules for testing



Picture 27. Filling till 3 m water column



Picture 28. Small leakage with low filling level



Picture 29. Transport of modules for testing



Picture 30. Transport of frame with bend module



Picture 31. Fixing for 7 m water column testing



Picture 32. Testing with 7 m water column



Picture 33. Testing with 7 m water column



Picture 34. Pump for testing with 7 m



Picture 35. Bended lower module water column



Picture 36. Bended lower module



Picture 37. Broken epoxy paint by bending

B Design drawings of the wave run-up simulator

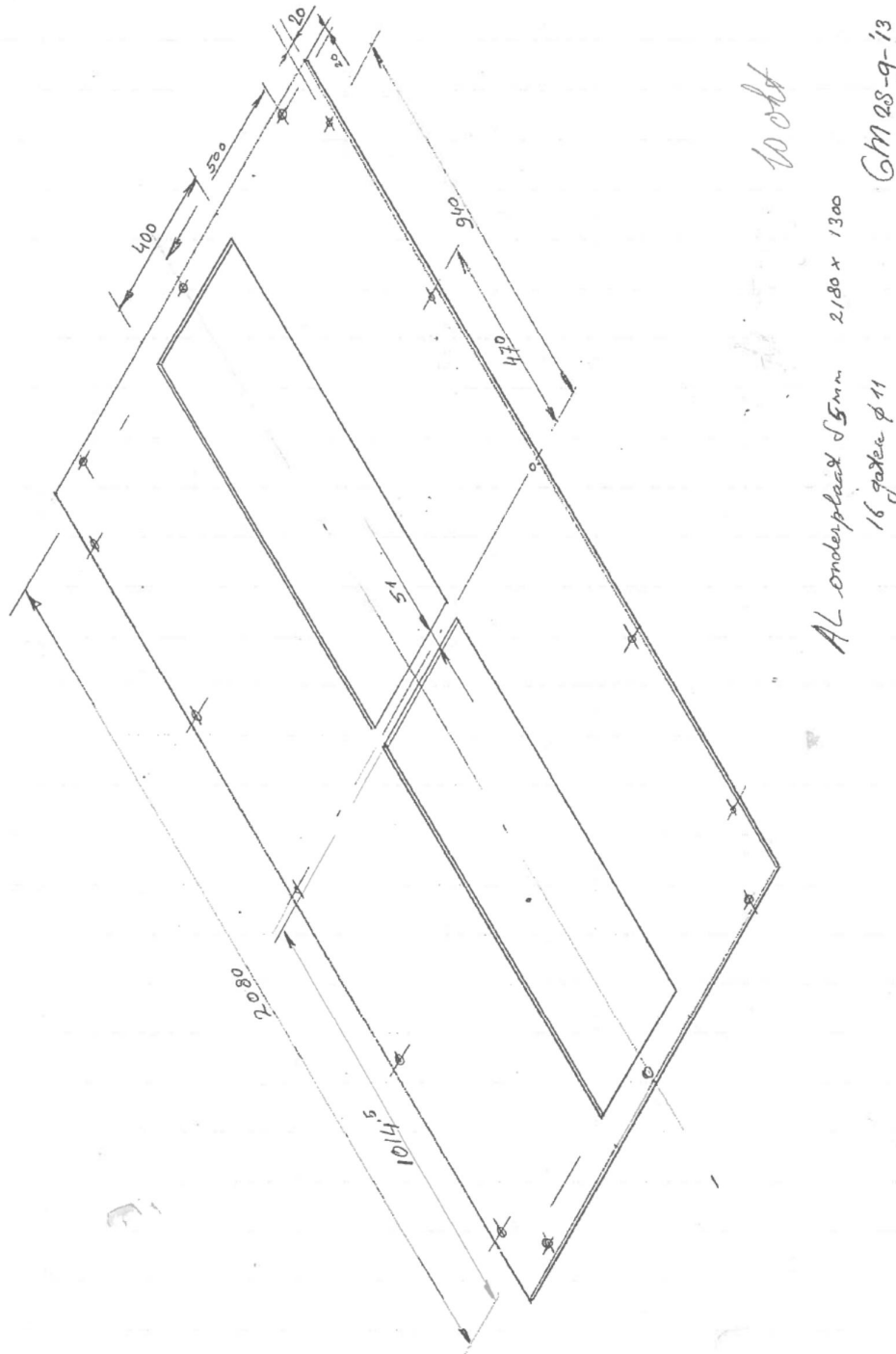


Figure 1 Lower plate of drawer type valve mechanism

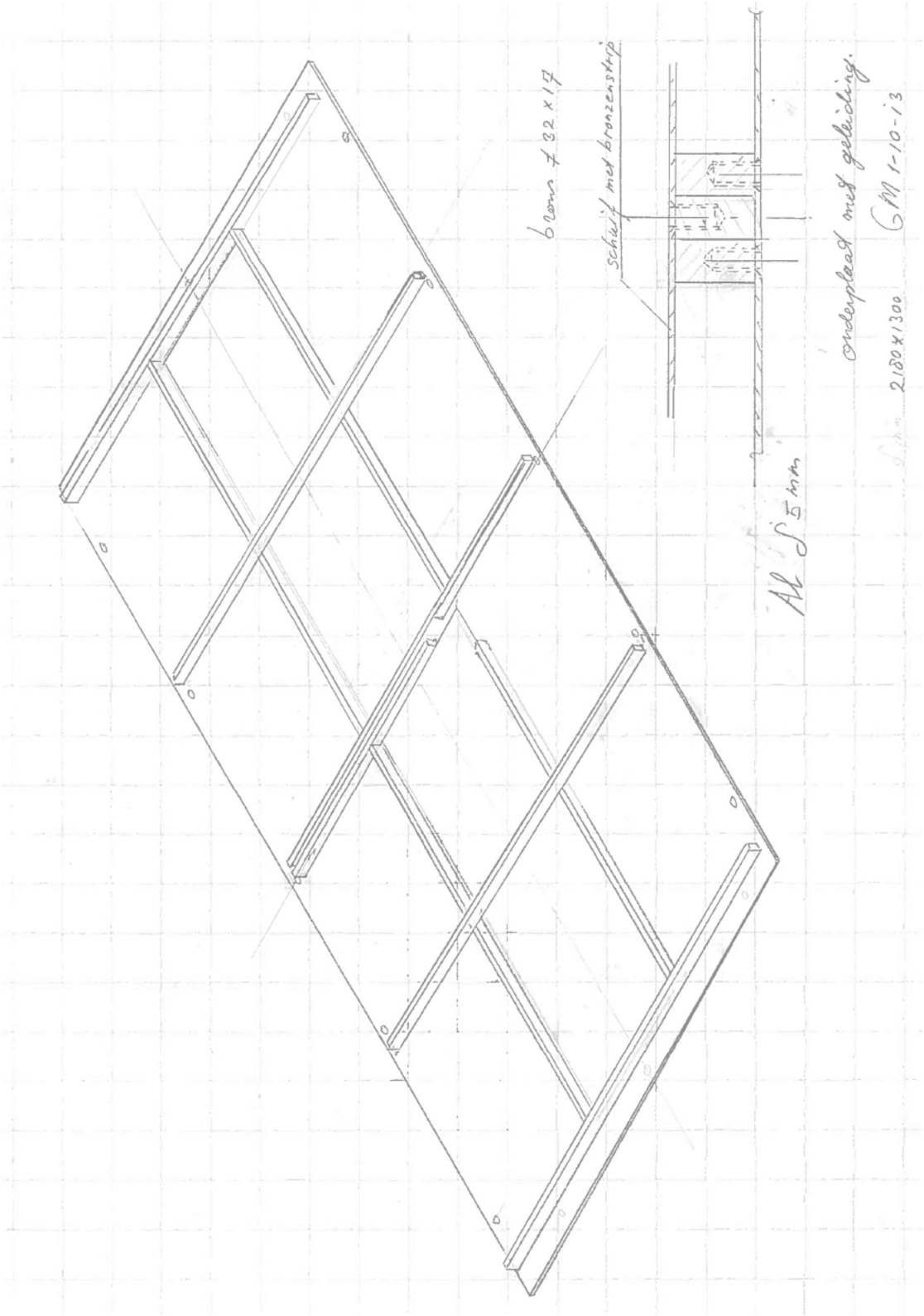


Figure 2 Lower plate with copper guiding of drawer type valve mechanism

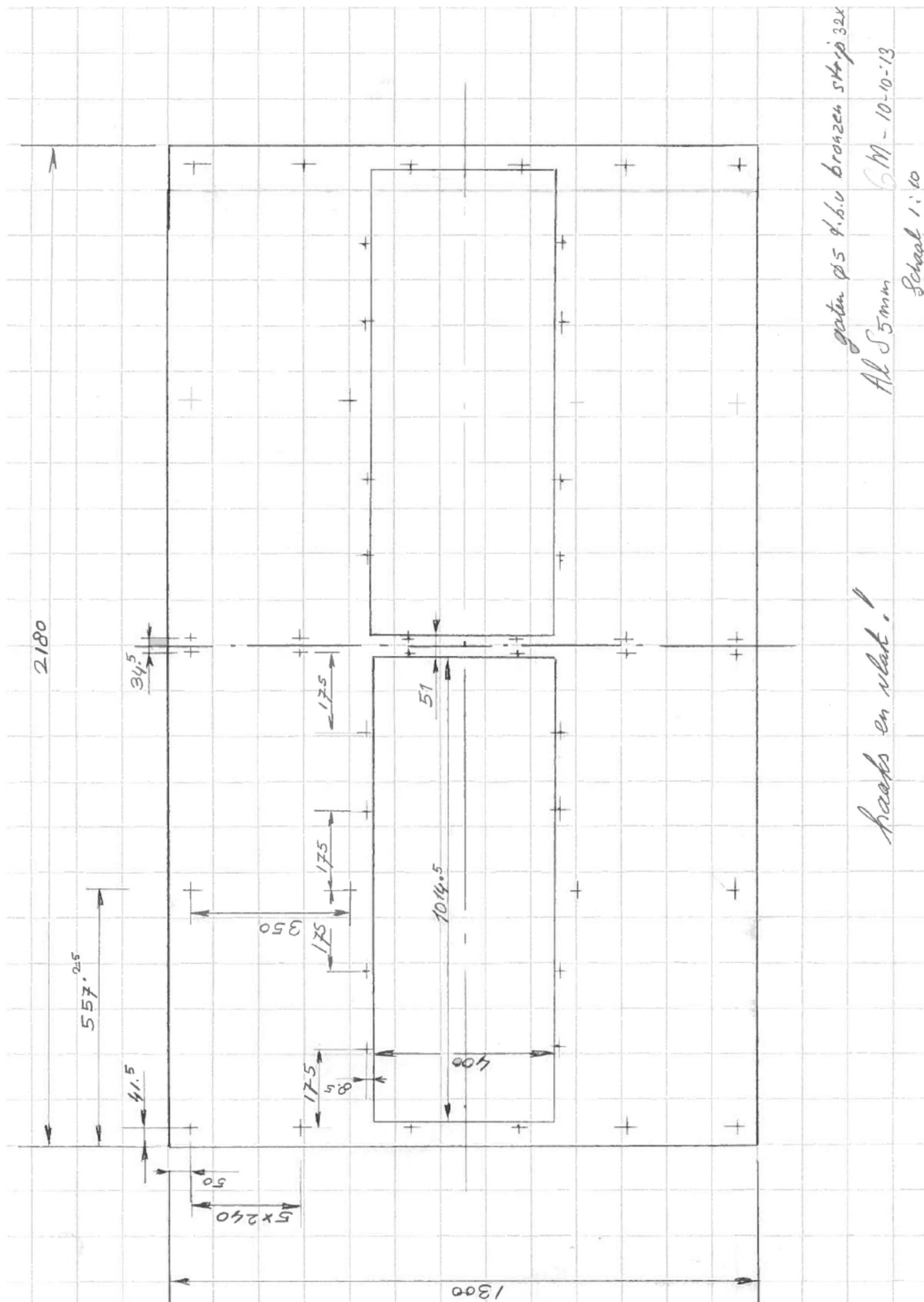


Figure 3 Upper plate of drawer type valve mechanism

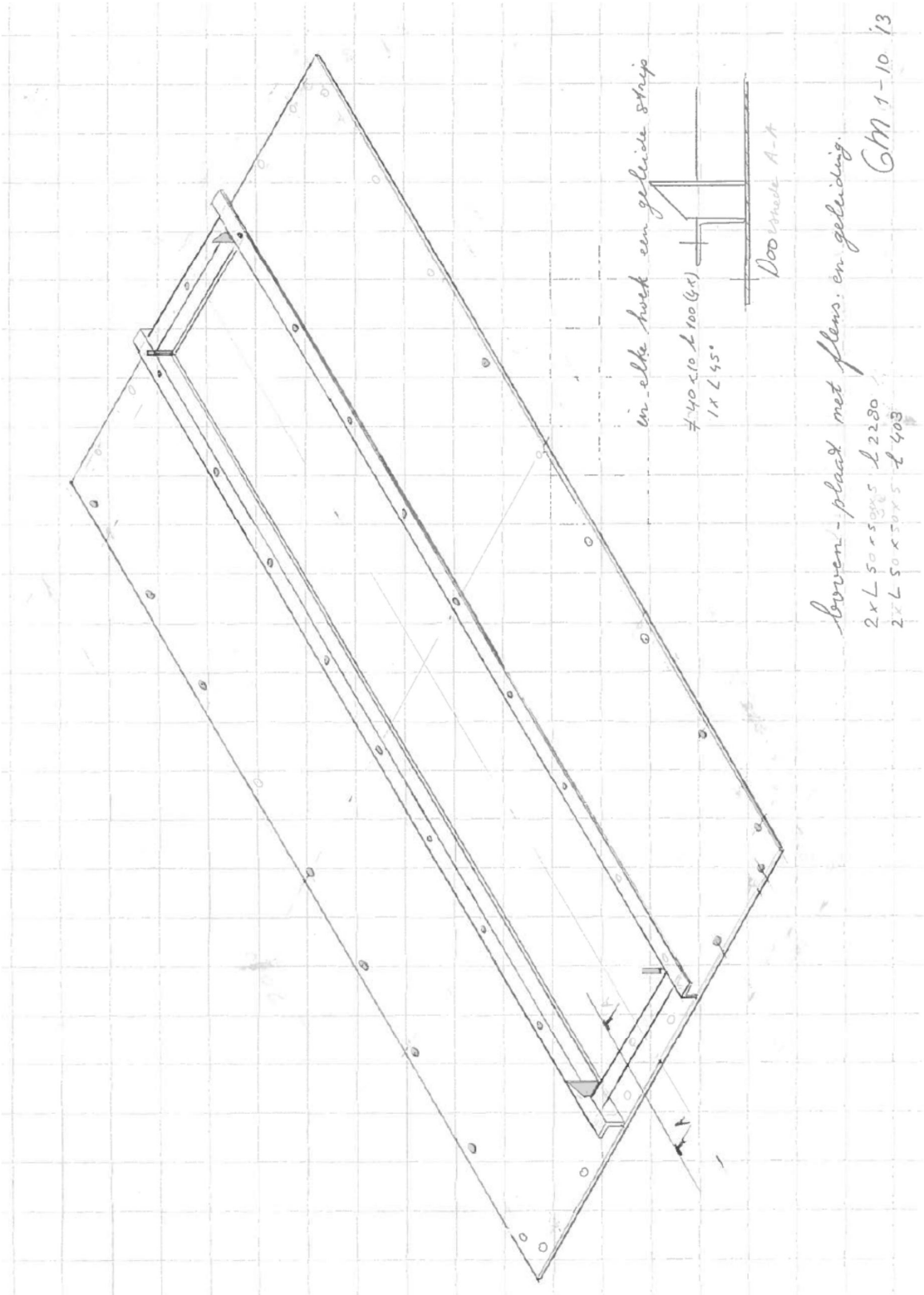


Figure 4 Upper plate of drawer type valve mechanism

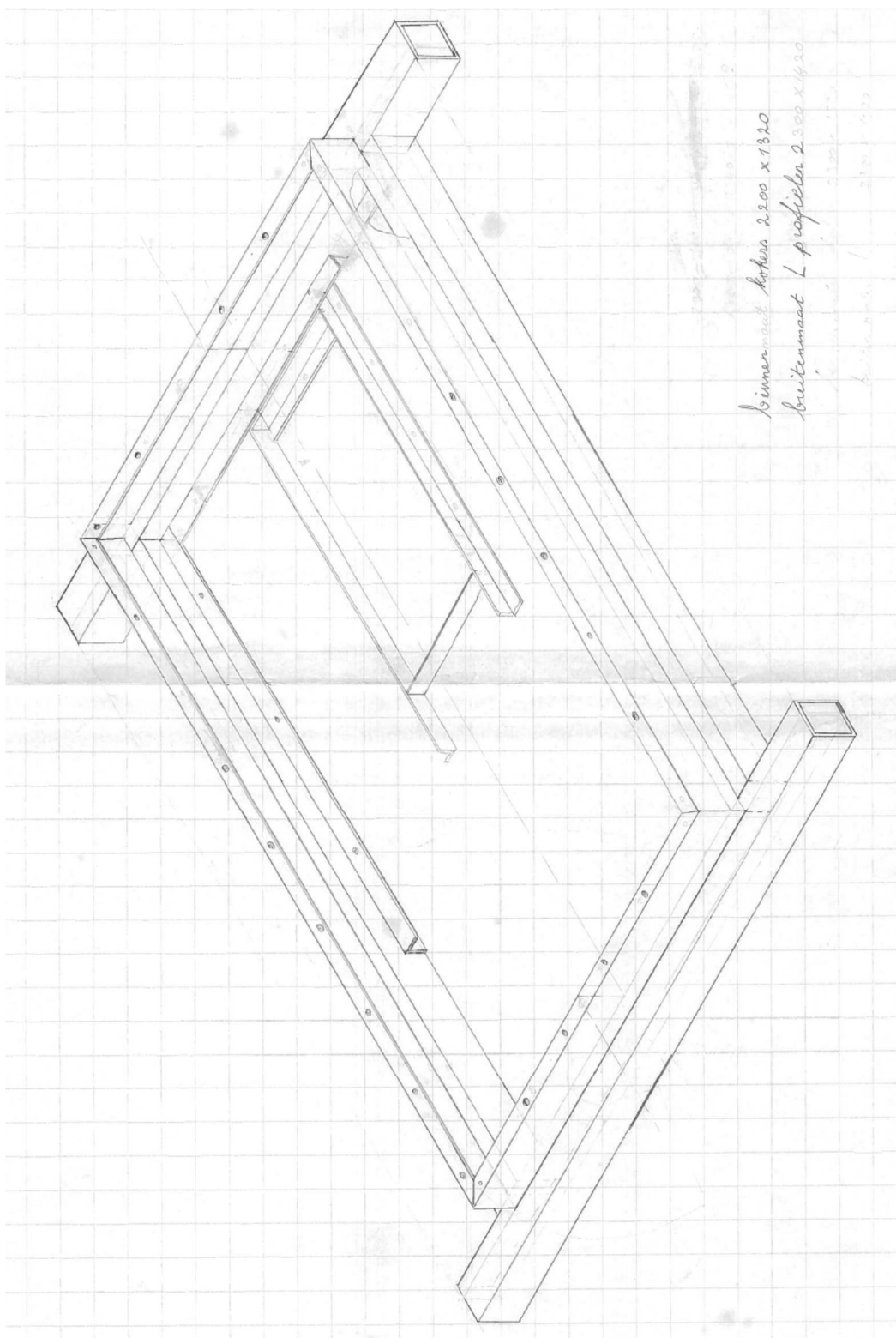


Figure 5 Frame

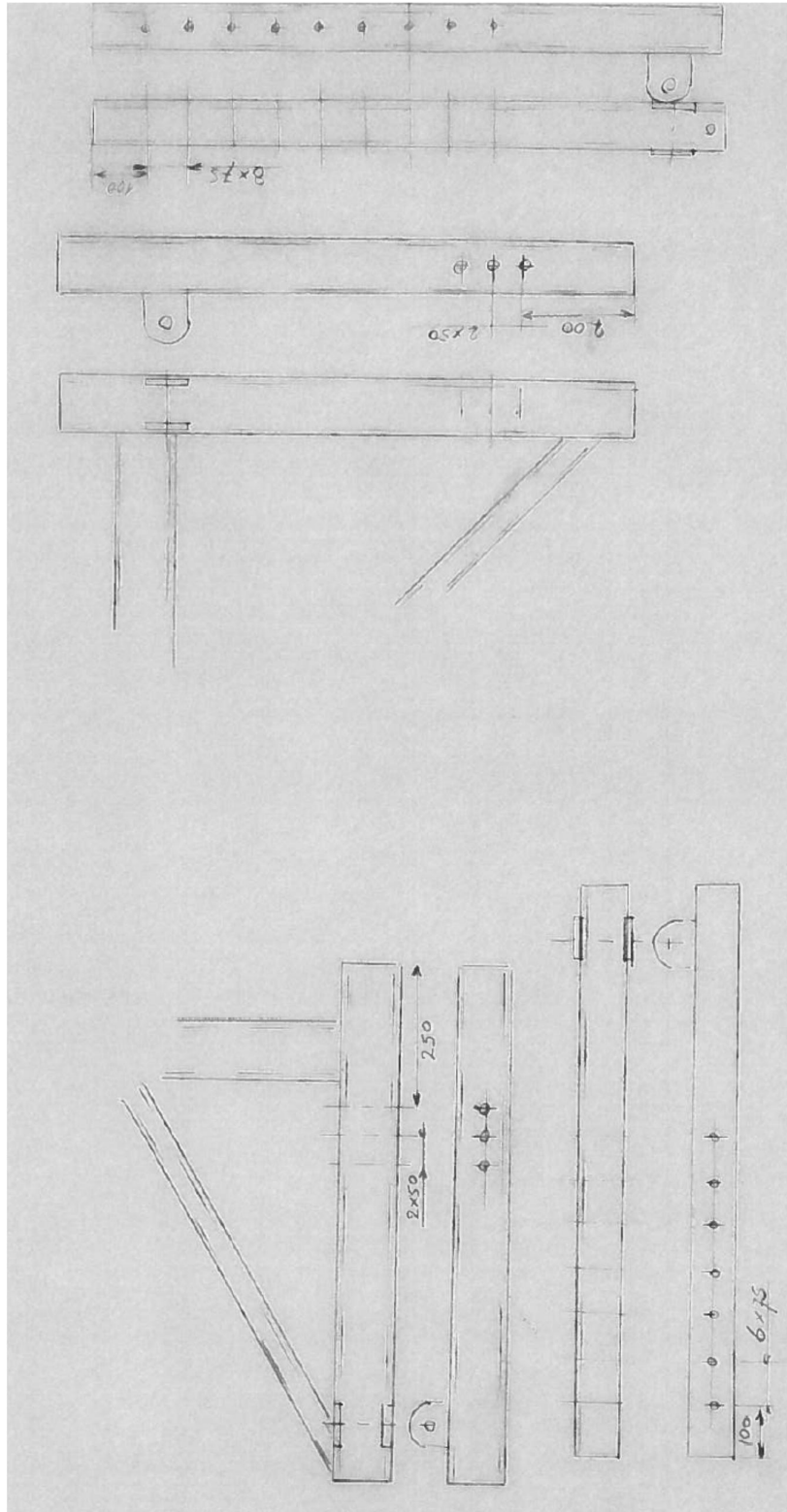


Figure 7 Details of frame with adjustable legs

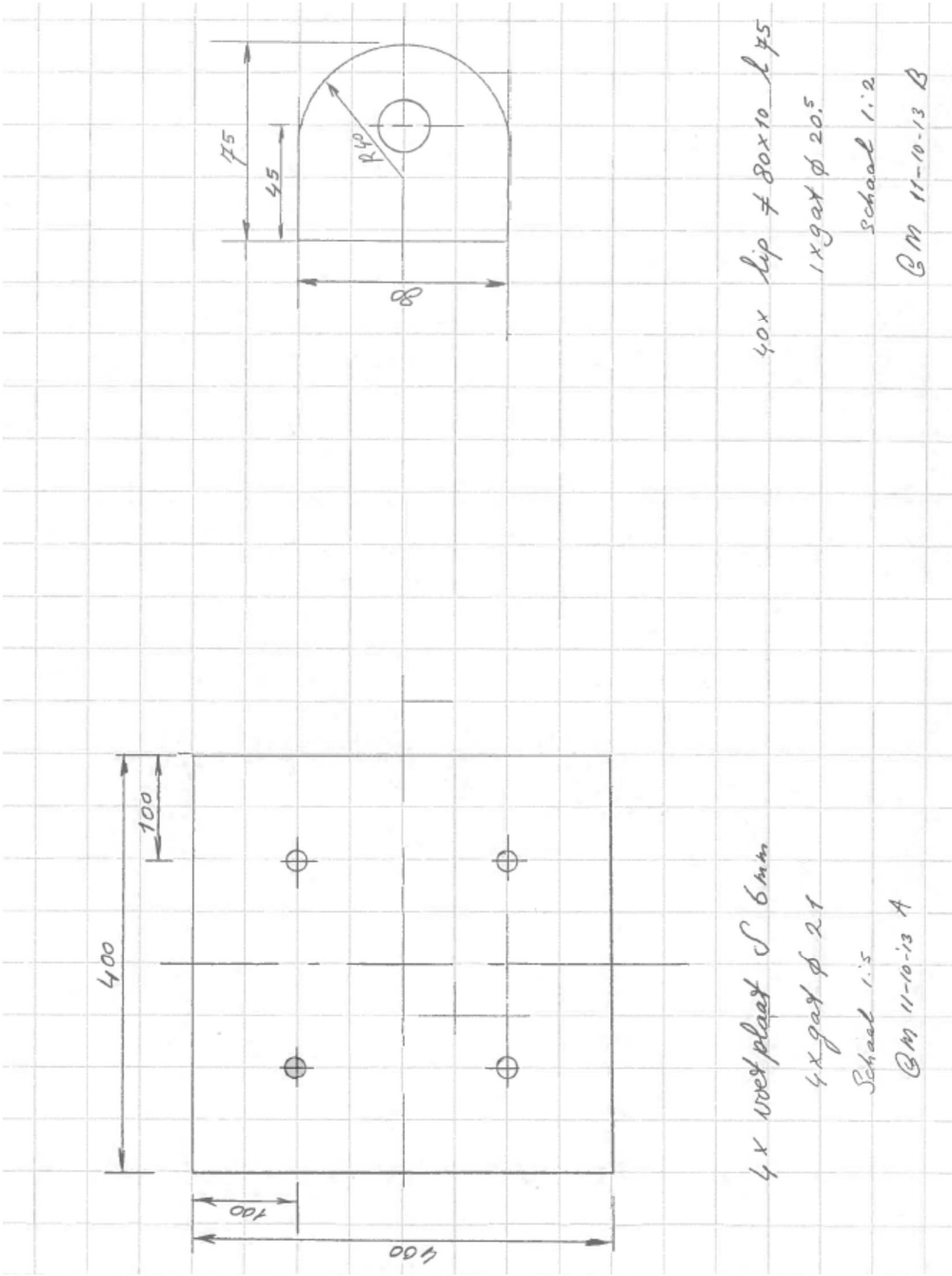


Figure 8 Footplate

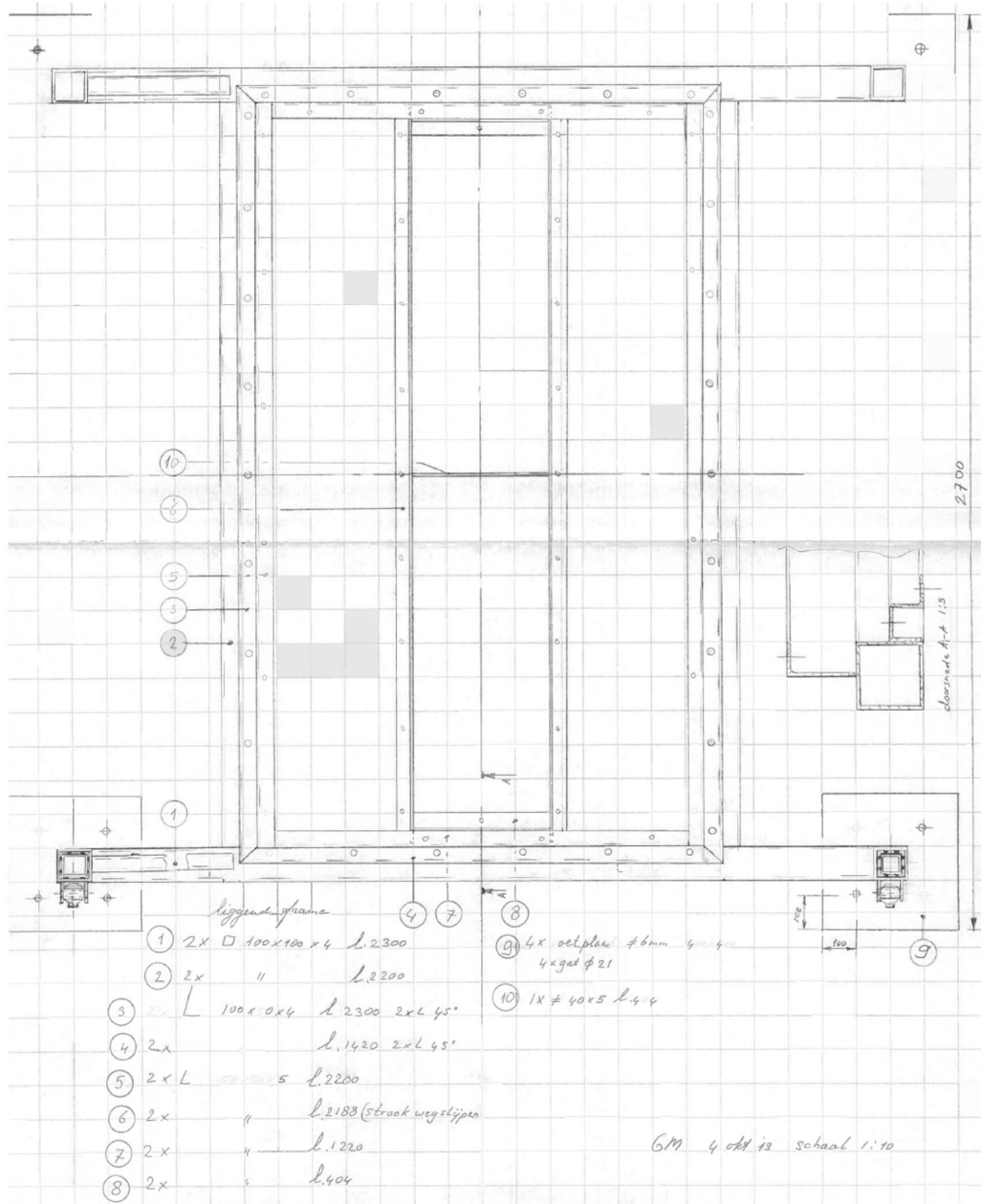


Figure 9 Frame

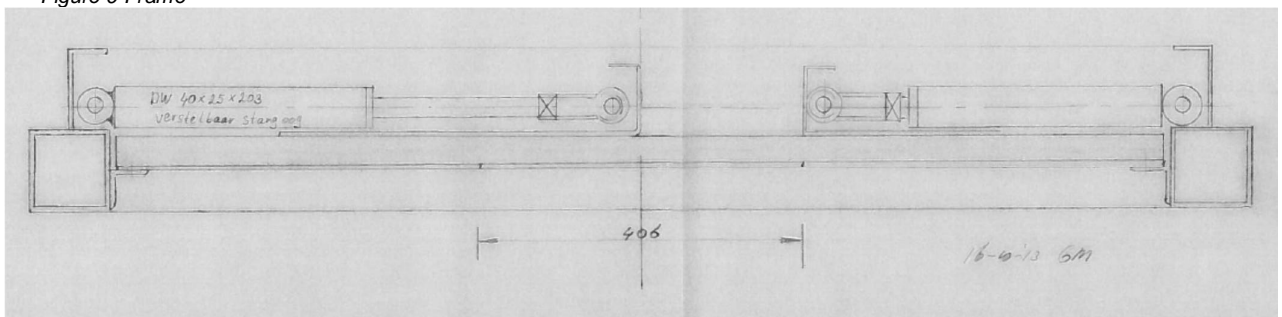


Figure 10 Adjustable leg of frame

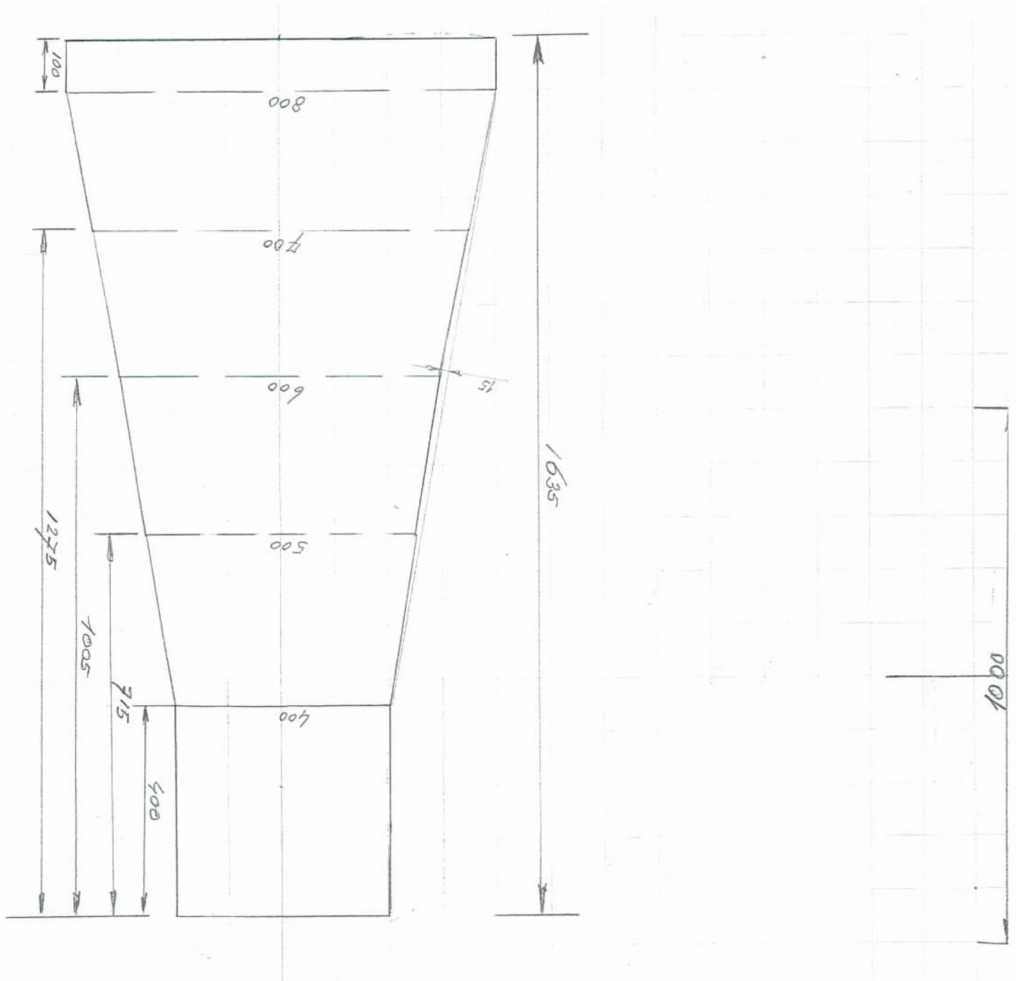


Figure 11 First design of transition module (later bended transition)

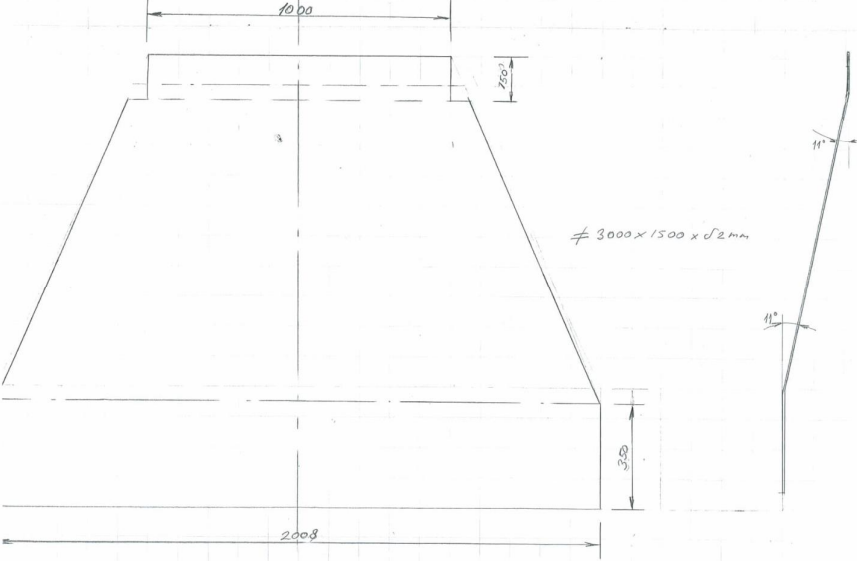


Figure 12 First design of transition module (later bended transition)

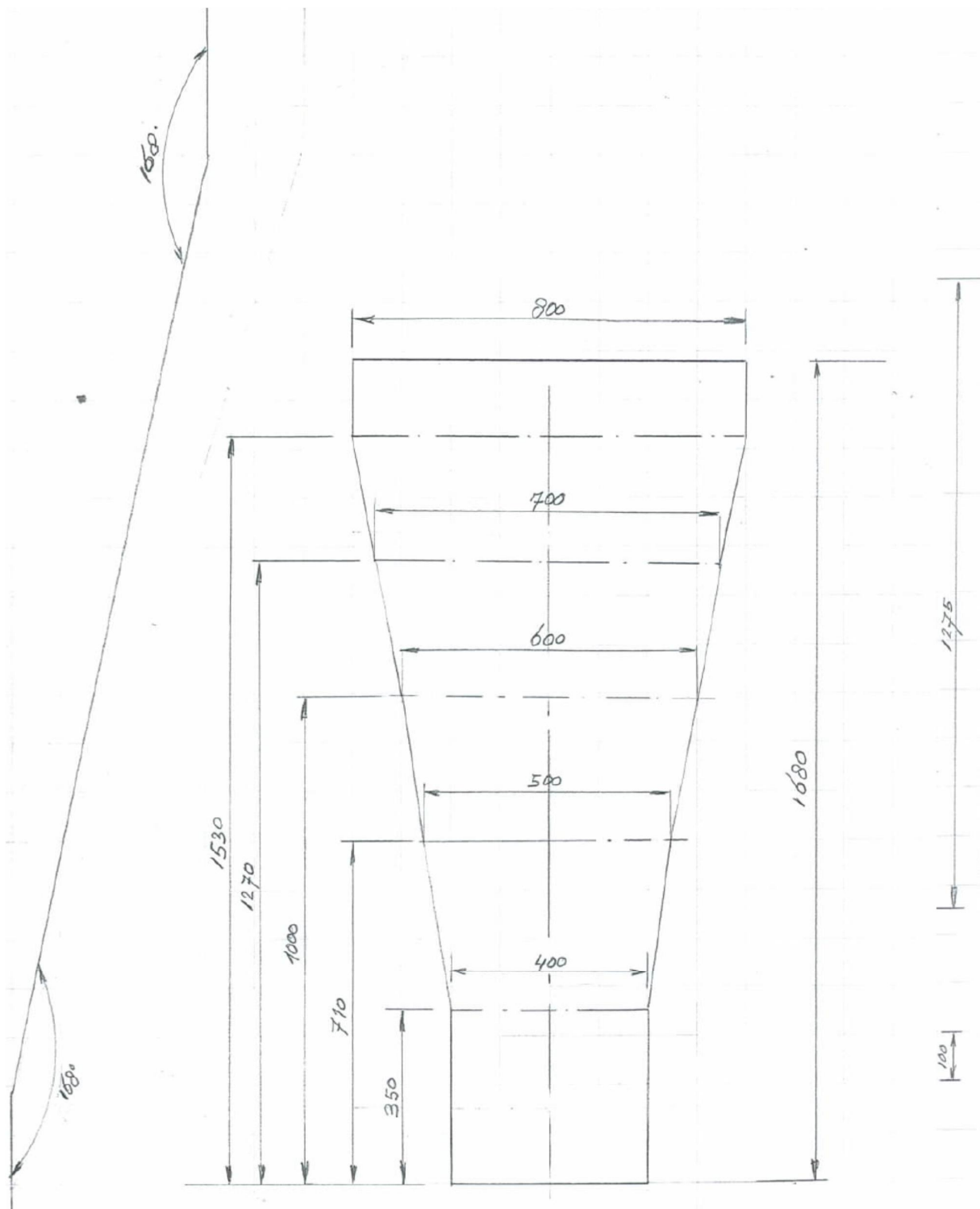


Figure 13 First design of transition module (later bended transition).

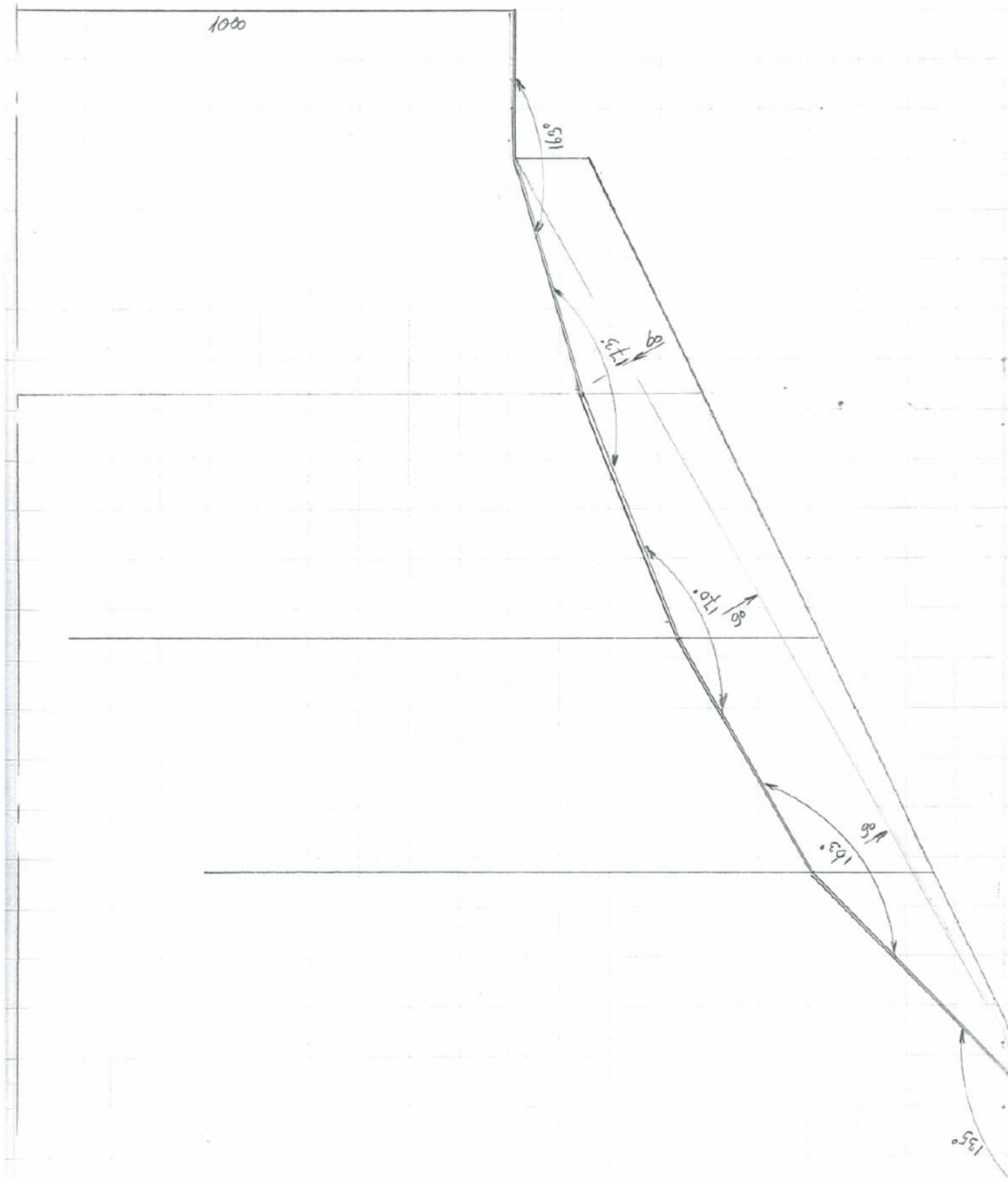
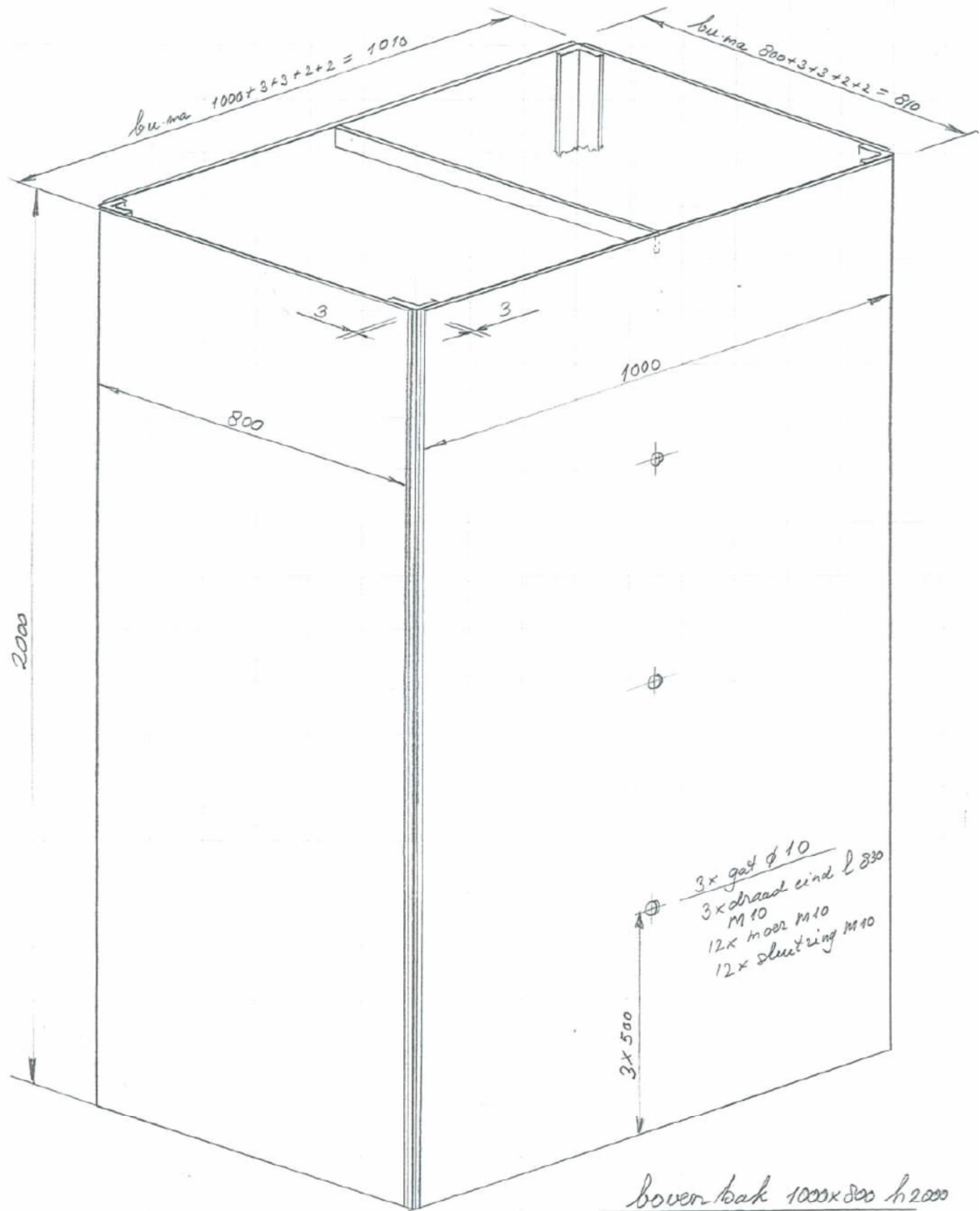


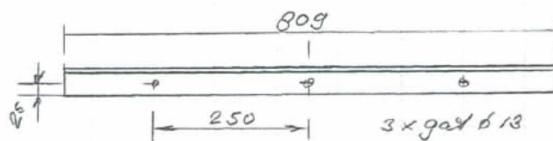
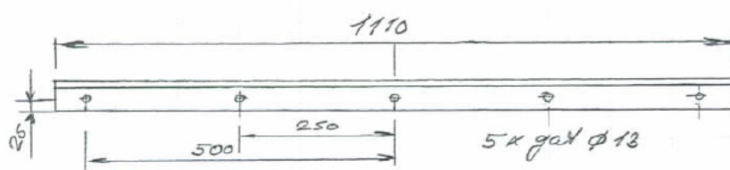
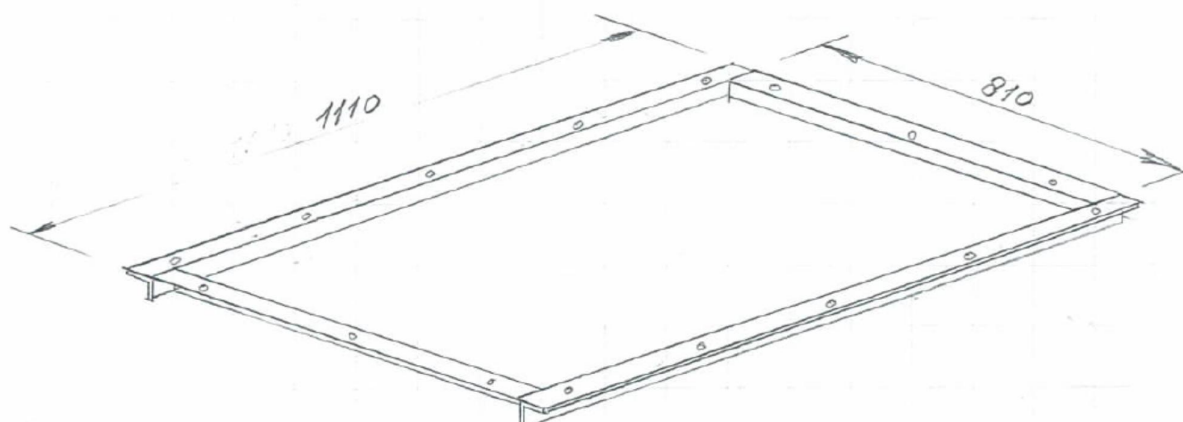
Figure 14 Bended transition module.



2x ≠ 2 x 2000 x 1000 blanke plaat
2x ≠ 2 x 2000 x 800 " "

19 okt 2013 Gm

Figure 15 Upper module



- 4x L 50x50x5 l 2000
- 4x L 50x50x5 l 1110
- 4x L 50x50x5 l 809
- 3x draad eind M10 l 830
- 12x moer M10
- 12x sluitring M10
- 2x ≠ 50x5 l 809
- 1 strip 2x gat $\phi 10$ v.b.v. kakeleu/hijzen

Figure 16 Details of upper module

C Pictures of the calibration at the Vossemeerdijk



Figure 1. Set-up



Figure 2. Set-up



Figure 3. Overall view with measuring cabin, crane, pump, simulator and "flume"



Figure 4. Set-up from the side



Figure 5. Set-up from the back



Figure 6. Set-up front with 8 paddle wheels



Figure 7. First two paddle wheels 3 cm above soil



Figure 8. Upper 6 paddle wheels



Figure 9. Full simulator, overflowing



Figure 10. Simulator shifted back 0.6 m



Figure 11. Damage at end of calibration



Figure 12. The run-up process for a filling level of 6 m.

D Measurements of velocity along the slope for various filling levels, during calibration at the Vossemeerdijk.

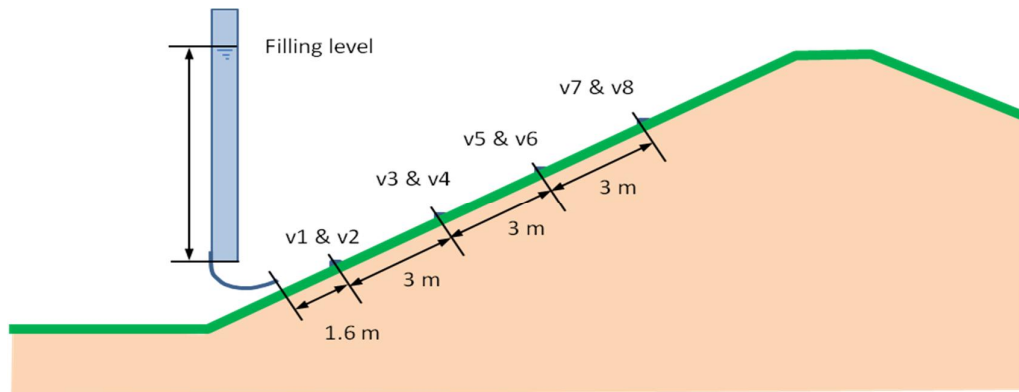
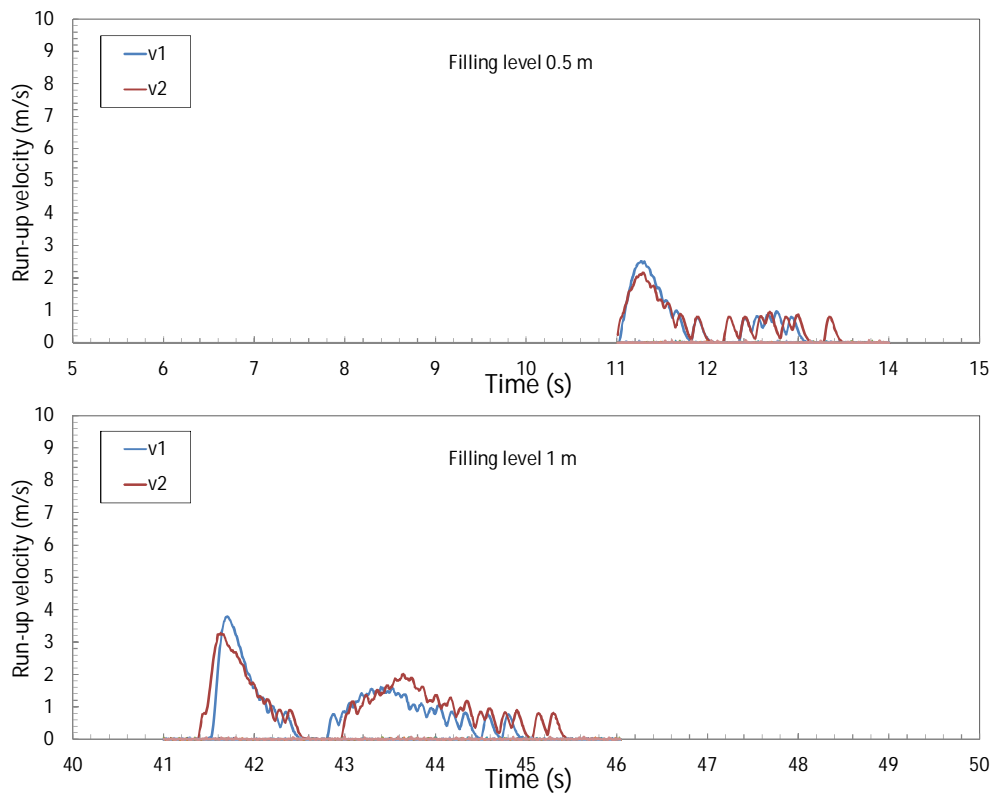
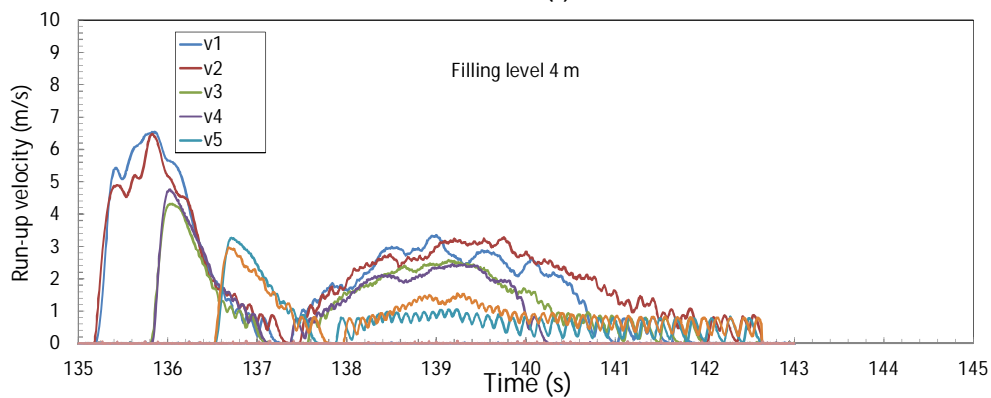
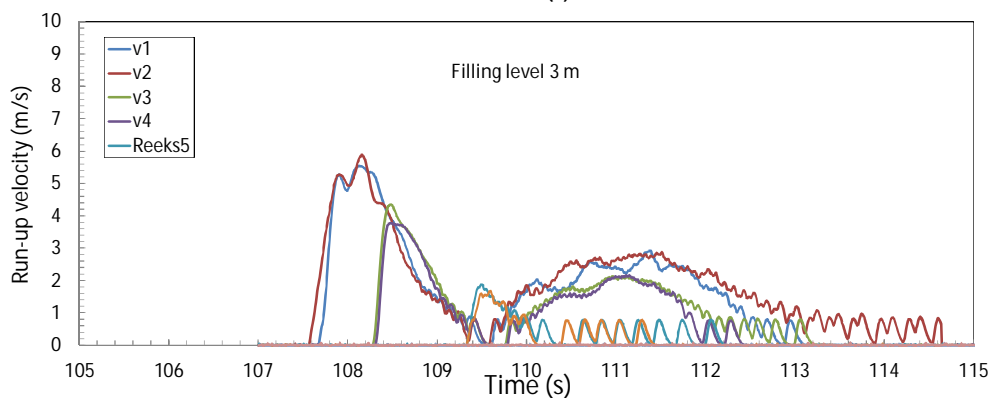
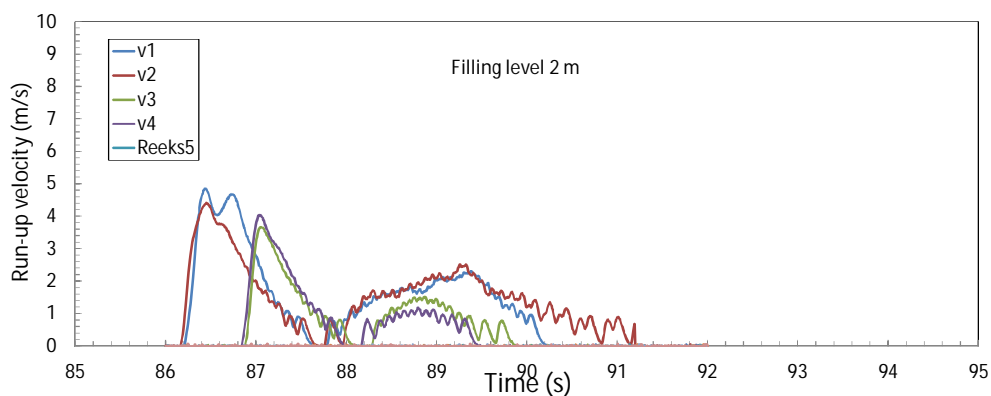
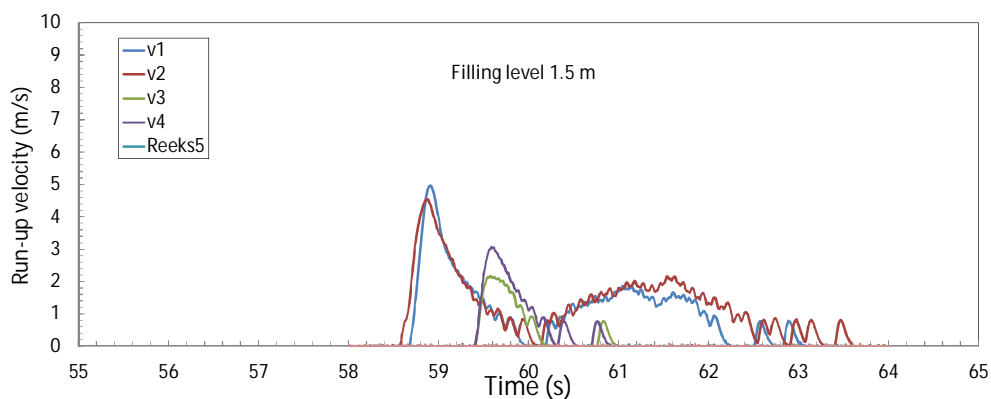
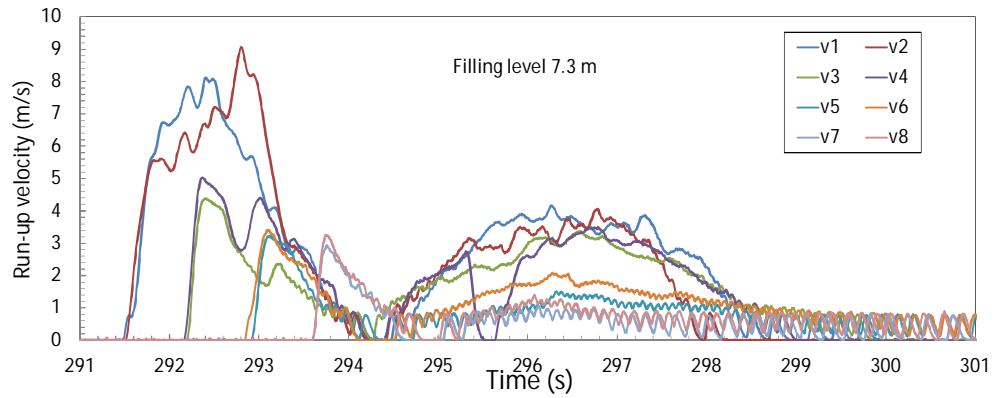
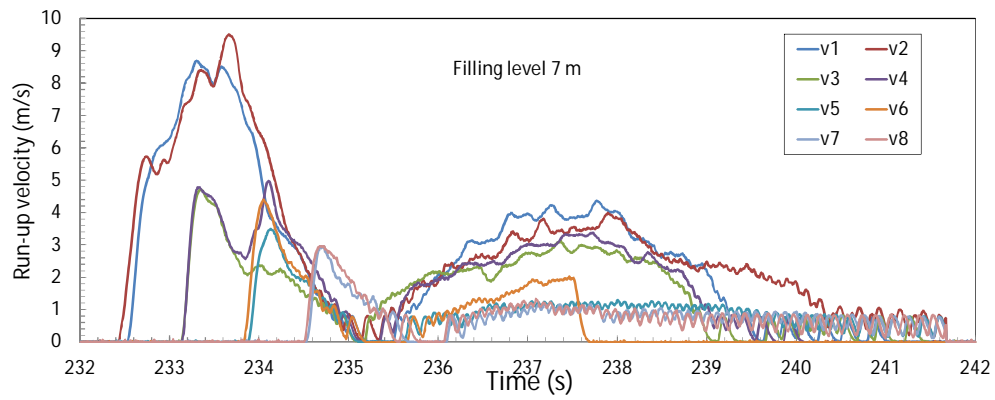
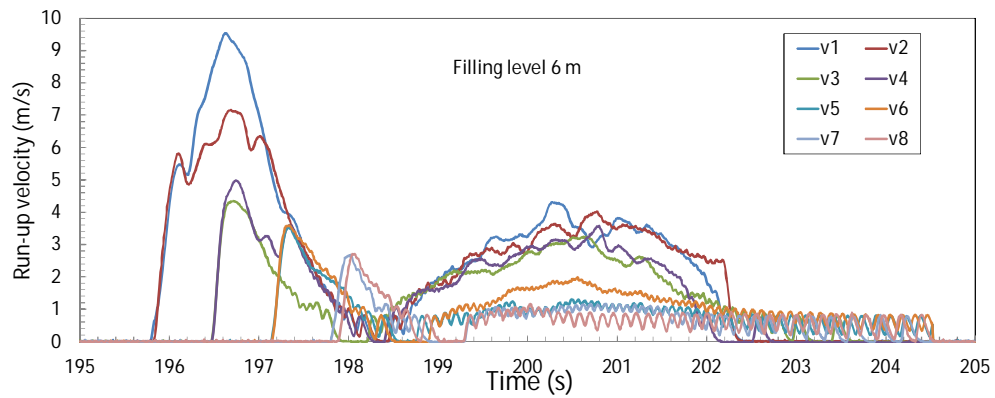
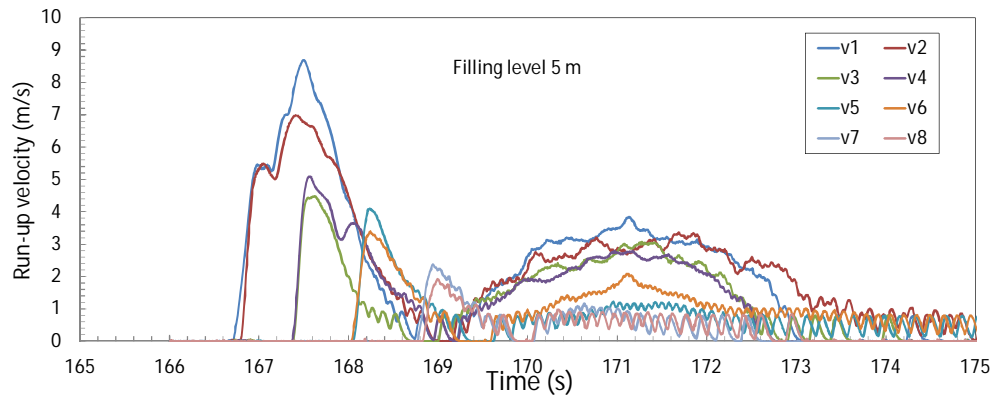


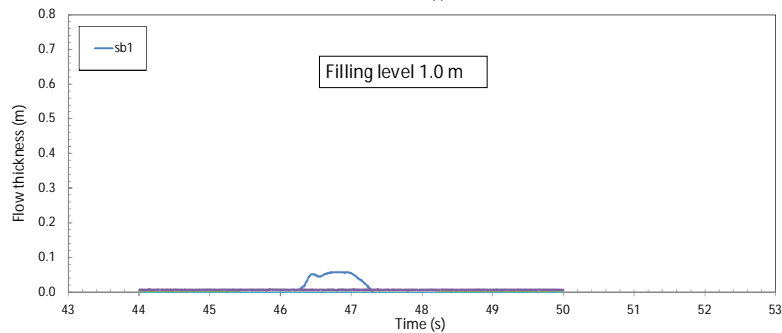
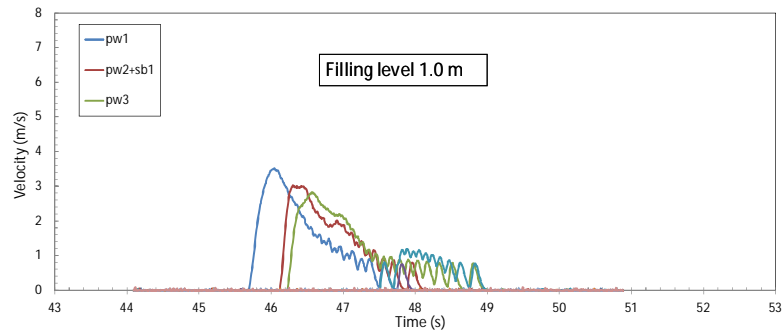
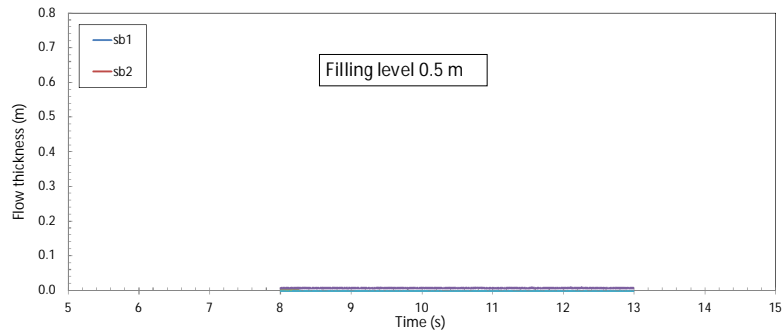
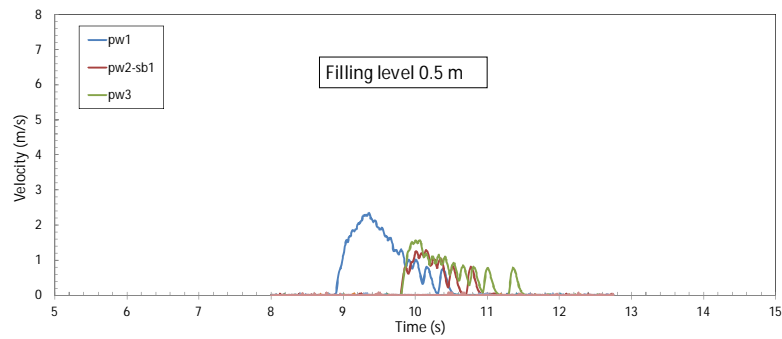
Figure D.1 Schematic representation of test set up, filling level and measurement locations along the slope surface

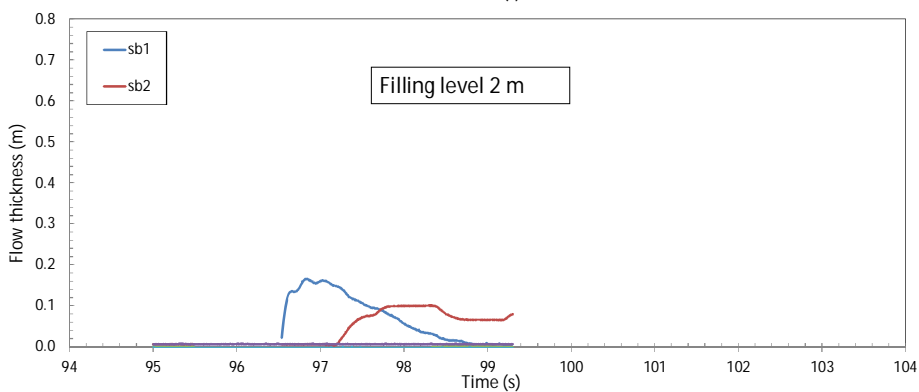
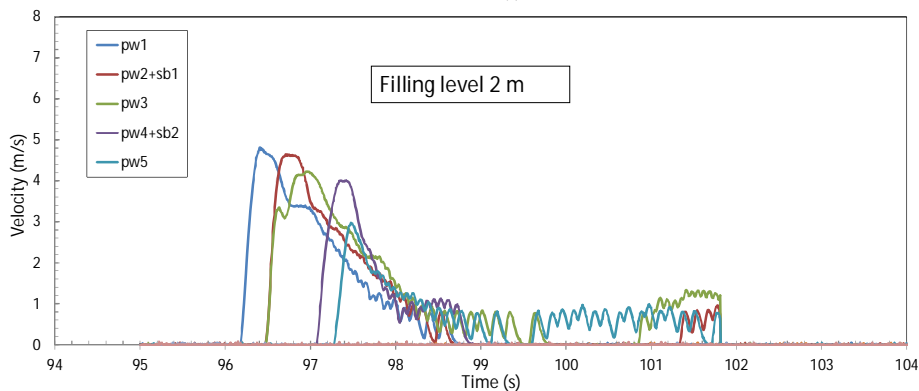
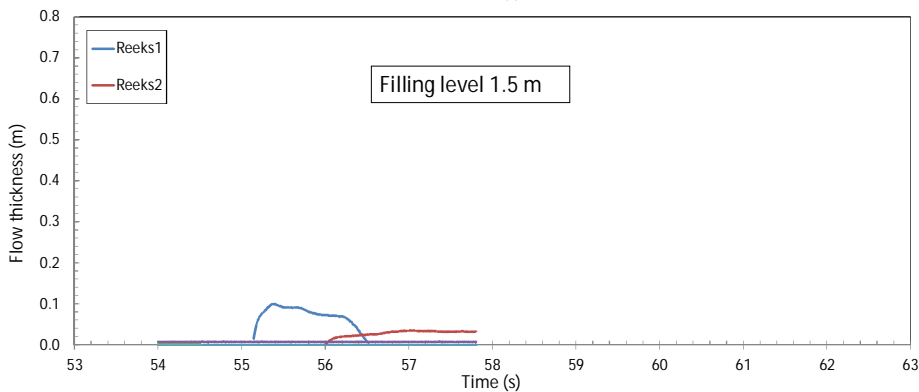
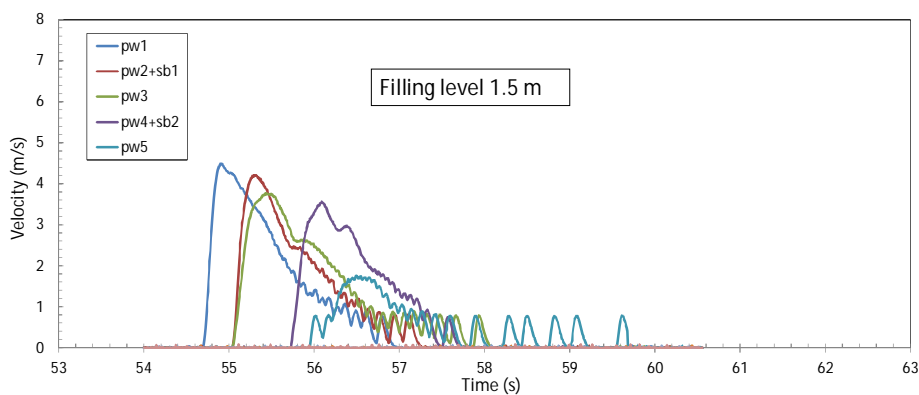


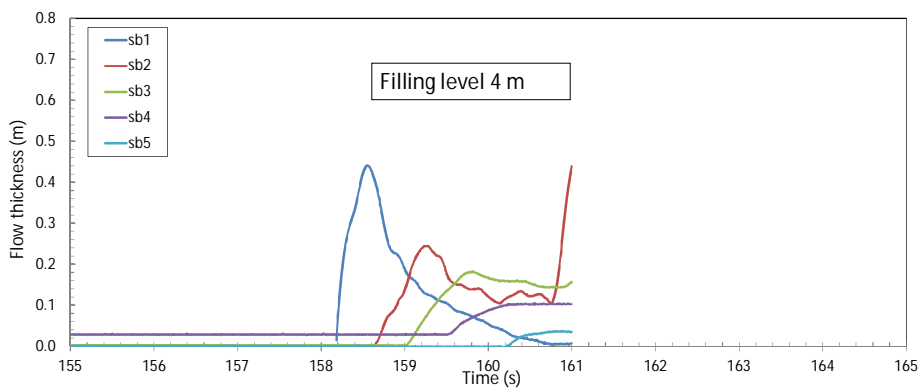
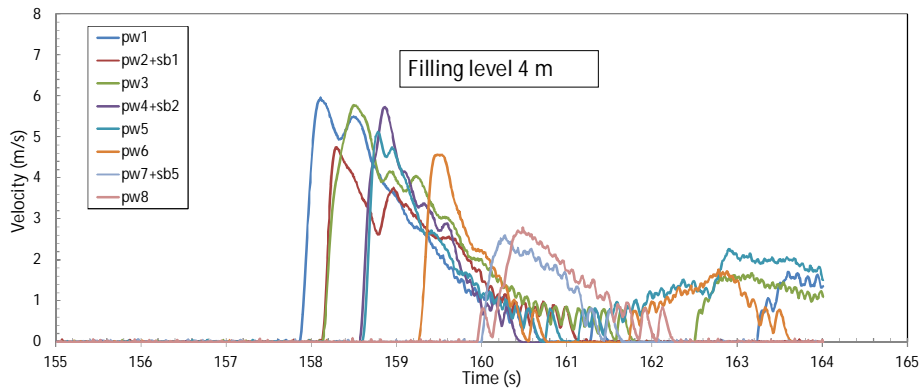
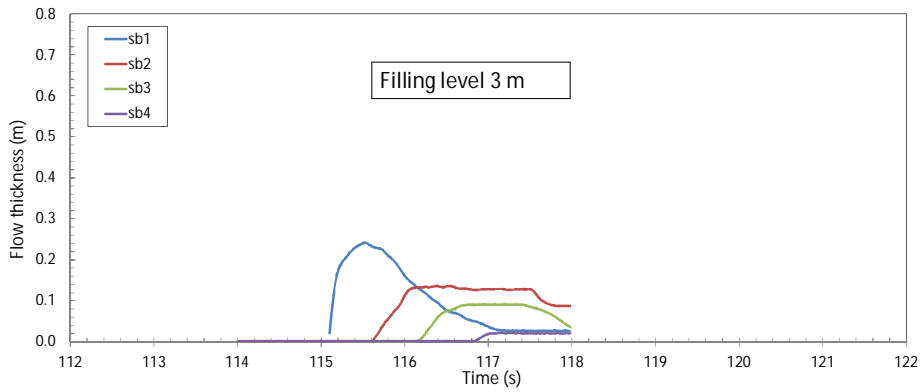
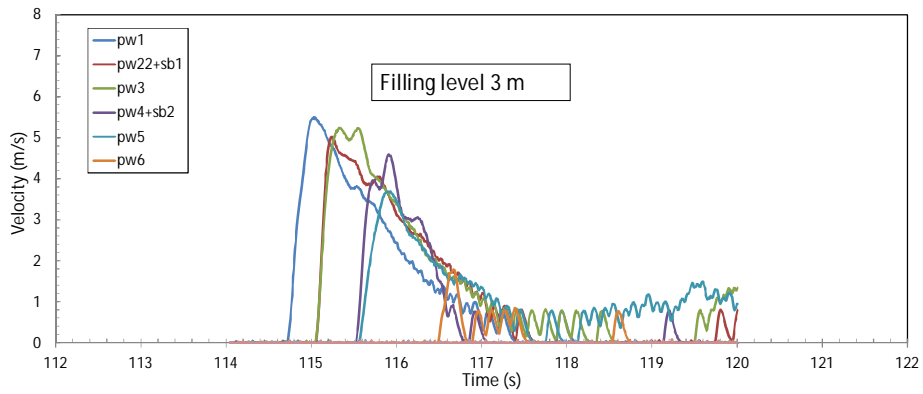


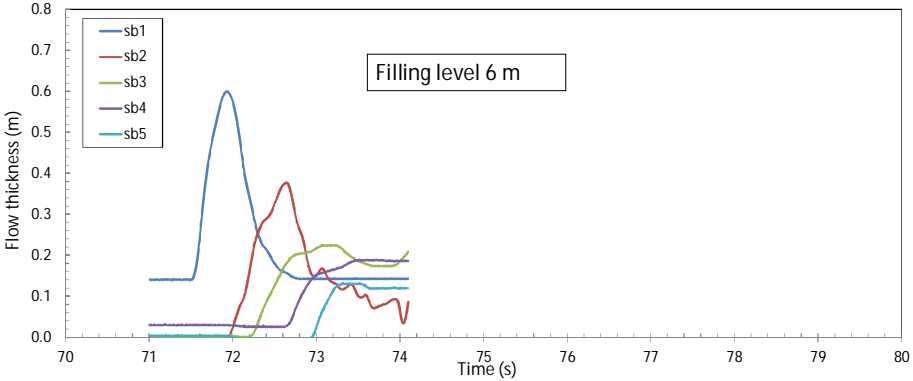
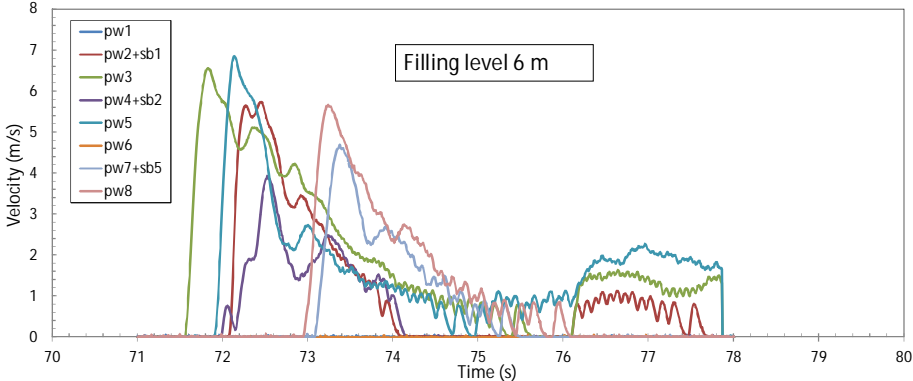
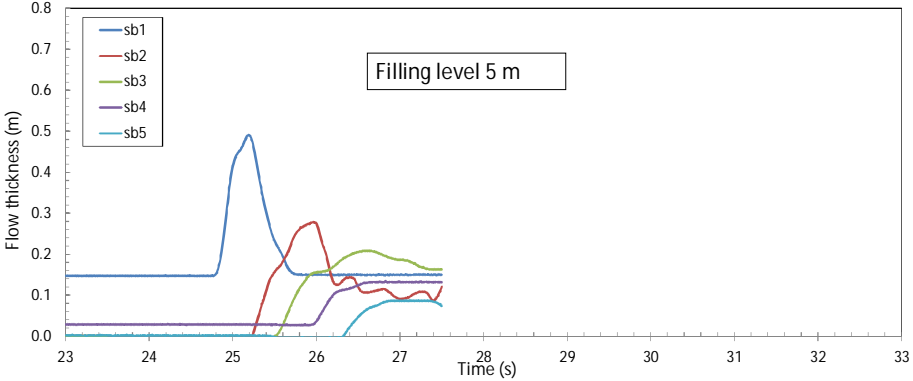
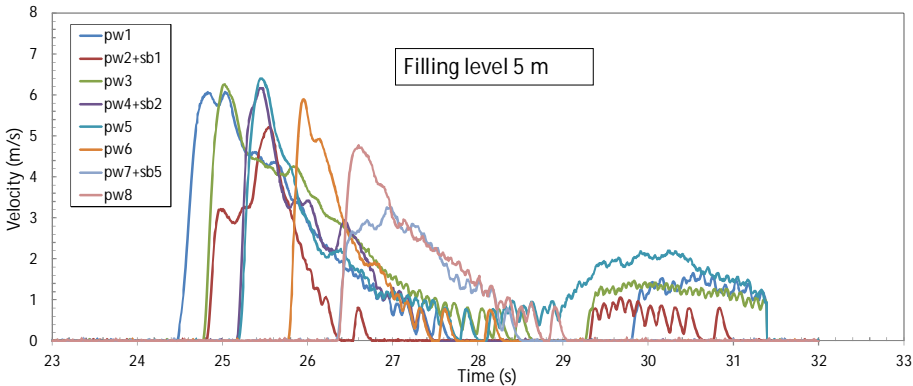


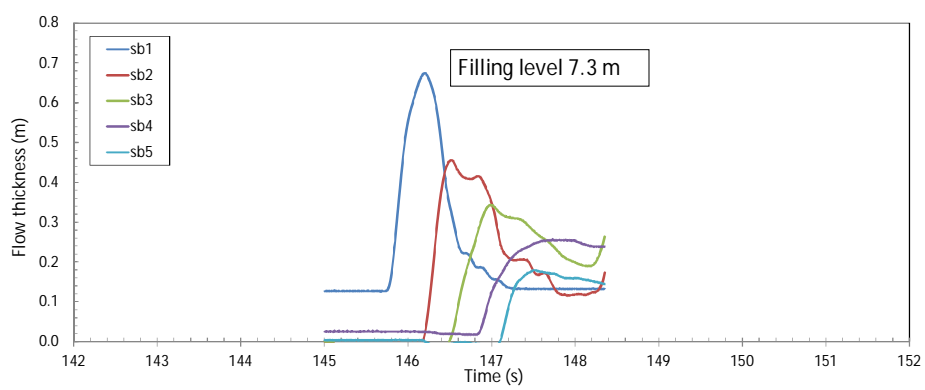
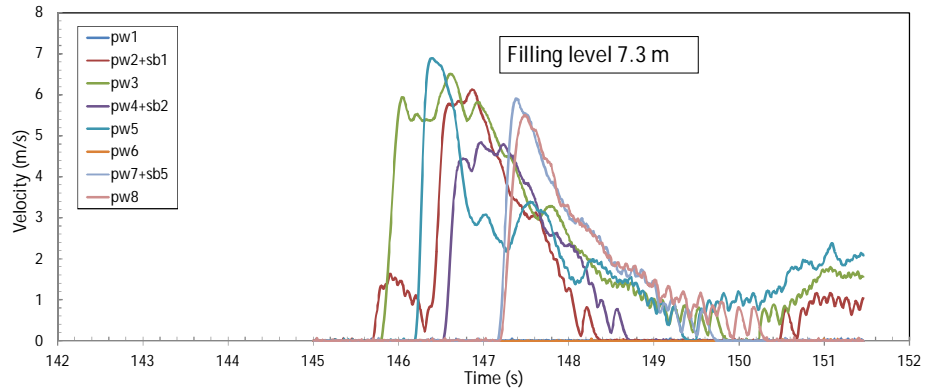
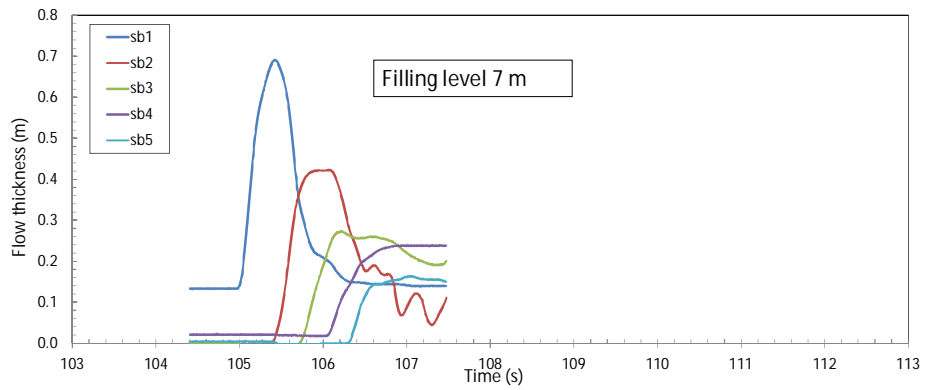
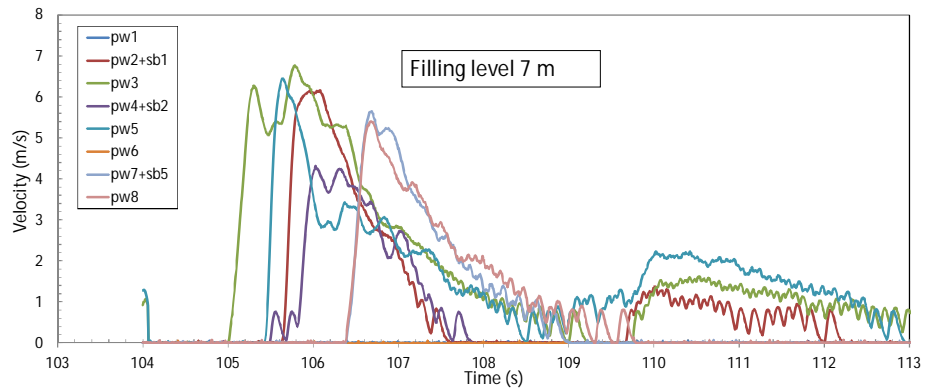
E Measurements of velocity and flow thickness along the slope during the hydraulic measurements at the Zeelandbrug and for various filling levels











F Cumulative overload for various test conditions and various acceleration factors

Duration hour	Average overtopping discharge l/s per m	$\Sigma (U^2 - U_c^2)$ at Comcoast; acceleration factor 1.36				
		$U_c=3\text{m/s}$	$U_c=4\text{m/s}$	$U_c=5\text{ m/s}$	$U_c=6.5\text{ m/s}$	$U_c=8\text{m/s}$
6	0.1	55	25	5	0	0
6	1	488	200	69	0	0
6	5	2629	1357	470	60	0
6	10	5444	2924	1154	186	5
6	20	11888	6974	3110	624	98
6	30	17524	10941	5513	1284	201
6	50	29205	20007	10497	3274	686

Duration hour	Average overtopping discharge l/s per m	$\Sigma (U^2 - U_c^2)$ at Comcoast; acceleration factor 1.44				
		$U_c=3\text{m/s}$	$U_c=4\text{m/s}$	$U_c=5\text{ m/s}$	$U_c=6.5\text{ m/s}$	$U_c=8\text{m/s}$
6	0.1	69	34	9	0	0
6	1	626	259	104	0	0
6	5	3184	1733	635	60	0
6	10	6653	3767	1612	285	53
6	20	14328	8865	4231	1006	203
6	30	20972	13688	7349	1993	458
6	50	34174	24976	13676	4807	1420

Duration hour	Average overtopping discharge l/s per m	$\Sigma (U^2 - U_c^2)$ at $H_s = 1\text{ m}$; acceleration factor 1.00				
		$U_c=3\text{m/s}$	$U_c=4\text{m/s}$	$U_c=5\text{ m/s}$	$U_c=6.5\text{ m/s}$	$U_c=8\text{m/s}$
6	0.1	0	0	0	0	0
6	1	10	0	0	0	0
6	5	157	3	0	0	0
6	10	543	31	0	0	0
6	30	3353	564	40	0	0
6	50	7189	1782	240	0	0
6	75	15008	4015	800	19	0

Duration hour	Average overtopping discharge l/s per m	$\Sigma (U^2 - U_c^2)$ at $H_s = 1\text{ m}$; acceleration factor 1.14				
		$U_c=3\text{m/s}$	$U_c=4\text{m/s}$	$U_c=5\text{ m/s}$	$U_c=6.5\text{ m/s}$	$U_c=8\text{m/s}$
6	0.1	4	0	0	0	0
6	1	50	0	0	0	0
6	5	517	40	0	0	0
6	10	1484	198	8	0	0
6	30	7078	1926	299	2	0
6	50	15682	4920	1158	46	0
6	75	26337	9635	2975	238	2

Duration	Average overtopping discharge l/s per m	$\Sigma (U^2 - U_c^2)$ at $H_s = 2$ m; acceleration factor 1.00				
		$U_c=3$ m/s	$U_c=4$ m/s	$U_c=5$ m/s	$U_c=6.5$ m/s	$U_c=8$ m/s
6	0.1	14	1	0	0	0
6	1	112	16	0	0	0
6	5	657	136	11	0	0
6	10	1488	384	51	0	0
6	30	5410	2015	496	18	0
6	50	9662	4251	1342	112	0
6	75	16021	7448	2794	339	0

Duration	Average overtopping discharge l/s per m	$\Sigma (U^2 - U_c^2)$ at $H_s = 2$ m; acceleration factor 1.15				
		$U_c=3$ m/s	$U_c=4$ m/s	$U_c=5$ m/s	$U_c=6.5$ m/s	$U_c=8$ m/s
6	0.1	29	8	0	0	0
6	1	249	66	7	0	0
6	5	1358	445	87	0	0
6	10	2907	1102	276	9	0
6	30	9547	4676	1721	199	4
6	50	16997	8966	3919	682	55
6	75	26015	14666	7244	1642	191

Duration	Average overtopping discharge l/s per m	$\Sigma (U^2 - U_c^2)$ at $H_s = 2$ m; acceleration factor 1.20				
		$U_c=3$ m/s	$U_c=4$ m/s	$U_c=5$ m/s	$U_c=6.5$ m/s	$U_c=8$ m/s
6	0.1	35	12	0	0	0
6	1	308	94	14	0	0
6	5	1650	602	140	2	0
6	10	3484	1449	417	23	0
6	30	11250	5843	2368	343	15
6	50	19696	10948	5176	1071	113
6	75	29656	18015	9296	2438	363

Duration	Average overtopping discharge l/s per m	$\Sigma (U^2 - U_c^2)$ at $H_s = 2$ m; acceleration factor 1.30				
		$U_c=3$ m/s	$U_c=4$ m/s	$U_c=5$ m/s	$U_c=6.5$ m/s	$U_c=8$ m/s
6	0.1	49	20	4	0	0
6	1	444	169	43	0	0
6	5	2316	1006	307	18	0
6	10	4783	2309	829	86	0
6	30	15131	8586	4064	838	82
6	50	25439	15495	8319	2269	368
6	75	37403	25762	14263	4722	1011

Duration	Average overtopping discharge l/s per m	$\Sigma (U^2 - U_c^2)$ at $H_s = 2$ m; acceleration factor 1.36				
		$U_c=3$ m/s	$U_c=4$ m/s	$U_c=5$ m/s	$U_c=6.5$ m/s	$U_c=8$ m/s
6	0.1	58	27	7	0	0
6	1	537	226	69	0	0
6	5	2766	1306	452	40	0
6	10	5652	2932	1170	159	4
6	30	17609	10484	5348	1300	170
6	50	29105	18696	10610	3303	652
6	75	42348	30707	17785	6586	1663

Duration	Average overtopping discharge l/s per m	$\Sigma (U^2 - U_c^2)$ at $H_s = 2$ m; acceleration factor 1.37				
		$U_c=3$ m/s	$U_c=4$ m/s	$U_c=5$ m/s	$U_c=6.5$ m/s	$U_c=8$ m/s
6	0.1	60	28	7	0	0
6	1	554	236	74	1	0
6	5	2845	1360	479	46	0
6	10	5803	3044	1234	175	5
6	30	18033	10819	5582	1391	190
6	50	29732	19323	11020	3500	712
6	75	43194	31553	18410	6934	1795

Duration	Average overtopping discharge l/s per m	$\Sigma (U^2 - U_c^2)$ at $H_s = 2$ m; acceleration factor 1.40				
		$U_c=3$ m/s	$U_c=4$ m/s	$U_c=5$ m/s	$U_c=6.5$ m/s	$U_c=8$ m/s
6	0.1	65	32	9	0	0
6	1	604	269	91	3	0
6	5	3086	1530	569	65	0
6	10	6266	3391	1439	227	10
6	30	19323	11852	6317	1690	259
6	50	31641	21232	12303	4138	915
6	75	45769	34128	20352	8047	2235

Duration	Average overtopping discharge l/s per m	$\Sigma (U^2 - U_c^2)$ at $H_s = 2$ m; acceleration factor 1.42				
		$U_c=3$ m/s	$U_c=4$ m/s	$U_c=5$ m/s	$U_c=6.5$ m/s	$U_c=8$ m/s
6	0.1	68	34	11	0	0
6	1	638	292	104	4	0
6	5	3252	1649	635	80	0
6	10	6584	3634	1586	268	14
6	30	20198	12565	6835	1911	315
6	50	32937	22528	13199	4602	1072
6	75	47517	35876	21701	8844	2567

Duration	Average overtopping discharge	$\Sigma (U^2 - U_c^2)$ at $H_s = 2$ m; acceleration factor 1.44				
		$U_c=3$ m/s	$U_c=4$ m/s	$U_c=5$ m/s	$U_c=6.5$ m/s	$U_c=8$ m/s
<i>hour</i>	<i>l/s per m</i>					
6	0.1	72	37	13	0	0
6	1	674	316	118	5	0
6	5	3422	1773	704	97	0
6	10	6909	3885	1742	313	20
6	30	21086	13298	7375	2151	379
6	50	34251	23842	14127	5097	1247
6	75	49290	37649	23092	9687	2931

Duration	Average overtopping discharge	$\Sigma (U^2 - U_c^2)$ at $H_s = 2$ m; acceleration factor 1.45				
		$U_c=3$ m/s	$U_c=4$ m/s	$U_c=5$ m/s	$U_c=6.5$ m/s	$U_c=8$ m/s
<i>hour</i>	<i>l/s per m</i>					
6	0.1	73	39	14	0	0
6	1	692	329	125	6	0
6	5	3508	1837	741	106	1
6	10	7074	4014	1824	338	24
6	30	21535	13672	7654	2278	414
6	50	34915	24506	14604	5356	1342
6	75	50185	38544	23804	10126	3126

Duration	Average overtopping discharge	$\Sigma (U^2 - U_c^2)$ at $H_s = 2$ m; acceleration factor 1.46				
		$U_c=3$ m/s	$U_c=4$ m/s	$U_c=5$ m/s	$U_c=6.5$ m/s	$U_c=8$ m/s
<i>hour</i>	<i>l/s per m</i>					
6	0.1	75	40	14	0	0
6	1	710	342	133	7	0
6	5	3596	1902	779	117	2
6	10	7240	4145	1907	364	29
6	30	21987	14051	7938	2410	451
6	50	35583	25174	15088	5624	1441
6	75	51087	39446	24526	10576	3329

Duration	Average overtopping discharge	$\Sigma (U^2 - U_c^2)$ at $H_s = 2$ m; acceleration factor 1.48				
		$U_c=3$ m/s	$U_c=4$ m/s	$U_c=5$ m/s	$U_c=6.5$ m/s	$U_c=8$ m/s
<i>hour</i>	<i>l/s per m</i>					
6	0.1	79	43	16	0	0
6	1	748	368	149	10	0
6	5	3773	2036	858	139	4
6	10	7578	4413	2081	420	39
6	30	22900	14823	8523	2688	534
6	50	36934	26525	16081	6183	1657
6	75	52909	41268	26301	11511	3761

Duration	Average overtopping discharge l/s per m	$\Sigma (U^2 - U_c^2)$ at $H_s = 2$ m; acceleration factor 1.51				
		$U_c=3$ m/s	$U_c=4$ m/s	$U_c=5$ m/s	$U_c=6.5$ m/s	$U_c=8$ m/s
6	0.1	84	47	19	0	0
6	1	805	410	174	14	0
6	5	4047	2245	985	178	6
6	10	8098	4830	2358	515	58
6	30	24292	16015	9442	3142	677
6	50	38994	28585	17630	7082	2021
6	75	55689	44048	29081	12999	4478

Duration	Average overtopping discharge l/s per m	$\Sigma (U^2 - U_c^2)$ at $H_s = 3$ m; acceleration factor 1.00				
		$U_c=3$ m/s	$U_c=4$ m/s	$U_c=5$ m/s	$U_c=6.5$ m/s	$U_c=8$ m/s
6	0.1	21	9	0	0	0
6	1	147	45	9	0	0
6	5	923	355	87	1	0
6	10	1913	810	237	11	0
6	30	6054	3087	1203	159	0
6	50	10231	5736	2565	465	0
6	75	15864	9282	4627	1093	0

Duration	Average overtopping discharge l/s per m	$\Sigma (U^2 - U_c^2)$ at $H_s = 3$ m; acceleration factor 1.12				
		$U_c=3$ m/s	$U_c=4$ m/s	$U_c=5$ m/s	$U_c=6.5$ m/s	$U_c=8$ m/s
6	0.1	31	17	6	0	0
6	1	241	102	27	0	0
6	5	1459	703	248	21	0
6	10	2959	1529	604	77	0
6	30	8963	5329	2591	566	60
6	50	15093	9463	5103	1400	199
6	75	22578	14777	8642	2849	505

Duration	Average overtopping discharge l/s per m	$\Sigma (U^2 - U_c^2)$ at $H_s = 3$ m; acceleration factor 1.21				
		$U_c=3$ m/s	$U_c=4$ m/s	$U_c=5$ m/s	$U_c=6.5$ m/s	$U_c=8$ m/s
6	0.1	41	26	12	0	0
6	1	323	161	54	6	0
6	5	1933	1050	444	65	0
6	10	3875	2230	1031	195	12
6	30	11514	7406	4056	1149	193
6	50	19130	12832	7654	2612	584
6	75	28113	19923	12538	4959	1409

Duration	Average overtopping discharge	$\Sigma (U^2 - U_c^2)$ at $H_s = 3$ m; acceleration factor 1.35				
		$U_c=3$ m/s	$U_c=4$ m/s	$U_c=5$ m/s	$U_c=6.5$ m/s	$U_c=8$ m/s
<i>hour</i>	<i>l/s per m</i>					
6	0.1	58	40	22	3	0
6	1	473	277	125	22	0
6	5	2783	1731	894	215	21
6	10	5505	3578	1972	560	87
6	30	16073	11260	7051	2669	694
6	50	26029	18987	12689	5528	1763
6	75	37573	29383	20020	9742	3668

Duration	Average overtopping discharge	$\Sigma (U^2 - U_c^2)$ at Durme; acceleration factor 1.00				
		$U_c=3$ m/s	$U_c=4$ m/s	$U_c=5$ m/s	$U_c=6.5$ m/s	$U_c=8$ m/s
<i>hour</i>	<i>l/s per m</i>					
1	1	0	0	0	0	0
1	10	33	0	0	0	0
1	30	493	68	2	0	0
1	50	1095	235	24	0	0

Duration	Average overtopping discharge	$\Sigma (U^2 - U_c^2)$ at Durme; acceleration factor 1.35				
		$U_c=3$ m/s	$U_c=4$ m/s	$U_c=5$ m/s	$U_c=6.5$ m/s	$U_c=8$ m/s
<i>hour</i>	<i>l/s per m</i>					
1	1	11	0	0	0	0
1	10	466	68	0	0	0
1	30	2830	952	245	10	0
1	50	5179	2102	722	72	0

Duration	Average overtopping discharge	$\Sigma (U^2 - U_c^2)$ at Durme; acceleration factor 1.36				
		$U_c=3$ m/s	$U_c=4$ m/s	$U_c=5$ m/s	$U_c=6.5$ m/s	$U_c=8$ m/s
<i>hour</i>	<i>l/s per m</i>					
1	1	12	0	0	0	0
1	10	489	74	0	0	0
1	30	2925	999	263	12	0
1	50	5315	2238	766	80	1

$\Sigma (U^2 - U_c^2)$ HM Vecht; acceleration factor 1.2				
$U_c=3$ m/s	$U_c=4$ m/s	$U_c=5$ m/s	$U_c=6.5$ m/s	$U_c=8$ m/s
1325	1065	776	417	1685

Duration	Average overtopping discharge	$\Sigma (U^2 - U_c^2)$ at Nijmegen; acceleration factor 1.00				
hour	l/s per m	$U_c=3\text{m/s}$	$U_c=4\text{m/s}$	$U_c=5\text{ m/s}$	$U_c=6.5\text{ m/s}$	$U_c=8\text{m/s}$
6	1	0	0	0	0	0
6	10	453	10	0	0	0
6	50	6168	760	13	0	0
6	100	20021	3885	254	0	0
6	200	47029	16873	2766	4	0

Duration	Average overtopping discharge	$\Sigma (U^2 - U_c^2)$ at Nijmegen; acceleration factor 1.10				
hour	l/s per m	$U_c=3\text{m/s}$	$U_c=4\text{m/s}$	$U_c=5\text{ m/s}$	$U_c=6.5\text{ m/s}$	$U_c=8\text{m/s}$
6	1	0	0	0	0	0
6	10	1046	72	0	0	0
6	50	11221	2287	151	0	0
6	100	31052	9017	1300	0	0
6	200	65047	34891	8543	194	0

Duration	Average overtopping discharge	$\Sigma (U^2 - U_c^2)$ at Nijmegen; acceleration factor 1.37				
hour	l/s per m	$U_c=3\text{m/s}$	$U_c=4\text{m/s}$	$U_c=5\text{ m/s}$	$U_c=6.5\text{ m/s}$	$U_c=8\text{m/s}$
6	1	78	0	0	0	0
6	10	4357	1040	105	0	0
6	50	32599	13029	3443	99	0
6	100	66084	40800	13692	1127	2
6	200	122267	92111	53339	9065	400

Duration	Average overtopping discharge	$\Sigma (U^2 - U_c^2)$ at Nijmegen; acceleration factor 1.40				
hour	l/s per m	$U_c=3\text{m/s}$	$U_c=4\text{m/s}$	$U_c=5\text{ m/s}$	$U_c=6.5\text{ m/s}$	$U_c=8\text{m/s}$
6	1	102	0	0	0	0
6	10	4881	1262	149	0	0
6	50	35263	14855	4274	164	0
6	100	70449	45165	16170	1598	11
6	200	129397	99241	60469	11557	670

Duration	Average overtopping discharge	$\Sigma (U^2 - U_c^2)$ at Nijmegen; acceleration factor 1.42				
hour	l/s per m	$U_c=3\text{m/s}$	$U_c=4\text{m/s}$	$U_c=5\text{ m/s}$	$U_c=6.5\text{ m/s}$	$U_c=8\text{m/s}$
6	1	119	0	0	0	0
6	10	5247	1427	185	0	0
6	50	37071	16140	4893	221	0
6	100	73412	48128	17949	1982	22
6	200	134237	104081	65309	13433	916

Duration	Average overtopping discharge	$\Sigma (U^2 - U_c^2)$ at Nijmegen; acceleration factor 1.50				
		$U_c=3\text{m/s}$	$U_c=4\text{m/s}$	$U_c=5\text{ m/s}$	$U_c=6.5\text{ m/s}$	$U_c=8\text{m/s}$
<i>hour</i>	<i>l/s per m</i>					
6	1	202	0	0	0	0
6	10	6842	2214	391	0	0
6	50	44560	23119	7917	612	0
6	100	85682	60398	27890	4188	143
6	200	154280	124124	85352	22719	2620

Duration	Average overtopping discharge	$\Sigma (U^2 - U_c^2)$ at N-Beveland; acceleration factor 1.00				
		$U_c=3\text{m/s}$	$U_c=4\text{m/s}$	$U_c=5\text{ m/s}$	$U_c=6.5\text{ m/s}$	$U_c=8\text{m/s}$
<i>hour</i>	<i>l/s per m</i>					
6	0.06	51	13	0	0	0
6	0.84	664	258	45	0	0
6	6.25	2305	1053	254	0	0

Duration	Average overtopping discharge	$\Sigma (U^2 - U_c^2)$ at N-Beveland; acceleration factor 1.37				
		$U_c=3\text{m/s}$	$U_c=4\text{m/s}$	$U_c=5\text{ m/s}$	$U_c=6.5\text{ m/s}$	$U_c=8\text{m/s}$
<i>hour</i>	<i>l/s per m</i>					
6	0.06	164	103	46	2	0
6	0.84	1830	1312	721	148	4
6	6.25	6023	4518	2747	747	33

G Experimental results force and displacements (grass sods)